The Dissertation Committee for Dharhas Pothina
certifies that this is the approved version of the following dissertation:

A multimodel approach to modeling bay circulation in shallow bay - ship channel systems

Committee:

Ben Hodges, Supervisor

Clint Dawson

Spyros Kinnas

David Maidment

Daene McKinney

A multimodel approach to modeling bay circulation in shallow bay - ship channel systems

by

Dharhas Pothina, B.Tech.; M.S.E

DISSERTATION

Presented to the Faculty of the Graduate School of

The University of Texas at Austin

in Partial Fulfillment

of the Requirements

for the Degree of

DOCTOR OF PHILOSOPHY

THE UNIVERSITY OF TEXAS AT AUSTIN

May 2009

Dedicated to my family

Acknowledgments

The road to the completion of this dissertation was long and bumpy. I would not have made it to the end without the help and support of family, friends and colleagues. First, I would like to thank my wife, Jada for her support, encouragement and perseverance the last few years. Without her editing skills and her belief in me, this work would not have been completed.

I would like to thank Vadym Aizinger who planted the seed of the idea and Clint Dawson who encouraged me to pursue my doctorate in civil engineering. To my advisor Ben Hodges, I give thanks for his guidance, patience and support throughout my research, especially as I juggled work, family and research responsibilities. Thanks is also required for Barney Austin, Ruben Solis, Carla Guthrie and the Texas Water Development Board for their support and flexibility at work that allowed me the time and resources to complete this research.

This dissertation would not have happened if not for the support my family received from friends and family. To the Lansings, the Wests, the Browns and both Jada's family and mine, I give special thanks. Without their prayers, encouragement and many forms of practical support, my family would not have been able to manage while I was distracted by research.

Finally, the joy I could see in my daughter Seraya's face every time we played sustained me through long days and nights of research. Her desire to spend more time with me and the impending arrival of our second daughter, Arlyn are what gave me the strength for that final push to finish.

A multimodel approach to modeling bay circulation in shallow bay - ship channel systems

Publication No. _____

Dharhas Pothina, Ph.D.
The University of Texas at Austin, 2009

Supervisor: Ben Hodges

Numerical modeling of shallow microtidal semi-enclosed estuaries requires the effective simulation of physical processes with a wide range of temporal and spatial scales. In theory, application of sufficient grid resolution in both the horizontal and vertical should result in a reasonable simulation. However, in practice, this is not the case. Fully resolving the finest scales can be computationally prohibitive, and various algorithmic assumptions can break down at fine resolutions, leading to spurious oscillations in the solution. One method of simulating inherently cross-scale phenomena is to use multimodel approaches in which domain decomposition is used to divide the region into multiple subregions, each modeled by different submodels. These submodels are coupled to simulate the entire system efficiently. In general, the different models may involve different physics, they may be dimensionally heterogeneous or they may be both physically and dimensionally heterogeneous. A reduction in computational expense is obtained by using simpler physics and/or a reduced dimension model in the submodels.

In this research, we look at the particular case of modeling shallow bays containing narrow, deep ship channels. In order to accurately model bay circulation, a model should capture the effect of these spatially localized navigational channels. Our research shows that modeling techniques currently used to simulate such systems using 2 dimensional or coarse resolution 3 dimensional estuary models misrepresent wind driven surface circulation in the shallow bay and tide driven volume fluxes through the channel. Fully resolving the geometry of the ship channel is impractical on all but large parallel computing clusters.

We propose a more efficient method using the multimodel approach. This approach splits the estuary into a shallow bay region and a subsurface ship channel region. By separating the physical domain into two parts in this way, simpler models can be used that are targeted at the different physical processes and geometries dominant in each region. By using a low resolution 3D model (SELFE) in the shallow bay region, coupled through appropriate interface conditions with a 2D laterally averaged model, the effects of the ship channel on bay circulation are accurately represented at a fraction of the computational expense. In this research, this coupled model was developed and applied to an ideal shallow bay- ship channel system. The coupled model approach is found to be an effective strategy for modeling this type of system.

Table of Contents

List of Tables

List of Figures

Chapter 1

Introduction

1.1 Motivation

An estuary, together with the tidal freshwater river upstream of it, comprises a pathway for exchange of water and materials between a drainage basin and coastal region. Rivers carry nutrients, sediments and pollutants into the estuary. Bay circulation also influences estuarine conditions such as hypoxia and the extent of salinity intrusion [19]. To characterize these transport processes, it is necessary to understand the underlying hydrodynamics and the turbulence structure of the flow. This is often done by means of numerical hydrodynamic models [5, 10, 11, 19, 29, 32, 70].

In this dissertation, we look at the particular case of modeling shallow microtidal semi-enclosed estuarine systems. In other words, estuaries with a tidal amplitude of less than 2m, consisting of a shallow bay containing a ship channel and separated from the ocean by barrier islands. This type of estuary is common around the world and especially along the Texas coast. Galveston Bay, Corpus Christi Bay and Matagorda Bay are examples of estuarine systems within Texas that fit this description. Mobile Bay (Alabama), Hillsborough Bay (Florida), Hawkesbury River Estuary (Australia) and Randers Fjord (Denmark) are other examples. The ship channels in these bays are usually an order of magnitude deeper than the surrounding bay and are spatially localized. While our research is valid for any shallow bay system containing a ship channel, we

use examples from Texas to guide this study.

While the presence of these ship channels can impact bay circulation and transport processes, the significance of these impacts has not been studied in detail. Klinck *et al* [28] studied the effect of changes in the ship channel configuration in Galveston Bay under different freshwater inflow regimes on oyster population. They noted that channel enlargement increases saltwater intrusion into the bay and that increased salinity is normally disadvantageous to oyster populations. However, they predicted that the introduction of an enlarged ship channel into Galveston Bay would result in increased oyster biomass over a 50-year assessment time. This was because channel enlargement would move optimal salinities over more of the existing reef tracts where hard substrate was plentiful and, consequently, production would increase.

Results from another study modeling the effect of deepening and widening the Houston Ship Channel in Galveston Bay [5], demonstrate the three dimensional nature of the flow regime caused by channelization. Under certain inflow conditions, parts of the lower bay had lower simulated salinities when the channel was deepened. They attributed this to increased stratification within the ship channel which caused the higher salinity water from the Gulf of Mexico to propagate up the channel instead of spilling out into the lower bay.

Winds, tides, heat fluxes, Coriolis forces and freshwater inflows, as well as the pressure from human activities, serve as the forcing agents of the physical and ecological processes in many estuaries. In our research, we explore the effect of wind and tidal forcing on shallow bay-ship channel systems. The most common approaches to the numerical solution of this problem include models based on either the 2D depth averaged or the 3D shallow-water equations(SWE) [58, 60, 63, 70, 72, 73]. It is our contention that both of these methods have

significant flaws when used to model shallow bay-ship channel systems. The 2D depth averaged approach underestimates the influence of wind forcing on circulation patterns in the bay, while the 3D models can be impractical due to the computational expense required. In both approaches, the narrowness of the ship channel makes accurately resolving it in the computational grid challenging. These issues are explored in detail in chapter 2.

To address these shortcomings, we propose a new multi-model approach that splits the estuary into a shallow bay region and a subsurface ship channel region (see figure 1.5). By separating the physical domain into two parts, we can use simpler models targeted at the different physical processes dominant in each region. The shallow bay is modeled using a 3D hydrodynamic model, while the subsurface portion of the ship channel is modeled using a 2D laterally averaged model. These models are coupled through appropriate interface conditions. This technique allows us to capture the salient features of the flow regime with greater accuracy than a 2D depth averaged approach and with a significantly lower computational cost than a high resolution 3D model.

While this type of system could potentially be modeled effectively using a high resolution 3D model running on a parallel computing cluster, our research is motivated by the way studies of estuarine systems are typically conducted in non academic settings. Government agencies and private consulting companies do not usually have the resources or expertise to take advantage of high performance parallel computing facilities. This is in contrast to universities and research centers where the presence of powerful supercomputing facilities has become the norm in recent years. Consequently, this modeling problem that in a sense can be '*solved*' in an academic sense by use of a high resolution computational grid in conjunction with a 3D hydrodynamic solver, remains unsolved in

a practical engineering sense in the commercial and government sectors. Thus, the need for a more efficient approach.

1.2 Background

1.2.1 Physical Setting

Texas has officially classified its coastal regions into 7 major and 5 minor bays and estuaries (see figure 1.1). These estuaries are typically warm, shallow systems separated from the Gulf of Mexico by barrier islands. The bays are often connected to the Gulf though a number of passes that are also dredged channels designed for shipping. They have relatively weak tidal signals with a typical tidal range of 0.6m[17] and have low freshwater discharge coming in from their rivers[23]. Strong prevailing winds with an average annual velocity of 12 miles per hour originate from the southeast through most of the year [57].

In many estuaries, the primary forcing agents influencing circulation are tides and freshwater discharge [22]. Other agents such as wind and Coriolis are still significant, modifying the circulation patterns but not driving them. The Satilla River estuary in Georgia, which has a tidal amplitude of 3m and an average depth of 4m, is tidally dominated [72] while the Columbia river estuary in Oregon, which has the second largest freshwater discharge in the United States, is heavily influenced by this discharge [70]. The confluence of the weak tides and low freshwater discharge in many Texas estuaries, along with the strong wind field can make the wind driven circulation in these estuaries more significant than in other locations. Therefore, any model used to conduct simulations in Texas should accurately capture the effect of this wind-driven circulation.

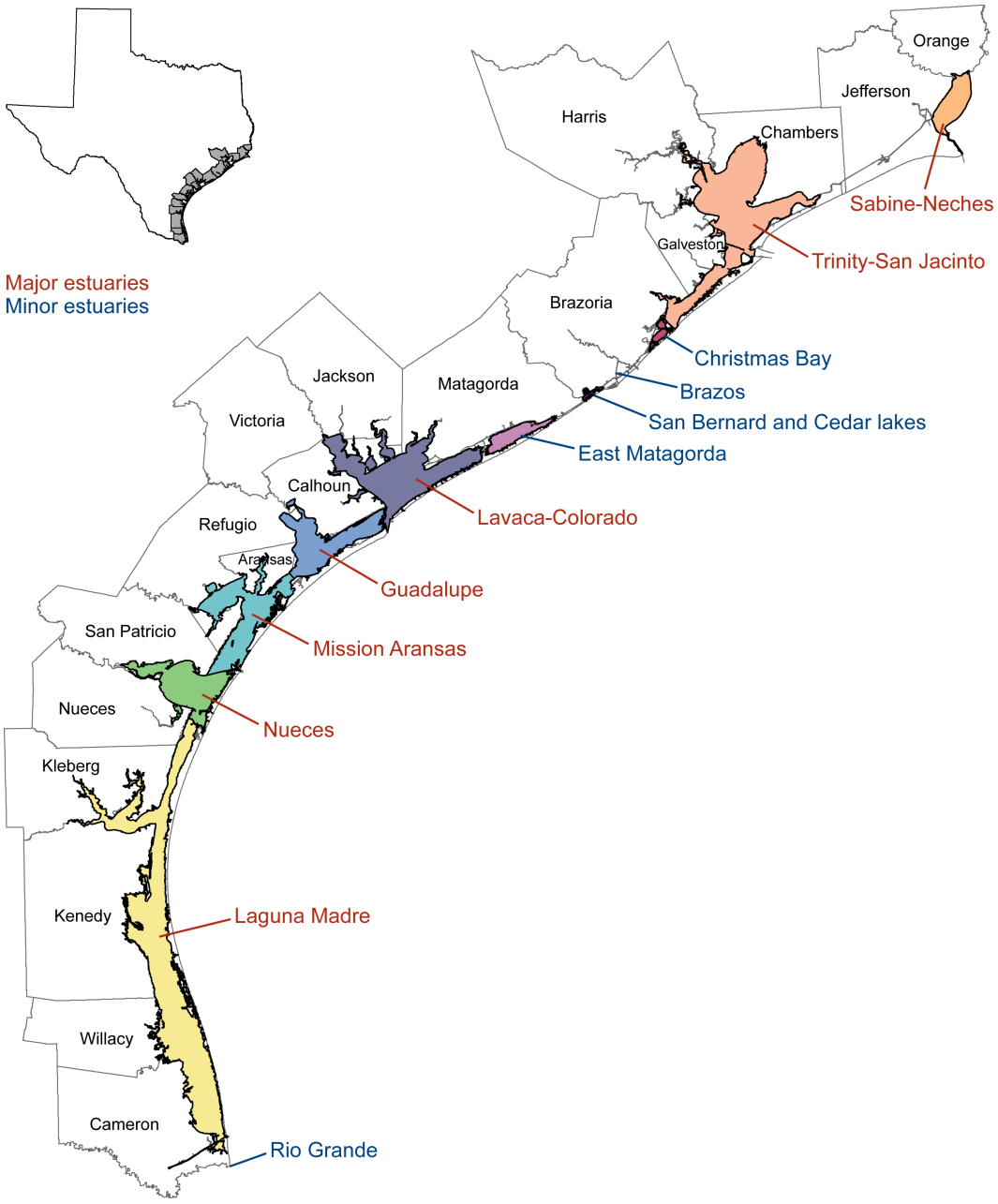

Figure 1.1: Major and Minor Bays and Estuaries of Texas [1], used with permission.

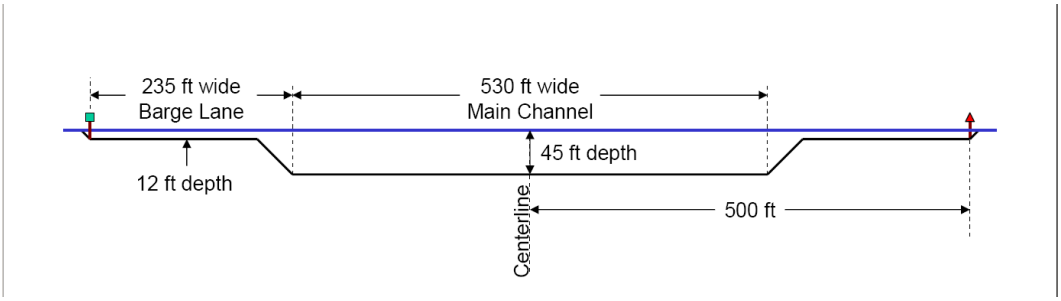

Figure 1.2: Design Dimensions of the Houston Ship Channel

The importance of Coriolis effects in Texas bays is unclear. In section 1.2.2 we show that while Coriolis-driven flow may be significant at a bay wide scale, we expect it to have little effect on the dynamics in and around the ship channel.

In Texas, Corpus Christi Bay, Matagorda Bay and Galveston Bay are good examples of shallow bays enclosed by barrier islands that contain dredged ship channels which are significantly deeper than the rest of the bay. These bays have depths ranging from 2-3 meters for much of their extent and bay widths of well over 16km [17]. The ship channels in these bays are spatially-localized features that can vary from 100-400m wide and are tens of kilometers long. At their centerline they can be over 15m deep. Figure 1.2 shows the design dimensions of the Houston Ship Channel which extends for 80km through Galveston Bay. Galveston Bay has an average depth of 2m and is around 32km wide. Figure 1.3 shows the physical features of Galveston Bay, including its bathymetry, the ship channel and the barrier islands separating it from the Gulf of Mexico. Some average dimensions for some Texas bays and estuaries are shown in Table 1.1.

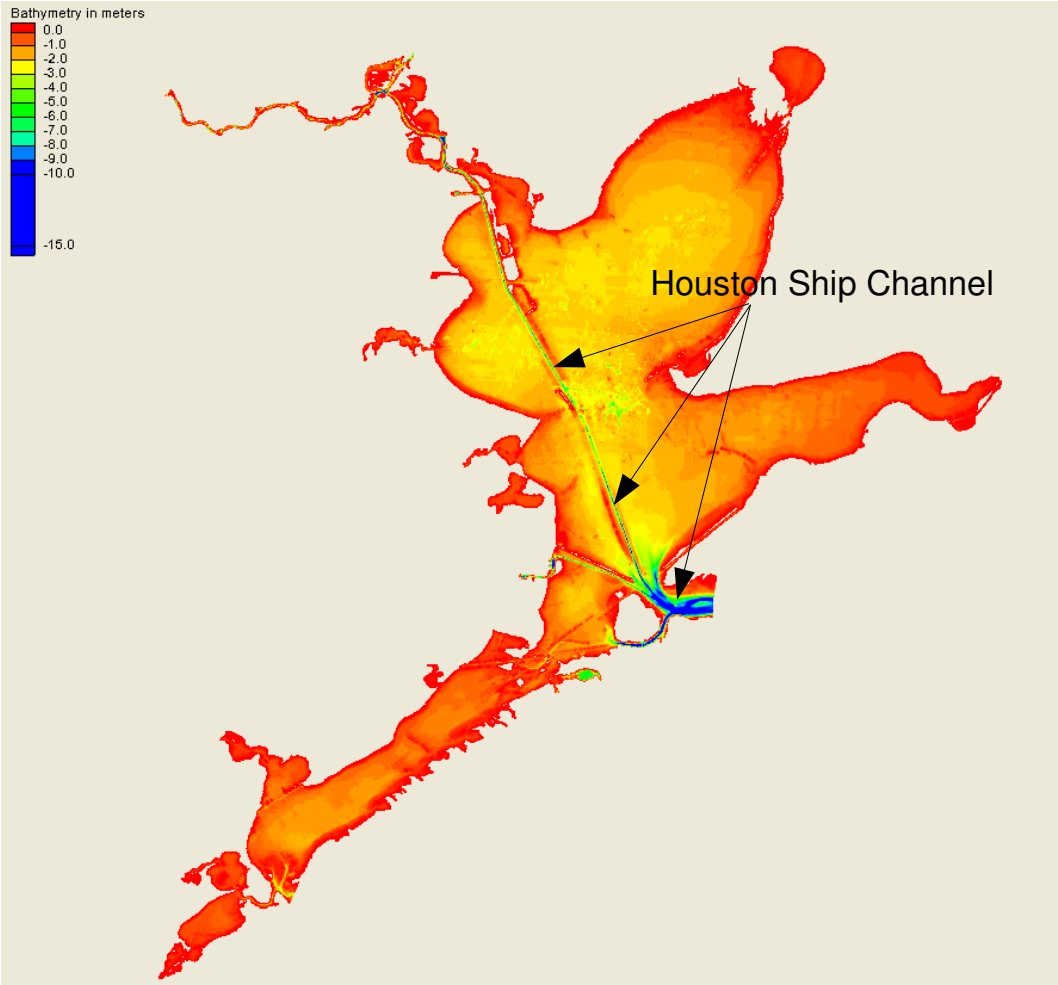

Figure 1.3: Galveston Bay Bathymetry

Bay	Width of Bay (m)	Width of Ship Channel (m)	Depth of Ship Channel (m)	Average Tidal Amplitude (m)	Surface Area (km^2)	Average Daily Freshwater Inflow (m^3/s)	Average Bay Depth (m)
Matagorda Bay	34000	60-90	11.5	0.3	1,100	150	2
Galveston Bay	32000	120-340	10.3-13.7	0.3	1,400	430	2
Corpus Christi Bay	17500	400-360	13.7-15.5	0.22	500	34	3

Table 1.1: Characteristics of various bays in Texas that have dredged navigational channels. Information compiled from [17, 44] and some ad-hoc measurements using GIS mapping software

1.2.2 Underlying Physics

Wind and Tide Forcing

While the current in the bottom layers of flow is driven more by tidal influences, the wind forcing in semi-enclosed basins can affect the circulation patterns of the surface layers. This can cause a bidirectional flow regime in which the surface layers of the water column have a dramatically different circulation pattern from the lower layer of the water column. Indeed, it has been observed that in some estuaries such as the Galician Ria (NW Spain), wind speeds higher than 4 m/s are able to dominate the current near the surface, even against tidal effects. In some cases these winds are able to force water to leave or enter the estuary against the tide [14]. Studies of the correlation of salinity with wind in the Maipo Estuary in central Chile have shown significant wind induced diurnal variability in the salinity regime of the estuary with the lowest coastal salinity being observed daily during the spring and summer at the time that coincided with the end of the onshore phase of the sea breeze [50].

In a shallow bay, we expect to see similar wind-driven effects in the surface current. Flow in a deep, narrow ship channel is expected to be less

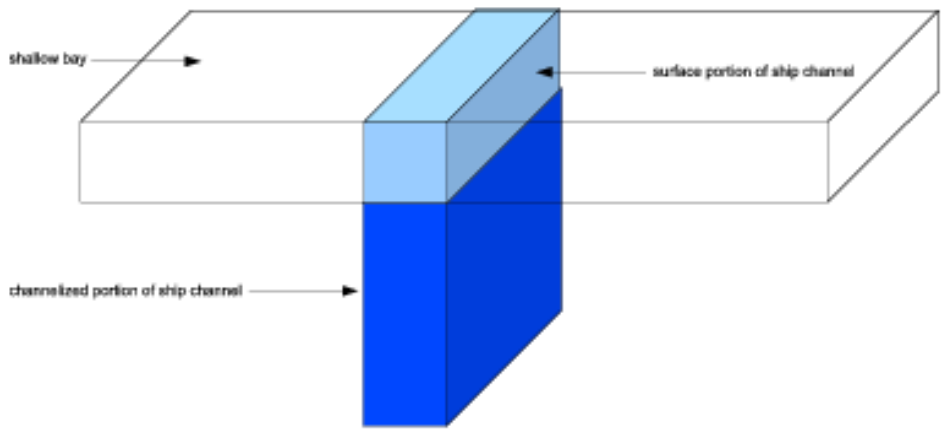

Figure 1.4: Sketch showing relative depths of the channelized part of the ship channel and surface portion. The greater volume of water in the channelized portion causes it to dominate when quantities are vertically averaged

influenced by the wind stresses and driven primarily by tidal influences below the surface current. We expect the tides to push the flow in and out in an oscillatory pattern along the direction of the channel within the deep channel itself. However, since the direction of the wind is often oblique to the direction of the ship channel, a decoupling occurs between the wind-driven current in the upper part of the basin (including the water overlying the ship channel) and a tidally-driven current at the lower depths.

This decoupling of flow regimes has implications for the accurate modeling of the system because the direction of the surface currents is not the same as the direction of currents at deeper depths in the ship channel. Models based on the 2D SWE solve for vertically integrated quantities and are inherently unable to resolve this decoupling; instead, they present a vertically averaged effect. From Table 1.1 we see that in Texas, the ship channel can be upto 5 times deeper than the surrounding bay. Figure 1.4 shows the relative depths of the

channelized part of the ship channel and overlying surface portion. The greater volume of water in the channelized portion causes it to dominate when quantities are vertically averaged. As we will discuss in chapter 2, this causes 2D models of the circulation in the bay to be dominated by the ship channel in an unrealistic manner (see appendix A.5).

Coriolis

To determine the importance of Coriolis, we compute a typical Rossby number for Corpus Christi Bay and the ship channel. Taking the approximate latitude of Corpus Christi Bay to be 29.5 °N and choosing the length scale of the bay to be 17km and the length scale of the ship channel to be 400m, we calculate their Rossby numbers as 0.4 and 17.3 respectively.

Since Coriolis accelerations are significant when Rossby numbers are small [46], these numbers indicate that Coriolis effects may be seen on bay wide circulation. Even so, we expect Coriolis to be a secondary effect when compared to tidally and wind driven flow. At the ship channel scale, we see that the influence of Coriolis is small. So while the Coriolis effect may be important in determining bay wide circulation patterns, it is expected to have little effect on the dynamics in and around the ship channel. For the purpose of our research we focus on wind and tide driven circulation patterns.

Freshwater Inflows

The volume, timing and quality of freshwater inflows into an estuary are important factors contributing to the health of an estuary and the circulation and mixing of water within the estuary [24]. In order to make accurate predictions of bay circulation and transport, the effects of riverine inflows need to be

correctly captured. However, we do not expect the presence of river inflows to change the basic nature of decoupling of the wind driven surface flow and tide driven flow in the deeper ship channel we described earlier in this section. This decoupling and effective ways to model it efficiently is the primary aim of our research. Hence, in this dissertation we do not consider the effect of freshwater inflows to the estuary.

1.2.3 Numerical Modeling of Estuaries

Governing Equations

The physics of the free surface hydrodynamics in estuarine systems are ultimately governed by the full 3D Navier Stokes equations; however, an effort to numerically solve these equations over the large spatial extent of an estuary is computationally expensive. This has led to the development of simplified systems of equations for representing such systems [41]. The most commonly used are the shallow-water equations (SWE). The SWE are used to describe free surface hydrodynamics in vertically well mixed bodies where the horizontal scales are much greater than the fluid depth. The 3D SWE are derived from the incompressible Navier-Stokes equations by approximating the pressure gradient with hydrostatic pressure distribution and by taking account of density variations only in the gravity term (the Boussinesq approximation) [60]. The 2D SWE are obtained by a further step of integrating them along the depth of the fluid body to obtain a depth averaged form of the equations. The SWE are a standard mathematical representation valid for most types of flow encountered in coastal sea, river, and ocean modeling. The SWE have been used to study many physical phenomena of interest, such as storm surges, tidal fluctuations, tsunami waves, forces acting on offshore structures, and contaminant and salin-

ity transport [26]. We present the 3D SWE and laterally averaged version of the 2D SWE in chapter 3. A complete derivation of the SWE is found in [60].

Numerical solution of the SWE is challenging due to the following factors. The SWE are a system of coupled nonlinear conservation laws which need to be solved on complicated physical domains arising from irregular coastlines and islands. The sea bed (bathymetry) is often irregular. Shallow water systems are subjected to the Coriolis force, density gradients, surface wind stress, atmospheric pressure gradients, and tidal potential forces. As a result, flow regimes can vary greatly throughout the domain, from very smooth to high gradients and shock waves. Apart from these physical factors there are additional difficulties arising from the mathematical nature of the SWE. One problem is that numerical solutions of the SWE can be unstable with small oscillations leading to catastrophic instabilities in the model. Also, the coupling between the fluid depth and the horizontal velocity field can lead to spurious spatial oscillations if the numerical algorithms are not chosen with care[3].

In this dissertation, we do not intend to explore the myriad of numerical techniques that have been applied to solve the SWE [60] and to overcome some of these difficulties [2]. Instead we focus on the particular issue of computational grid resolution and its effects on the solution of the model and computational cost when using the SWE to model our shallow bay-ship channel system.

Grid Resolution

The initial step in the development of a numerical model is the discretization of the domain into a computational grid on which the discrete equations will be solved. The motion of water in an estuarine system is characterized by a wide spectrum of space and time scales, due to the coexistence of physical

phenomena of different natures. In developing the computational grid we balance the use of smaller elements sizes needed to resolve certain flow features with the increased computational cost that this entails in terms of the number of unknowns. Section 2.2 presents results that show how dramatically computational cost can increase as we refine the computational grid.

Useful simulations require both an ability to accurately represent the various phenomena which are resolved, and an ability to parameterize those scales of variability which are not resolved. In looking at the effect of the presence of a deep ship channel in a shallow bay, we are presented with two choices: We could use a computational grid with grid elements small enough to capture this localized physical feature, or we could somehow represent the net effect of the ship channel on the rest of the system. Our research focuses on the second choice. To justify this, we explore some of the problems inherent in the first approach.

For the first approach, the horizontal grid must represent the ship channel with sufficient grid cells to resolve the physical processes. As shown in Table 1.1, Texas Bays are 2 orders of magnitude wider than the ship channels present in them. It is shown in chapter 2 that the grid cell size required to resolve the ship channel physics leads to a model with so many grid cells that it becomes impractical for common engineering and management use.

In the vertical dimension, the simplest models are based on the 2D depth averaged form of the SWE which are equivalent to the 3D SWE with a single vertical layer. Although the use of 2D shallow water models can be justified for applications involving calculations of depth-integrated transport and water level changes, such models are unsuited for simulations of three-dimensional water motion near river and inlet mouths where significant salinity (density)

fronts exist [49]. Horizontal salinity (density) gradients in these regions induce cross-front circulation and support wind-driven motions with characteristics different from those predicted by 2D shallow water models. The lack of vertical variations of water circulation may lead to unrealistic estimates of horizontal transport of vertically stratified quantities such as pollutants, nutrients, biota and general flotsam [67]. The 2D representation is also (by definition) unable to capture vertical gradients in the horizontal flow caused by the steep bathymetric gradient between the bay and the ship channel [45].

Models based on the 3D SWE allow representation of both vertical gradients in the horizontal flow field and vertical density stratification. The trade off is higher computational cost as we add more vertical layers to the model. We will show in appendix A that this computational cost can be prohibitive at the resolutions required to accurately capture the flow features.

In our wind-forced system, insufficient vertical grid resolution can cause the presence of a ship channel to dominate bay wide circulation patterns in an unrealistic manner. As we see in some of the numerical experiments in appendix A, in a bay system with a deep channel that is forced by both tides and wind, insufficient vertical grid resolution can lead to dramatically different circulation patterns than are obtained by using a fine resolution model.

In general, applying sufficient horizontal and vertical grid resolution along with a reasonable turbulence closure model should result in an accurate simulation. Sufficient resolution is typically defined by a grid resolution test [55], wherein modeling is conducted on a grid finer than required to show that the model solution is invariant with further grid refinement. However, in the commercial and state government sectors computational resources are often limited. Rarely is there the capability to conduct a detailed grid resolution

study, and models are run at the finest practical resolution. Thus, the present work focuses on developing methods that are practical at a coarse grid resolution where the detailed flow in the ship channel may not be fully resolved. Chapter 2 explores the importance of grid resolution in greater detail.

Parameterization of vertical turbulent mixing

Recognizing that the parameterization of turbulent vertical mixing remains an open question in coastal modeling, and that there are many approaches of widely varying complexity that have been proposed in the literature, we will not make choice of turbulence closure model a focus of this research. For a discussion of various turbulent closure models and their comparative application to estuarine problems see [25, 32, 33, 56, 59, 62].

In this research, the initial work used a constant eddy viscosity that is independent of vertical position. Other turbulence closure schemes were tested but not used for reasons explored further in section 5.3

1.2.4 Domain Decomposition and Model Coupling

Theory

Domain decomposition has historically been done for a variety of different reasons. The advent of cheap high performance computing clusters has driven research into decomposition techniques that take into account load balancing and efficient partition of the problem among numerous processors. These techniques have been used to conduct large scale simulations that encompass the entire eastern seaboard and Gulf of Mexico [65]. In our research we are more interested in the other applications of domain decomposition: those that are driven by differing physics or physical features in the domain. In these al-

ternate applications, different mathematical models can be used simultaneously and the most complex ones are solved only where it is strictly necessary; that is, on restricted regions of the domain.

As an example, consider a typical aerodynamics problem: the simulation of the flow field around an airfoil where the equations for compressible and incompressible fluids are merged [16, 52, 53]. The Navier-Stokes equations are solved in the boundary layer and in the downstream wake, the Euler equations in the surrounding region where the shock may develop, and the full potential equation in the far field where the flow is irrotational. Accordingly the domain is decomposed into a number of subdomains with differing physics and the appropriate transmission conditions based on the physical properties [12].

In modeling free surface flows, much work has been done on using multimodel approaches for river-estuary systems [41]. These coupled strategies divide the river-estuary system into different zones and apply different models to each zone [4, 40, 41]. Miglio *et al* [42] discusses an application in which the 2D and 1D St. Venant equations are coupled at a river bifurcation. Dallimore *et al* [13] present a multimodel approach in which a separate underflow model is coupled to a 3D estuary and lake model. The underflow equations are solved on a 2D grid underlying the 3D model grid. The underflow model entrains ambient water whose properties are given by the fluid properties of the bottom boundary cells in the 3D model. This approach allows improved representation of underflow effects by reducing numerical convective entrainment.

In general, the different models may involve different physics, they may be dimensionally heterogeneous or they may be both physically and dimensionally heterogeneous. A reduction in computational expense is obtained by using simpler physics and/or a reduced dimension model in the submodels. The aero-

dynamics example is a dimensionally homogeneous, physically heterogeneous coupling wherein the submodels invoke different physical processes. A reduction of the computational cost is provided by ensuring that the most complex physical model is solved on a reduced zone of the domain. The work by Miglio is an example of dimensionally heterogeneous, physically homogeneous coupling. In this case the submodels have the same underlying physics, but the submodels have different dimensionality. Reduction in dimensionality can considerably reduce the computational cost of the approximation procedure. The work by Dallimore is an example that uses both types of coupling, reducing the dimensionality from 3D in the lake model to 2D in the underflow model while at the same time modeling different physics in each domain. In each case, the increased efficiency of the multimodel approach needs to be balanced with the complexity of implementing interface conditions and errors that may be introduced through the interface.

From a mathematical standpoint, the multimodel approach relies on establishing a suitable set of matching conditions for variables at the grid interface separating the two sub regions[16]. Defining these interface conditions turns out to be an easy or a hard task depending on the level of physical and dimensional heterogeneity of of the involved models [41]. These multimodel approaches can only be justified in those situations where the difference between the solution obtained using this method and the solution using the full 3D solver with sufficient resolution is acceptably small relative to the physical scales of interest.

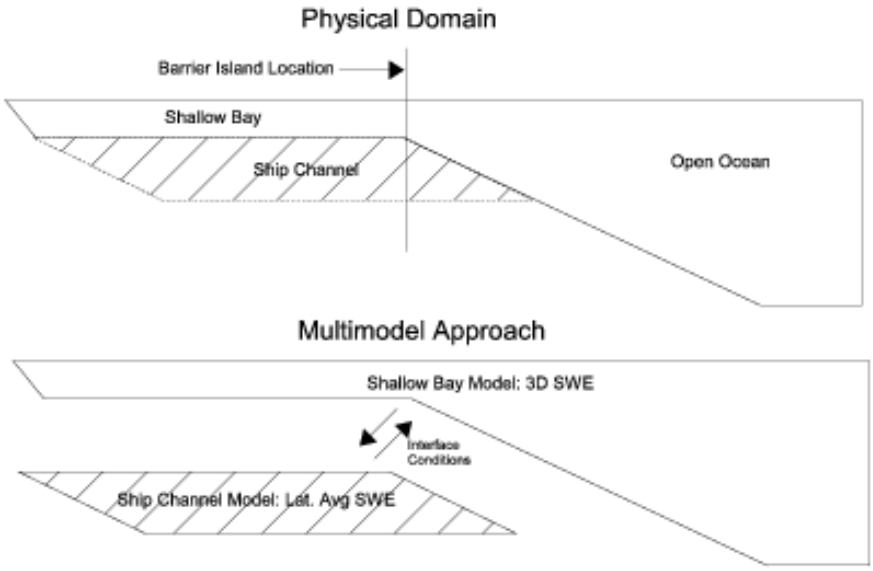

Figure 1.5: Schematic of the multimodel strategy. A vertical section along the axis of the ship channel is shown

Application

For our problem, we note that the basic physics governing the flow in the ship channel is the same as in the surrounding bay. We will see in chapter 2 that flow within the subsurface portion of the ship channel is oscillatory in nature while flow in the surface layers of the bay is wind driven. The absence of significant lateral flow within the subsurface portion of the ship channel coupled with the narrowness of the ship channel makes it reasonable to use a dimensionally lower order model to represent it. Based on this recognition of distinct flow regimes within the system, we choose a multimodel approach that uses a 3D model for the bay and horizontally contiguous water above the ship channel, while the dredged portion of the ship channel deeper than the adjacent bay will be modeled using a 2D laterally averaged model. The mathematical basis for this multimodel approach is presented in chapter 3. Section 2.5 discusses

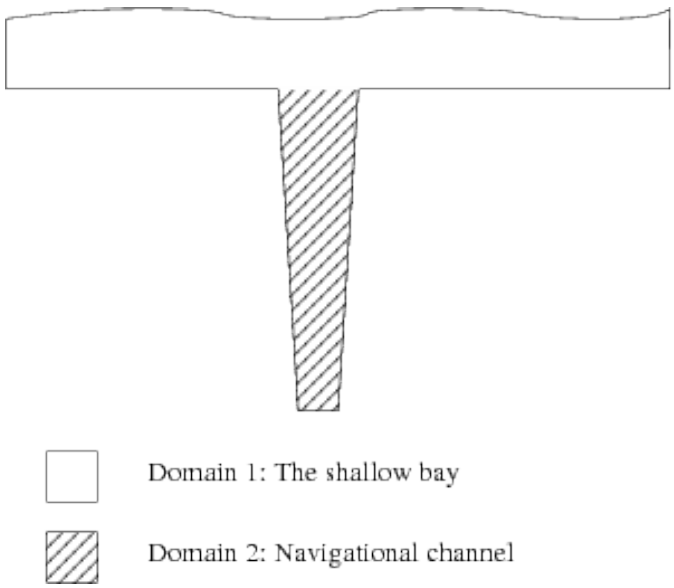

Figure 1.6: Subdomains in the multimodel strategy. A vertical section perpendicular to the axis of the ship channel is shown

in more detail the reasoning behind this choice of subdomains and multimodel strategy.

1.3 Reseach Objectives and Approach

The primary objective of our research is to develop a practical tool to model estuarine systems consisting of a shallow bay containing a ship channel separated from the ocean by barrier islands. We accomplish this using a multi-model approach that uses a 3D shallow bay model for the bay and horizontally contiguous water above the ship channel coupled with a 2D laterally averaged ship channel model that simulates the flow in the dredged portion of the ship channel deeper than the adjacent bay.

The development of the multimodel approach required a choice of models for the shallow bay and ship channel as well as appropriate interface conditions. For the shallow bay model, we used an off-the shelf model (SELFE [71]), that is already in use with various federal and state agencies and universities [69] and is being used by the Texas Water Development Board for modeling Texas estuaries. SELFE is a recently developed, unstructured-grid hydrodynamic circulation model designed for the effective simulation of 3-D baroclinic circulation across river-to-ocean scales. It uses a semi-implicit finite-element Eulerian-Lagrangian algorithm to solve the shallow water equations and is written to realistically address a wide-range of physical processes, including atmospheric, oceanic, and riverine forcings. The numerical algorithm is high-order, stable, and computationally efficient. Modifications will be made to the implementation of the bottom boundary conditions in SELFE to enable coupling of this model to the ship channel model.

For the subsurface portion of the ship channel, we developed a new finite difference model based on a 2D laterally averaged form of the SWE that we will henceforth refer to as the Laterally Averaged Channel Model (LACM). The mathematical basis for this model and details of its implementation can be found in chapters 3 and 4.

In order to achieve the primary goal of this project, we took several steps to develop and validate our approach.

1. Quantifying the effect of grid resolution on computational cost for a typical Texas embayment.

2. Quantifying the dependence of the numerical solution on grid resolution.

3. Exploring the relative importance of wind driven circulation and tidal circulation in a shallow estuarine system containing a ship channel.

4. Formulating a mathematical basis for coupling a 3D shallow bay model to a 2D laterally averaged model of the ship channel.

5. Implementing, verifying and validating this multimodel approach.

6. Showing that the multimodel approach can achieve equal or better accuracy than a medium resolution 3D SWE model at significantly lower computational cost.

The rest of this dissertation is outlined as follows: In chapter 2, we present analyses and numerical studies that explore the effect of grid resolution on wind and tidally driven circulation in a shallow bay-ship channel model. In chapter 3, we present the mathematical basis behind the 3D SWE and the laterally averaged SWE that are the basis of our multi-model approach. We also derive interface conditions and formulate a coupling strategy. In chapter 4, we outline the steps that were taken to implement and validate the coupled approach. In chapter 5 we present results from numerical runs used to validate our approach. Finally in chapter 6 we discuss what we learned from our research and make recommendations for future work.

Chapter 2

Resolution Issues in the Numerical Modeling of a Shallow Bay - Ship Channel System

2.1 Introduction

The scales necessary for an accurate numerical model of a shallow bay-ship channel system are not uniform over the entire physical domain. Hence, the numerical modeling of such systems will always involve compromises involving the resolution required to resolve the scales of different processes present and the numerical cost of that resolution. Even with advances in computer speed and memory capacity there still exists a practical limit for the resolution of any model. This limit is even more evident when we restrict ourselves to models that run in serial on a single processor. Increasing a model's spatial resolution typically increases the model's need for computer storage space, run time memory and computational time. The increase in computational time results not only from the larger number of computational nodes and hence unknowns to be solved for, but also from the necessity of decreasing the model time step to satisfy various well known stability criteria.

In this chapter, we explore some of the issues caused by insufficient spatial resolution in the horizontal and vertical. We discuss how these issues affect the modeling of our shallow bay - ship channel system and how we expect our multimodel approach to improve our ability to simulate these type of systems.

2.2 Computational Time

While it is true that fine resolution 3D models require hefty resources in terms of disk storage and computer memory, these resources are relatively cheap and readily available. The limiting factor for practical modeling is often computer time. Recently, increases in the speed of computer chips have started to taper off, and the trend is toward multi-core chips and parallel solutions. This trend has in effect put an upper ceiling on the resolution that can be used in conventional non-parallel models.

To demonstrate that using a fine resolution in the horizontal and vertical is computationally expensive a series of simulations were conducted with the ELCIRC model ([70]) on an Intel Xeon 5160 3.00GHz processor with 2GB of memory. Full details of these simulations are presented in Appendix A. Here, we summarize the results by presenting the increase in computational cost when the vertical and horizontal resolutions are increased. A 15 day time period was simulated. As we refine horizontally by increasing the number of elements across a 320m ship channel from 1 to 32, the number of elements in the grid increases from 3255 to 246852 (see Figure 2.1c) and the CPU time taken by the model increases from 3.5 minutes to 22 hours (see Figure 2.1a). The increase in computational cost is a little lower than second order.

Increasing the vertical resolution from 1 vertical layer to 128 layers while holding the number of horizontal elements at 8 increases the CPU time taken by the model from 72 minutes to 30.5 hours (see figure 2.1b). The computational cost increases linearly.

Extrapolating from figures 2.1a and 2.1b, we estimate that to run a 15 day simulation using a grid with 128 vertical layers and 32 elements across the

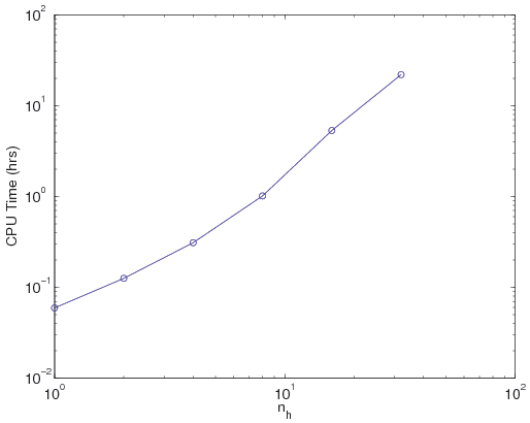

(a) Effect of increased horizontal resolution across ship channel on computational cost at $n_v = 4$.

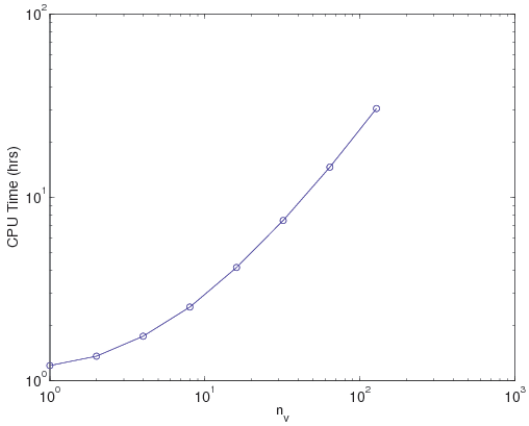

(b) Effect of increased vertical resolution on computational cost at $n_h = 8$.

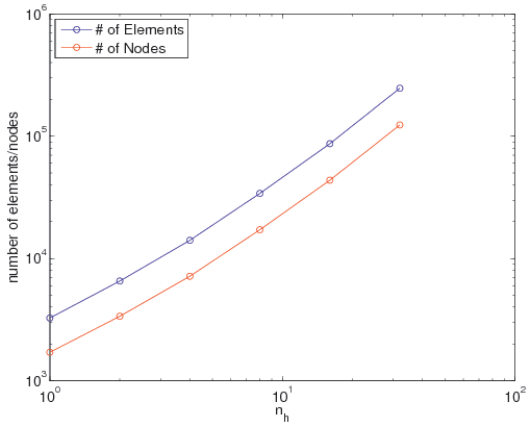

(c) Effect of increased horizontal resolution on number of elements and nodes in the computational grid

Figure 2.1: Effect of grid resolution on problem size and computational cost. n_h is the number of elements across the ship channel. n_v is the number of vertical layers used.

ship channel would take approximately 30 days. An initial attempt to conduct a model run at this grid resolution met with failure due to machine limitations.

2.3 Horizontal Resolution

2.3.1 Importance

Accurate representation of channels and sills that connect different bodies of water within a model domain is critical to obtaining meaningful simulations. When channels are represented with minimal resolution, it is difficult to simultaneously compute the appropriate water depth and cross-sectional area correctly. This leads to errors in phase speed and/or transport [21]. As an example, Kliem and Greenberg [27] found that, in the Canadian Arctic Archipelago, the smaller channels make a significant contribution to the transport from the Arctic to the North Atlantic and hence need to be properly resolved in the computational grid.

In our research we consider a shallow bay connected to the ocean through a narrow ship channel. The importance of resolution in such a system is illustrated in efforts to model the Maracaibo System in Venezuela, which is an example of a system where partially enclosed seas are linked to the ocean through restricted channels. The Maracaibo lake is joined to the Gulf of Venezuela through a narrow channel that runs through Tablazo Bay and the Maracaibo Strait. This originally narrow channel has been dredged to a depth of 14m and is 200-300m wide [31]. Molines et al. [43] modeled tides in this system, focusing on issues relating to grid orientation and transport through the narrow channels at low resolutions. Lynch et al. [37] established the relevance of the explicit inclusion and resolution of the channels connecting the Gulf by demonstrating that when the subdomains of the Gulf, the Bay and the Lake were decoupled into sepa-

rate subdomains, the model produced a result for each subdomain that differed greatly from the result obtained when the system was run as a single unit. Other studies by Lynch and Werner [35, 36] and Lynch et al. [37] considered the effects of tidal and baroclinic processes in their tidal model. The researchers were able to concentrate high (and variable) resolution through the narrow straits, and accurately model the system's tidal response. More recently, Laval et al [31] studied the effects of grid resolution on modeling volume and salt flux. They found significant differences in exchange between the water bodies when using different resolutions for the channel. The results of their study indicated that the more rapid the variation in bathymetry and the greater the tidal velocity, the greater the differences in fluxes.

In another physically similar situation in the Bras dÓr Lakes, Nova Scotia, Canada, Petrie [47] and Petrie and Bugden [48] have demonstrated that the frictional effects of the constricted channels effectively damp the diurnal and semi-diurnal tidal frequencies, but the longer period motions, mostly meteorological, originating outside the Lakes, propagate into the system largely unaffected.

Greenberg *et al* [21] contains an excellent discussion of the resolution issues encountered in the numerical modeling of oceanic and coastal circulation. It includes a section on the importance of the resolution of channels and sills from which much of this material is taken.

2.3.2 Representation of Channel Cross Section

As shown by previous researchers, horizontal resolution in channels can have a significant effect on the volume and salt flux through the channel. In our research we are looking at enclosed shallow bay systems connected to the

ocean by a deep ship channel. In this type of system, the pass where the ship channel cuts across the barrier island is the primary source of salt water in the bay. Accurately accounting for the salt flux through this pass becomes a priority in modeling this type of system

As the level of grid resolution is increased, the level of physical parameter resolution can change. The scale of definition of bathymetry depends on the grid resolution [21, 34, 55]. As the grid is refined, we can either interpolate the coarsely resolved bathymetry from the coarse grid onto the fine grid or we can increase the resolution of the bathymetry by re-interpolating actual bathymetry onto the fine grid. If the first technique is used, the channel cross section will continue to be misrepresented with the associated errors in fluxes. Using the second technique can cause new features to appear in the bathymetry as the grid becomes fine enough to resolve them, causing the channel cross section to vary with grid resolution until a fine enough grid is used. This confounds efforts to conduct horizontal grid resolution studies. Westerink and Roach [64] notes that under resolution in the grid leads to over predictions in the response while under resolution in the bathymetry leads to under predictions in response. Thus under resolution in the grid and the inherent under resolution in the bathymetry can lead to a cancellation of errors which corresponds to a cancellation of truncation errors from the grid and bathymetric terms. This type of truncation error cancellation can lead to effective convergence rates being lower than formal convergence rates. We have seen this effect in convergence studies done with ELCIRC where the error can sometimes actually increase as the grid is refined from one level to the next.

In Section A.4, we present a horizontal grid convergence study that indicates that a horizontal resolution of 8 elements across a 320m wide deep

ship channel was sufficient to accurately capture the flow. In this study, the bathymetry was held constant at the average depth of 9m across the ship channel rather than using the actual variable bathymetry (4m to 15m) that had been defined for the channel. Freezing the parameter definition can aid in *code verification* but is not helpful in error estimation [64]. Hence, while the 8 elements may be sufficient from a numerical point of view this conclusion may be inaccurate in answering the question of whether eight elements is sufficient to capture all the variations in the bathymetry across the channel and the associated changes in fluxes.

2.3.3 Maintaining Channel Connectivity

The vast majority of existing bathymetric data, particularly in estuarine systems, have been collected using a single beam echo sounder. In order to use this type of depth data for numerical modeling it becomes necessary to interpolate the data on to the computational grid used by the model. Several interpolation methods exist and produce good results over areas smooth, uniformly trending water depths. However, when applied to estuarine bathymetry, consisting of mudflats crossed by a narrow, relatively deep channel, prominent interpolation artifacts are produced [8, 9]. Even in cases where high resolution multi-beam surveys exist artifacts can be produced by the alignment and position of the usually lower resolution computational grid.

Burroughs [9] gives examples of these artifacts, appearing as ridges across the deep channel, when single beam echo sounder data for the Truro River, in Southwest Cornwall, UK, were interpolated to a model grid. A similar effect can be seen in the modeling of the Keith Lake system near Port Arthur [51], TX where the initial grid generation caused an artificial ridge to form

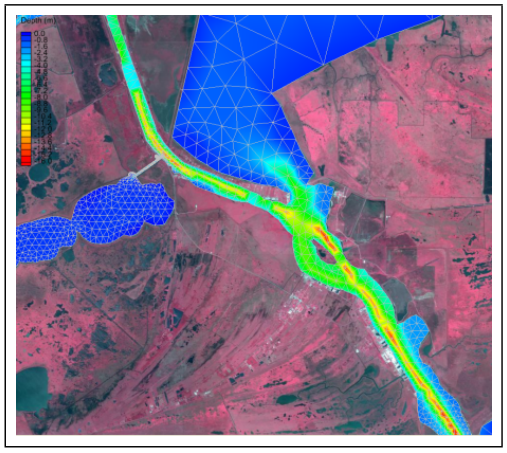

(a) Low Resolution Grid containing artificial ridges across the Sabine-Neches Waterway

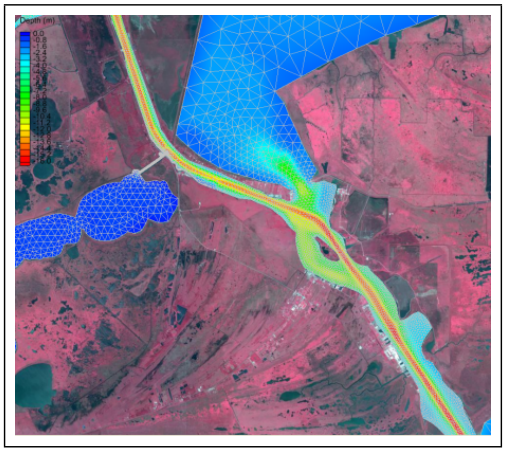

(b) High Resolution Grid that represents the Sabine-Neches Waterway bathymetry more accurately

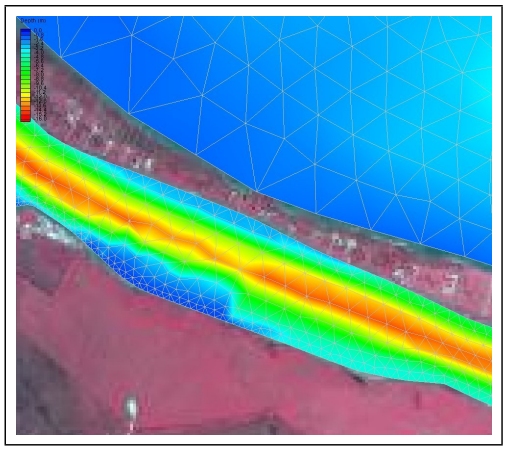

(c) Zoomed in portion of Medium Resolution Grid showing artificial pinching of the channel

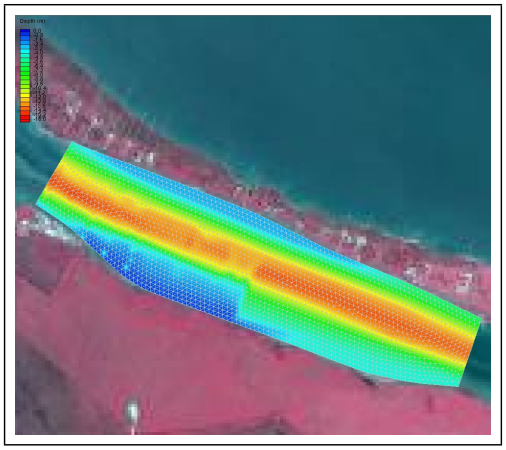

(d) Zoomed in portion of High Resolution Grid showing accurately resolved bathymetry

Figure 2.2: Effect of grid resolution and alignment on channel connectivity. Example from modeling studies in the Keith Lake System near Port Arthur,TX.

across the Sabine-Neches Waterway (see Figure 2.2). Figures 2.2a and 2.2b shows the difference grid resolution and alignment made in the way the grid represents the Sabine-Neches Waterway while figure 2.2c shows that even using higher resolution if care is not taken the channel can be misrepresented based on the exact locations of the element nodes.

Merwade *et al.* [39] contains of discussion and comparison of various anisotropic interpolation techniques for river channels aimed at mitigating some of these issues. However, this analysis is based on generating a representative bathymetry and not so much on maintaining channel connectivity, which is arguably more important in an estuarine system where the presence of an artificial ridge could effect transport, stratification and circulation patterns. While there have been other efforts to maintain channel connectivity by using methods like zonal inverse distance weighting [8, 9] and transformation to flow oriented coordinate systems [20], the fact remains that care must be taken during the generation of the computational grid and the interpolation of bathymetry to that grid.

2.4 Vertical Resolution

2.4.1 Importance

Simulating vertical processes in coastal and oceanic systems requires numerical discretization in the vertical. Over the years, many types of vertical discretizations have been used, the main ones being z coordinate models, terrain following sigma transformation models, isopycnal coordinate models and hybrids of the various schemes. Each of these discretization techniques has its particular advantages and also its own problems. For a discussion of the various vertical discretizations and a summary of their strengths and weaknesses look

at [21]. Here we do not explore these issues, rather we look at the more basic effect insufficient vertical resolution has on circulation in the presence of the ship channel.

Ideally, a 3D circulation model should have enough vertical levels to represent the physics of the surface and bottom boundary layers where strong gradients are found with coarser resolution in between. The present state-of-the-art ocean models with 40 to 50 levels are actually still behind these basic requirements [21]. The level of vertical resolution required in a shallow estuary system with a ship channel is less clear. Estuarine systems often have complex bathymetry and shorelines necessitating higher horizontal resolution, which can reduce the resources available for increased vertical resolution. Applications to systems found in literature typically use 1 (i.e. 2D models) to 10 vertical layers. The NOAA nowcast/forecast system for Galveston Bay and the Houston Ship Channel uses 6 layers [54]. The choice of vertical resolution seems to be driven more by computational limitations than by rigorous study of needed resolution.

2.4.2 Flow Decoupling

In appendix A.5 we qualitatively show that circulation patterns are dramatically different when the model is under resolved in the vertical. We show that in a shallow estuary, the presence of the ship channel along with the winds and tides can cause the flow regime to be three dimensional in nature. Flow within the channel is constrained in an along channel direction. Water above the channel is not constrained in this manner and is free to move in any direction. When a wind shear exists oblique to the channel direction, the result is that the the upper layers move in the wind direction, the lower layers above the channel move in the opposite direction, and the channel flow driven by tides

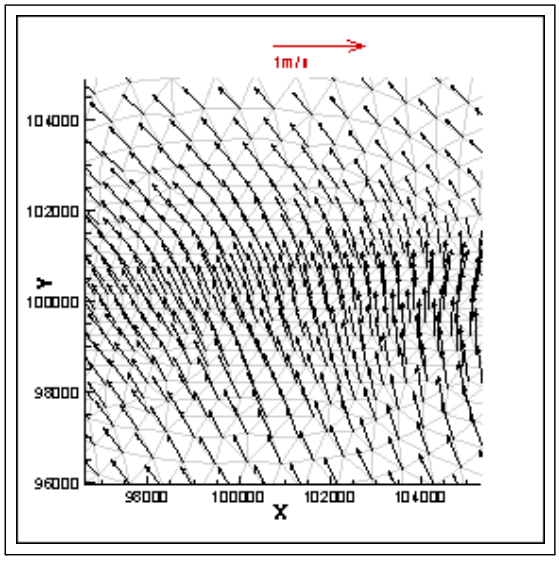

(a) Surface Circulation with n_v=32

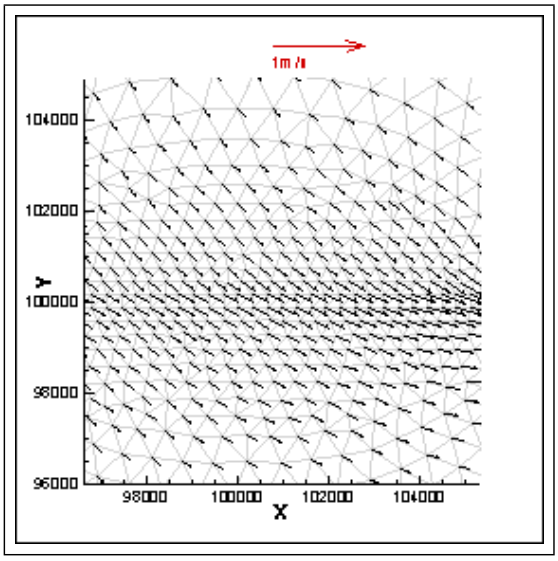

(b) Shallow Bay Bottom Circulation with n_v=32

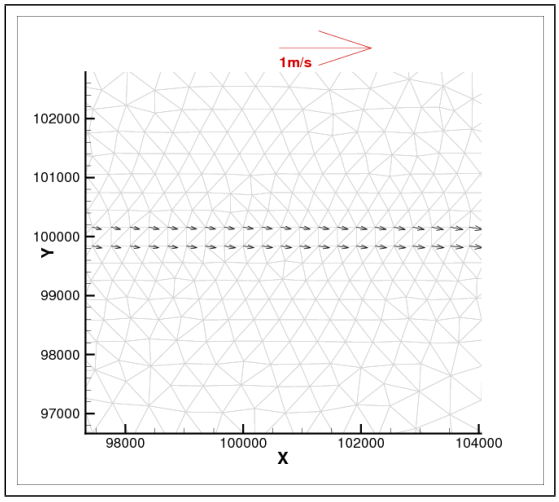

(c) Ship Channel Bottom Circulation with n_v=32

Figure 2.3: Comparison of surface and bottom layer circulation patterns at vertical grid resolution n_v=32 with n_h=1. n_v and n_h are the number of vertical layers and number of elements across the channel respectively. The shallow bay bottom layer shown is just above the top of the ship channel. Model run forced with ideal diurnal wind and semi diurnal tide. Constant eddy viscosity of 10^{-4} used for turbulence closure

moves in the along channel direction. This bidirectional flow is demonstrated qualitatively in the simulations conducted with ELCIRC (see appendix A.5 for complete details) on a idealized bay domain in the presence of wind and tides. The bidirectional nature of the flow field in the shallow bay can be seen in figure 2.3. The surface circulation and the bay bottom circulation are shown in the area close to the center of the shallow bay. The surface velocity field is driven along the direction of the wind and is fairly strong (figure 2.3a). The bottom velocity field is in the reverse direction and is weaker(figure 2.3b). The flow inside the portion of the ship channel below the bay depth is oscillatory and parallel to its walls (figure 2.3c).

2.5 Advantages of Multimodel Approach

2.5.1 Discussion

In summary, based on the arguments presented in this chapter, we make the following statements about the modeling of a shallow bay-ship channel driven by wind and tidal forces.

- Using a high resolution in the horizontal and vertical is computationally expensive.
- Insufficient horizontal resolution causes a misrepresentation of the channel cross section which leads to errors in volume and salt fluxes.
- Misalignment of grid elements and physical channel can cause channel connectivity to be misrepresented in the model.
- Insufficient vertical resolution causes a misrepresentation of along channel and cross channel fluxes.

- The flow regime is essentially 3D in nature.
- A single layer (or 2D) model is inadequate to model such systems.

We are essentially faced with three issues. First, fluxes and velocities through the channel can be modeled incorrectly due to inaccurate representation of the channel depth and cross section. Second, unless care is taken to align the computational grid with the physical ship channel, channel connectivity may be misrepresented. Third, 2D and low resolution 3D models are unable to capture the decoupled flow regimes present in the system.

The coupled model approach we propose is able to avoid these problems because :

- Using a laterally averaged model for the channel can represent bathymetry much more accurately.
- Channel connectivity can be enforced without the need for careful grid alignment.
- This technique naturally allows for the flow decoupling to be represented.
- This technique reduces the computer time in two ways : 1) It reduces the resolution required in the vertical and horizontal for the 3D shallow bay model. 2) It uses a simpler 2D model for the subsurface ship channel.

In the next chapter we describe the mathematical basis for our coupled model approach and in chapter 4 we detail its implementation.

Chapter 3

Mathematical Formulation of the Multimodel Approach

3.1 Introduction

The motion of water in an estuary is ultimately governed by the full 3D Navier Stokes equations. The shallow bay-ship channel system under consideration could be solved by using these equations. However, solving a 3D Navier Stokes problem is computationally more demanding than solving the 3D SWE for two reasons. First, it is necessary to solve a 3D Poisson equation for the pressure distribution in each time step; in the SWE case this is replaced by a 2D problem. Secondly, it is not clear whether elongated grid cells (high aspect ratio $\delta x/\delta z$) such as are usually used in estuarine modeling can be used in a Navier-Stokes code for accuracy reasons [60]. A Navier-Stokes solver would hence require more grid points and thus be more computationally demanding.

The models based on the simpler 3D SWE have been widely used for modeling estuarine systems [10, 60, 65, 70]. In chapter 2 we have discussed how the 3D SWE are unable to accurately capture the flow regime in a shallow bay ship channel system unless very fine grid resolution is used.

In this chapter, we explain the reasoning behind our multimodel approach, and we present the formulation of the governing equations that will be used on each subdomain. The 3D SWE will be used in the shallow bay subdomain and the laterally averaged 2DV SWE will be used in the ship channel

subdomain. We end with the mathematical formulation of interface conditions that will be used to couple these models. We limit our research to developing a multimodel approach that solves for the flow field and free surface elevation in our domain. Hence, we do not present the transport equations in this formulation.

3.2 Nomenclature

t	time
u, v, w	cartesian velocity components
$\overline{u}, \overline{v}, \overline{w}$	laterally averaged cartesian velocity components
u', v', w'	deviation of cartesian velocity components from laterally averaged velocity com
x, y, z	cartesian spatial coordinates
$\overline{n}$	overbar operator represents lateral averaging
p_a	atmospheric pressure
b, c	subscripts representing the bay model and channel model respectively.
ρ_o	density of water at STP
g	acceleration due to gravity
f	body forces
ν^v, ν^h	vertical and horizontal viscosity
τ_{sx}, τ_{sy}	bottom shear stresses
$\tau_{cx'}, \tau_{bx'}$	interface shear stresses in the along channel direction
η	free surface elevation
C_f	coefficient of bottom friction
ξ	width of channel
$\Omega, \partial\Omega$	entire bounded domain and its boundary
$\Omega_b, \partial\Omega_b$	bounded bay domain and its boundary
$\Omega_c, \partial\Omega_c$	bounded channel domain and its boundary
Γ	interface between Ω_b and Ω_c

3.3 Multimodel Approach

The NOAA nowcast/forcast system for Galveston Bay is an example of a coupled model approach. It uses a coarse resolution bay model to provide boundary conditions for a fine resolution spatially-localized ship channel model to obtain more accurate velocities and elevations within the Houston Ship Channel [54]. This application of model coupling is unidirectional and the results from the fine resolution Houston Ship Channel model are not propagated back to the bay model. In our application this kind of coupling is less than ideal since we are interested in the effect of the presence of the ship channel on bay wide circulation and transport. Hence a two way coupling is required. We are also interested in greatly reducing the computational cost of the model.

The development of a strategy for modeling the shallow bay-ship channel system under the influence of wind and tide requires some exploration of the flow patterns that dominate the system. Here we reiterate some of the points presented in chapter 2 and some of the findings of our numerical studies in appendix A.

We note that the development of distinct flow regimes can be seen within the system. A examination of the high resolution model results (see figure 2.3) shows a mainly wind-driven bi-directional circulation forming in the surface layers of the bay. The flow in the sub-surface portion of the ship channel is tide-driven, mainly oscillatory and parallel to the walls of the channel. The flow in the ship channel has little effect on the surface layers. It has a stronger influence on the lower layers of the bay especially those that are in the vicinity of the channel.

Considering the presence of these dissimilar flow regimes confined to separate sections of the physical domain, we choose to decompose the entire

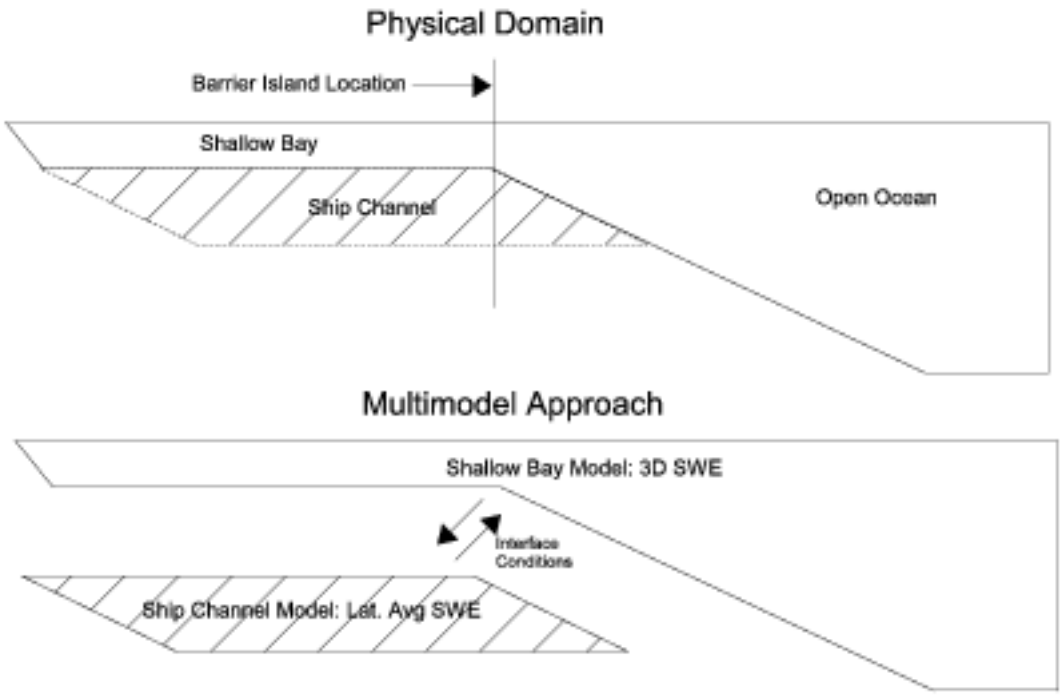

Figure 3.1: Schematic of the multimodel strategy

domain into two subdomains and to model these flow regimes separately. We choose to decompose the domain into a bay subdomain and a sub-surface ship channel subdomain as shown in figure 3.1.

3.3.1 Shallow Bay Model

We choose to use the 3D SWE to model the shallow bay subdomain. While a 2D depth averaged SWE could be used to model the bay subdomain at reduced computational cost, it may not be the most appropriate choice. In the shallow bay, wind forcing causes a bidirectional flow with the surface layers moving in the direction of the wind stress and the lower layers moving in the opposite direction (see figure 2.3). Density differences can also induce a 3D

flow structure, and it is known that the ship channel can influence salinity intrusion and stratification [5, 28]. Work by Pandoe *et al*[45] on 3D simulations of an idealized ship channel in a rectangular bay, shows that near the sloping bank of a ship channel with a one-third gradient, the vertical velocity becomes important. They show that these vertical velocities can be important for accurate modeling of sediment movement when combined with deposition and suspension processes. It is this essentially 3D nature of the flow that makes the 3D SWE a good choice of governing equations for the bay model.

3.3.2 Ship Channel Model

We choose a laterally averaged form of the SWE to model the ship channel subdomain. The sub-surface portion of the ship channel is a narrow, long canyon with steep walls. The physical dimensions of the ship channel and the oscillatory nature of the flow present between its walls allow us to neglect variations in the lateral direction without much loss of accuracy. Studies have shown that stratification can happen in the ship channel [5]. The 2DV SWE model allows us to continue to take into account any vertically varying features in the flow regime within the ship channel while still reducing the computational cost compared to a full 3D model. The use of this type of channel model also enables us to represent the channel more accurately and maintain channel connectivity, both of which are important for accurate representation of fluxes through the channel (see sections 2.3.2 and 2.3.3 for a discussion on this issue).

3.4 3D Shallow Water Equations

3.4.1 Equations

The 3D SWE are derived from the incompressible Navier-Stokes equations by approximating the pressure gradient with hydrostatic pressure distribution and by taking account of density variations only in the gravity term (the Boussinesq approximation) [60]. The 3D SWE are presented below:

$$\frac{\partial u}{\partial t}+u\frac{\partial u}{\partial x}+v\frac{\partial u}{\partial y}+w\frac{\partial u}{\partial z}-fv=-g\frac{\partial \eta}{\partial x}-\frac{1}{\rho_o}\frac{\partial p_a}{\partial x}dz-\frac{1}{\rho_o}\int_z^\eta \frac{\partial \rho}{\partial x} + \nu^h\left(\frac{\partial^2 u}{\partial x^2}+\frac{\partial^2 u}{\partial y^2}\right)+\frac{\partial}{\partial z}\left(\nu^v\frac{\partial u}{\partial z}\right) \tag{3.1}$$

$$\frac{\partial v}{\partial t}+u\frac{\partial v}{\partial x}+v\frac{\partial v}{\partial y}+w\frac{\partial v}{\partial z}+fu=-g\frac{\partial \eta}{\partial y}-\frac{1}{\rho_o}\frac{\partial p_a}{\partial y}dz-\frac{1}{\rho_o}\int_z^\eta \frac{\partial \rho}{\partial y} + \nu^h\left(\frac{\partial^2 v}{\partial x^2}+\frac{\partial^2 v}{\partial y^2}\right)+\frac{\partial}{\partial z}\left(\nu^v\frac{\partial v}{\partial z}\right) \tag{3.2}$$

$$\frac{\partial u}{\partial x}+\frac{\partial v}{\partial y}+\frac{\partial w}{\partial z}=0 \tag{3.3}$$

(3.1) and (3.2) represent the momentum equation in the x and y directions. (3.3) represents the continuity equation. The equations for the transport of temperature and salt are not presented.

3.4.2 Vertical Boundary Conditions

The surface and bottom boundary conditions come in two kinds: The *kinematic* conditions are based on the principle that water particles will not

cross the boundary, while *dynamic* conditions describe the forces acting at the boundary.

Surface

At the free surface $z = \eta(x, y, t)$, we have three conditions:

$$\text{kinematic,} \qquad \frac{\partial \eta}{\partial t} + u\frac{\partial \eta}{\partial x} + v\frac{\partial \eta}{\partial y} - w = 0 \tag{3.4}$$

$$\text{dynamic: pressure,} \qquad p = p_a \tag{3.5}$$

$$\text{dynamic: shear stress,} \qquad \nu^v \rho_o \frac{\partial}{\partial z}(u, v) = (\tau_{sx}, \tau_{sy}) \tag{3.6}$$

In principle, the surface level η can be computed from (3.4), once the velocity field is known from the momentum and continuity equations. However, a more robust equation is obtained by integrating the continuity equation (3.3) over depth, which gives (3.7):

$$\text{kinematic,} \qquad \frac{\partial \eta}{\partial t} + \frac{\partial}{\partial x}\int_z^\eta u dz + \frac{\partial}{\partial y}\int_z^\eta v dz = 0 \tag{3.7}$$

Bottom

At the bottom $z = z_b(x, y)$, there are two conditions:

$$\text{kinematic,} \qquad u\frac{\partial z_b}{\partial x} + v\frac{\partial z_b}{\partial y} - w = 0 \tag{3.8}$$

$$\text{dynamic: no slip,} \qquad u = v = 0 \tag{3.9}$$

Formally, 3.9 is the correct dynamic condition at the bottom. It is somewhat complicated to handle numerically because it usually leads to very strong velocity gradients (logarithmic profile) near the bottom. A common alternative in

turbulence modeling is using the *law of the wall*[60]. It assumes that near the very bottom a constant-stress layer exists in which a logarithmic velocity profile can be deduced using a mixing-length model. The velocity at the margin of that layer, that is at some distance δ from the bottom, can then be related to the bottom stress, which by assumption equals the stress at level δ:

$$(\tau_{zx}, \tau_{zy}) = \nu^{\nu} \rho \frac{\partial}{\partial z}(u, v) = c_f(u, v) \tag{3.10}$$

where, c_f is a drag coefficient depending on bottom roughness.

3.5 2D Vertical Shallow Water Equations

3.5.1 Description

Averaging laterally yields the computational efficiency of a two-dimensional model, while retaining some effects associated with variable domain width such as flow acceleration through contracting channels [7]. The application of these models is best suited to cases where the lateral dimension of the domain is small compared with the longitudinal dimension[7, 30, 61]. The main advantages of these 2D models are that much finer resolution in the longitudinal and vertical directions may be achieved and numerical dispersion can be better controlled than in comparable 3D models. In addition, laterally averaged 2D models are computationally less expensive than 3D models [30]. For a summary of laterally averaged estuary models and their application see [18]. The implementation of our model, henceforth called Laterally Averaged Channel Model (LACM) is largely based on the formulation found in [6].

At this point we are not considering bifurcations in the channel or the intersection of the main ship channel with other navigational channels; hence, there are no sources or sinks in the sides of the subdomain. Since the ship

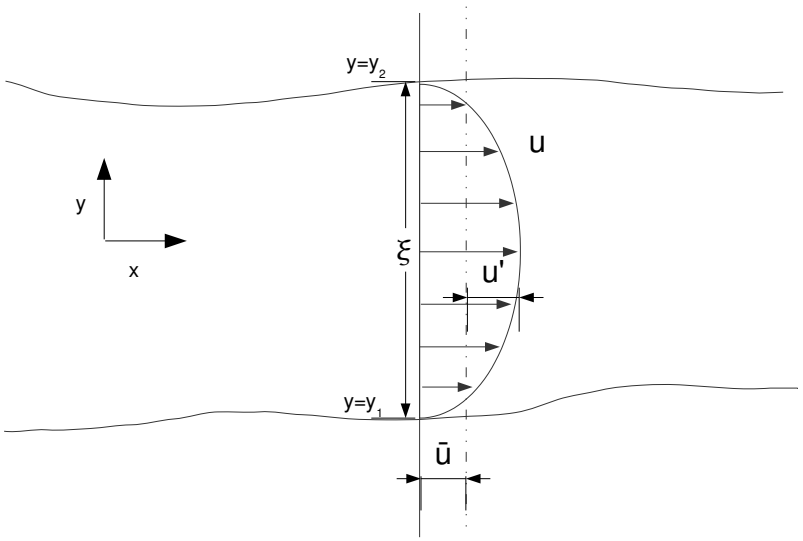

Figure 3.2: Lateral averaging of the x component of velocity

channel subdomain ends at the depth of the surrounding shallow bay (see figure 3.1), we no longer have a temporally varying free surface, rather we have an fixed interface between the two subdomains.

3.5.2 Derivation

To obtain the laterally averaged SWE we start with the full 3D SWE (equations 3.1 to 3.3). We rewrite the variables as sums of a laterally averaged component and a deviation from the lateral average (see figure 3.2).

$$u = \overline{u} + u' \tag{3.11}$$

$$v = \overline{v} + v' \tag{3.12}$$

$$w = \overline{w} + w' \tag{3.13}$$

$$p = \overline{p} + p' \tag{3.14}$$

$$etc..., where \overline{(.)} = \frac{1}{\xi}\int_{y_1}^{y_2}(.)dy \tag{3.15}$$

We note that by definition the lateral averaging of the primed variables is zero, i.e.

$$\overline{u'} = \frac{1}{\xi}\int_{y_1}^{y_2}(u')dy = 0 \tag{3.16}$$

We chose to use a model with a fixed surface rather than a free surface, dropping the η terms and applying the lateral averaging the the 3D SWE leaves us with:

$$\frac{\partial \xi\overline{u}}{\partial x} + \frac{\partial \xi\overline{w}}{\partial z} = 0 \tag{3.17}$$

$$\frac{\partial \xi\overline{u}}{\partial t} + \frac{\partial \xi\overline{uu}}{\partial x} + \frac{\partial \xi\overline{uw}}{\partial z} - \frac{\partial}{\partial x}\left(\xi N_x \frac{\partial \overline{u}}{\partial x}\right) - \frac{\partial}{\partial z}\left(\xi N_z \frac{\partial \overline{u}}{\partial z}\right) + \kappa\overline{u}|\overline{u}|\frac{\partial \xi}{\partial z} + \frac{\xi}{\rho_o}\frac{\partial \overline{p}_\Gamma}{\partial x} + \xi g \frac{\partial}{\partial x}\left(z_\Gamma - z\right) = 0 \tag{3.18}$$

(3.17) and (3.18) represent the laterally averaged SWE with a fixed surface. $p_{\Gamma c}$ is the pressure at the fixed surface. The y-momentum equation vanishes. N_x and N_z are the horizontal and vertical turbulent viscosities. κ is a dimensionless boundary friction coefficient that represents sidewall friction [6].

3.5.3 Boundary Conditions

We present the boundary conditions for our channel model below:

Surface

At the fixed surface, we have three conditions:

$$\text{kinematic,} \qquad \overline{w} = \overline{w}_{\Gamma c} \tag{3.19}$$

$$\text{dynamic: pressure,} \qquad \overline{p} = \overline{p}_{\Gamma c} \tag{3.20}$$

$$\text{dynamic: shear stress,} \qquad N_z \frac{\partial \overline{u}}{\partial z} = (\tau_{sx}) \tag{3.21}$$

Bottom

At the bottom $z = z_b(x)$, there are two conditions:

$$\text{kinematic,} \qquad \overline{u}\frac{\partial z_b}{\partial x} - \overline{w} = 0 \tag{3.22}$$

$$\text{dynamic: no slip,} \qquad (\tau_{zx}) = N_z \frac{\partial \overline{u}}{\partial z} = c_f(\overline{u}) \tag{3.23}$$

where, c_f is a drag coefficient depending on bottom roughness.

3.6 Coupling Strategy

3.6.1 Non-overlapping Domain Decomposition

We consider a bounded domain Ω of R^3 divided into two subdomains Ω_b and Ω_c such that $\partial\Omega = \partial\Omega_b \cup \partial\Omega_c, \Omega_b \cap \Omega_c = \emptyset$ and $\partial\Omega_b \cap \partial\Omega_c = \Gamma$. Γ is the interface surface between the shallow water model and the ship channel model (see figure 3.3). We describe the motion of the fluid in Ω_b with the 3D SWE (3.3 through 3.2) and the fluid motion in Ω_c with the fixed level laterally averaged SWE (3.17 and 3.18).

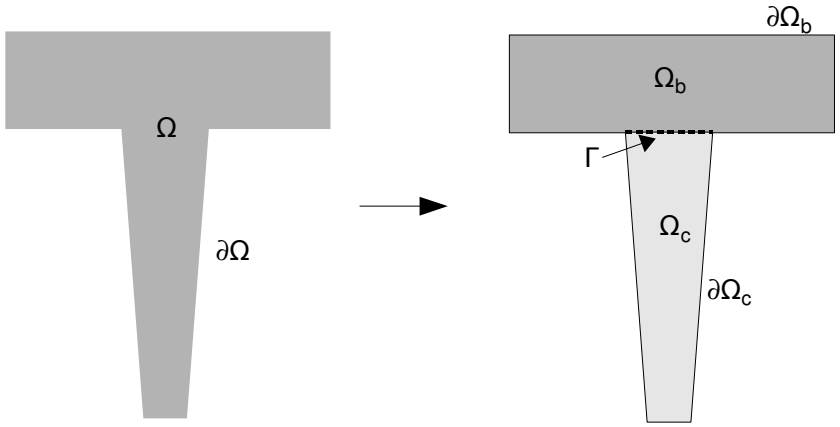

Figure 3.3: Domain Decomposition

3.6.2 Interface Conditions

To complete the mathematical formulation of our multimodel approach, we need to specify suitable matching conditions on the interface between Ω_b and Ω_c. For the coupled shallow bay-ship channel multimodel, we propose the following interface conditions on Γ :

$$\text{kinematic,} \qquad w_b = \overline{w}_c \tag{3.24}$$

$$\text{dynamic: pressure,} \qquad p_b = \overline{p}_c \tag{3.25}$$

$$\text{dynamic: shear stress,} \qquad \tau_{bx'} = \tau_{cx'} \tag{3.26}$$

where w_b, p_b and $\tau_{bx'}$ are the vertical component of velocity, the pressure and the shear stress in the direction along the ship channel at the bottom of the bay model on the interface Γ. Similarly, $\overline{w}_c, \overline{p}_c$ and $\tau_{cx'}$ are the laterally averaged

quantities at the top of the ship channel model. We observe that condition (3.24) imposes the continuity of the vertical component of the velocity, however it allows a discontinuity of its horizontal components.

In summary, we have presented the mathematical basis for the 3D SWE and our fixed surface laterally averaged channel model along with interface conditions suitable for coupling the two models. In the next chapter we will present details on how this coupled model is implemented.

Chapter 4

Implementation

4.1 Overview

Implementation of the multimodel approach requires the development of a new laterally averaged fixed surface model (LACM), modifications to the SELFE model to incorporate the interface conditions, and the choice of a time stepping strategy for the coupling between the two models. The objective of the multimodel is not to resolve small scale features near the interface but to capture the integrated effect of the flow within the ship channel on bay-wide circulation. The coupling strategy used for the model is guided by this objective. The rest of this chapter describes the details of the implementation.

4.1.1 Shallow Bay Model

For the shallow bay model, we used an off-the shelf model (SELFE [71]), that is already in use with other agencies and universities and is being used by the Texas Water Development Board for modeling Texas estuaries [51]. SELFE is an unstructured-grid model designed for the effective simulation of 3D baroclinic circulation across river-to-ocean scales. It uses a semi-implicit finite-element Eulerian-Lagrangian algorithm to solve the shallow water equations, written to realistically address a wide range of physical processes and of atmospheric, ocean and river forcings. The numerical algorithm is high-order, stable and computationally efficient. Modifications were made to the implementation

of the bottom boundary conditions to enable the coupling of this model to the ship channel model. These modifications are described in section 4.2.3

4.1.2 Ship Channel Model

For the subsurface portion of the ship channel, we developed a model based on the laterally averaged 2D vertical SWE, which we will refer to as the Laterally Averaged Channel Model (LACM). The implementation of this model is described in section 4.3

4.1.3 Solution Strategy

The Schwarz method is the earliest example of a domain decomposition approach for partial differential equations [53]. There exist two variants of the Schwarz method: the multiplicative Schwarz method and the additive Schwarz method. The latter is known for its natural parallelism because the subproblems can be solved simultaneously [15]. It has been widely used in the decomposition of large problems into multiple subdomains [65]. While the additive Schwarz method has attractive properties when considering parallelism, in a serial code it involves greater complexity for little advantage. During a multiplicative Schwarz iteration, the two subproblems are solved successively. This strategy fits well with our use of two submodels and the desire to minimize modifications to the shallow bay model. Hence, we chose to use the multiplicative Schwarz method.

Effective time stepping schemes are essential for multiphysics applications and coupled systems. It is critical to modeling large scale coupled multiphysics problems accurately and efficiently. For loosely coupled models like ours, it is appropriate to time-lag the solutions [66]. The ship channel and the

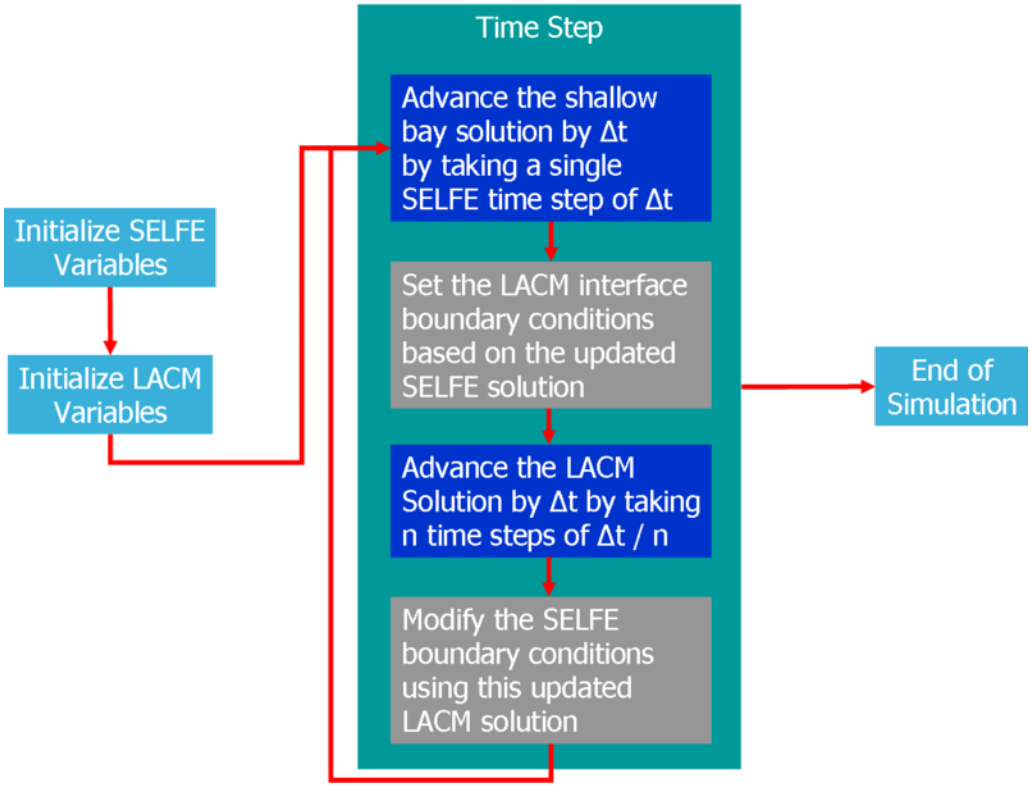

Figure 4.1: Solution Strategy

shallow bay models use a time-lagged algorithm. The time-lag introduces an error of the order $O(\Delta t)$ in the interface conditions and these errors (versus the more difficult and computationally expensive strategies of solving the both subdomains implicitly or iterating between the models to reach a converged solution each timestep) are small compared with other errors resulting from the change in grid sizes between the models and from poor knowledge of physical descriptors such as the bathymetry in geophysical flows.

The time step constraints on the shallow bay model and ship channel model are not the same. The ship channel model has higher spatial resolution and has a stricter time step constraint (see section 4.3.2). Hence, we allow the

ship channel model to take a number of smaller timesteps during each iteration of the larger shallow bay model. The solution strategy used is outlined below and in figure 4.1.

1. Initialize SELFE variables
2. Initialize LACM variables
3. Advance the shallow bay solution by Δt by taking a single SELFE time step.
4. Set the LACM interface boundary conditions based on the updated SELFE solution
5. Advance the LACM solution by Δt by taking n timesteps of $\frac{\Delta t}{n}$
6. Modify the SELFE boundary conditions using this updated LACM solution
7. Continue with such Timesteps until the simulation is complete

4.1.4 Computational Grids

Figure 4.2 shows a schematic of the spatial discretization that will be used for the individual models. These are described in more detail below.

Shallow Bay Model

One of the objectives of this research is to enable the use of large computational elements in the shallow bay model. For computational efficiency in the shallow bay model, we will use a triangular unstructured grid with elements whose sides are at least as wide as the width of the ship channel.

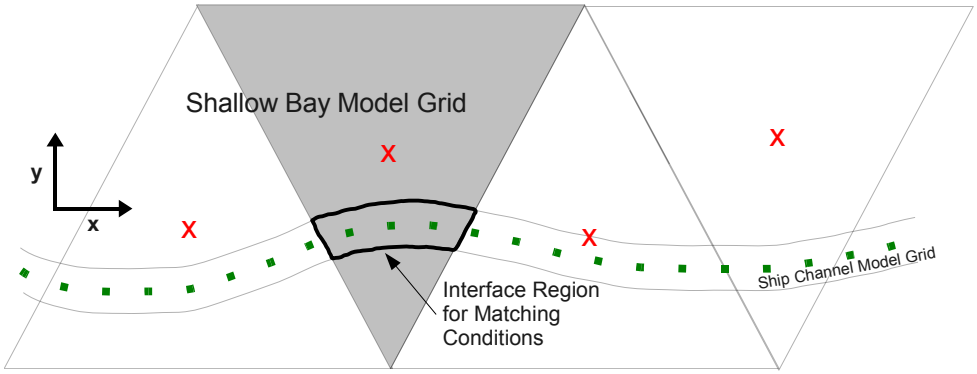

Figure 4.2: Interface between the shallow bay and ship channel models. The red crosses show where the shallow bay variables are defined. The green dots show where the ship channel model variables are defined.

Ship Channel Model

As a test case, we considered a sinuous ship channel as shown in Figure 4.2. We defined the model grid for the ship channel model by specifying points along the thalweg of the ship channel. At each of these points we defined the ship channel cross section by specifying the width of the channel at a fixed number of depths below the depth of the shallow bay. The depth of the fixed upper surface of the ship channel model was taken as the depth of the parent shallow bay model element. We then performed a coordinate transformation from cartesian space to (x', z) space as shown in Figure 4.3. The governing equations for the ship channel grid were solved in this transformed space.

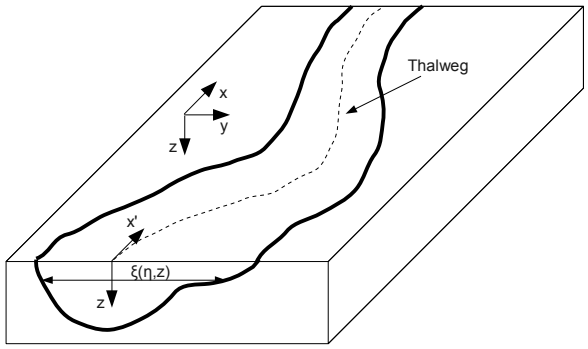

Figure 4.3: Sketch of ship channel geometry showing the relation between a cartesian coordinate system and (x', z) coordinate system.

4.2 Matching Conditions

The 3D shallow bay model uses an unstructured triangular grid while the ship channel model uses a simple structured grid. Although the two grids have a common interface, the location of defined quantities on each grid do not coincide. Hence, interpolation and averaging is needed each time step to accomplish the transfer of each sub model's solution for use as boundary conditions for the other sub model. In section 3.6.2, we presented matching conditions on the interface Γ that are required to couple the two subdomain models. They are repeated here for convenience:

$$\text{kinematic,} \qquad w_b = \overline{w}_c \tag{4.1}$$

$$\text{dynamic: pressure,} \qquad p_b = \overline{p}_c \tag{4.2}$$

$$\text{dynamic: shear stress,} \qquad \tau_{bx'} = \tau_{cx'} \tag{4.3}$$

The interface condition is simplified by specifying that any shallow bay model

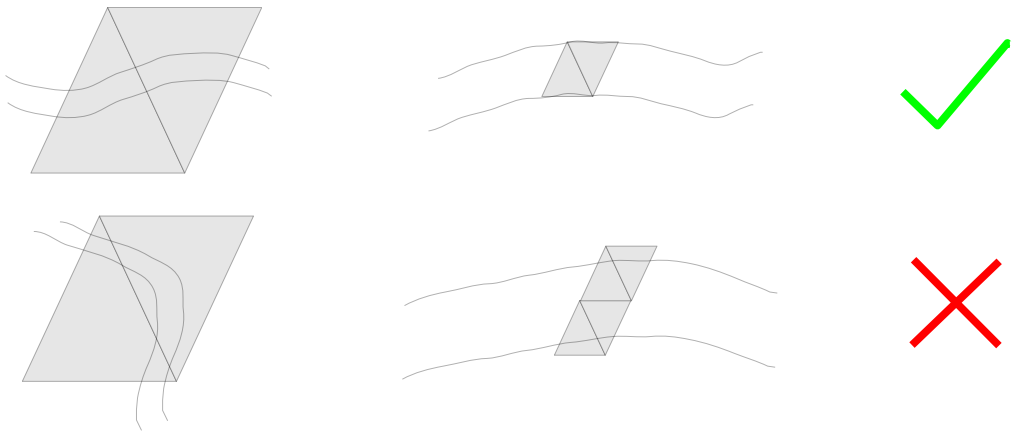

Figure 4.4: Sketch of correct and incorrect relationships between the model grids. The grey triangles represent the shallow bay computational grid while the lines represent the ship channel.

element only has one section of the ship channel passing through it(See Figure 4.4), and also that the bay elements must be equal or greater in size than the width of the ship channel that passes through them.

Care was taken in applying the interface conditions to ensure conservation of the quantities of interest. We looked at the interface conditions required at a single element E_i in the shallow bay channel model. Figure 4.5 shows the relationship between the computational nodes of each model and their coordinate spaces.

4.2.1 Pressure

The implementation of the pressure matching interface condition was straightforward. Due to our approximation of pressure as hydrostatic, the pressure at the interface only has contributions from the weight of the water column

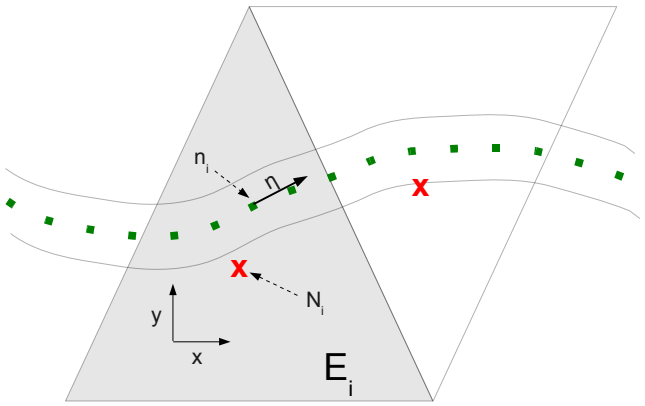

Figure 4.5: Sketch showing interface nodes N_i and n_i along with the respective coordinate systems in shallow bay element E_i.

above it. Hence, this value is calculated in the shallow bay model and specified as a known boundary condition in the ship channel model. We have $p_\Gamma = \rho_o g H$, where H is the total height of the water column at N_i and p_Γ is the pressure at the interface. This value will be used directly as a specified boundary condition for all the ship channel nodes contained within E_i.

4.2.2 Shear Stress

The continuity of the horizontal velocity field is established weakly through shear stresses. In each direction of the coupling, a diffusive flux (of the form $N_x \frac{\partial u}{\partial x}$) is calculated in each model using values of along channel velocity on either side of the interface boundary. This diffusive flux is imposed as a boundary condition for the other model. By definition the lateral components of the shear stress are neglected in the 2DV SWE ship channel model.

Ship Channel Interface Conditions

To impose the the surface shear stress boundary condition for the ship channel node n_i, first the components of horizontal velocity (u, v) are interpolated from the three nodal values in the bay model using area weighted averages. Then, the along-channel component of this interpolated velocity is used to calculate the along-channel shear stress ($\tau_{bx'}$) at N_i. This shear stress is imposed as a specified boundary condition in the ship channel model.

Shallow Bay Model

A reverse projection to transfer shear stresses from the ship channel model to the shallow bay model was also required. A two step procedure was used that first calculated an average along-channel velocity for all of the ship channel nodes n_i contained within the element E_i. This average along- channel velocity was then split into cartesian components and used to calculate the components of the shear stress for use in the bay model($\overline{\tau_{cx}}, \overline{\tau_{cy}}$). As a final step, the area weighted average shear stresses were calculated for element E_i using the following equations:

$$\tau_{bx} = a_i \overline{\tau_{cx}} + (A_i - a_i)\tau_{bdx} \tag{4.4}$$

$$\tau_{by} = a_i \overline{\tau_{cy}} + (A_i - a_i)\tau_{bdy} \tag{4.5}$$

where a_i and A_i are the area of E_i occupied by the ship channel and the area of E_i respectively. τ_{bdx} and τ_{bdy} are the contributions to shear stress from bottom drag in the shallow bay model.

4.2.3 Vertical Velocity

In the original 3D SWE, the bottom boundary condition specifies $w_b = 0$. This boundary condition is modified in the SELFE solver to allow a non-zero w_b. Care was taken in matching the vertical velocity components w_b and w_c. Improper specification of this interface condition would result in mass not being conserved in the coupled model. Conservation of mass is important for transport processes, and we wish to retain this property across the interface. Applying this conservation principle at the interface we get the relationship:

$$w_{b_i} A_i = \Sigma_1^{N_e} w_{c_i} \Delta z \xi_i \tag{4.6}$$

where, $w_{c_i} \Delta z \xi_i$ is the volume of water entering or exiting the ship channel model at n_i. N_e is the number of ship channel nodes n_i present in E_i. We added the total at all the ship channel nodes n_i present in E_i to get the overall volume contribution of the ship channel model to E_i. There was an inherent approximation when the entire volume of water from the ship channel nodes was transfered to the parent node E_i in the shallow bay model. This approach maintained conservation of mass without the added complexity of dealing with partial elements near the edges of E_i. We justify this approach by noting again that the goal of this research is to represent the integrated effect of the ship channel on bay circulation.

Hence, to set the vertical velocity interface condition in the ship channel model, we used the following equation:

$$w_{c_i} = \frac{1}{N_e} \frac{w_{b_i} A_i}{\Delta z \xi_i} \tag{4.7}$$

The volume of water transfered from the bay model to the ship channel model was equally distributed among the N_e ship channel nodes contained in E_i.

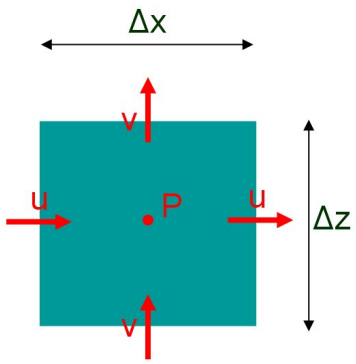

Figure 4.6: Location of variables in LACM grid

In the reverse direction, to set the vertical velocity interface condition in the shallow bay model we used the equations:

$$w_{b_i} = \frac{\Sigma_1^{N_e} w_{c_i} \Delta\Delta z \xi_i}{A_i} \tag{4.8}$$

4.3 Laterally Averaged Channel Model (LACM)

For the subsurface portion of the ship channel, we developed a model based on the laterally averaged 2D vertical SWE, which we called LACM. The LACM model was designed and coded as a separate FORTRAN module that can be easily coupled to existing 2D and 3D SWE models with relatively few modifications to the existing model code. More details on this are presented later in this chapter.

4.3.1 Finite Difference Representation

The LACM is based on the laterally averaged SWE equations presented in the previous chapter (equations 3.17 and 3.18). These governing equations along with the necessary boundary and interface conditions are solved using finite difference methods. The equations are discretized using central differences in space on a staggered Arakawa C grid as in [6]. The horizontal velocities are defined at the centers of the vertical sides of each cell, while the vertical velocities are defined at the centers of the top and bottom sides of each cell (see figure 4.6). All other quantities are represented at the cell centers. This staggered arrangement permits easy application of boundary conditions and permits evaluation of the dominant pressure gradient force without interpolation or averaging and is a common feature of other laterally averaged models found in literature ([6, 18, 61]).

Since the vertical gradients of velocity of the shallow estuaries of interest in this research are much larger than their horizontal gradients, the vertical grid spacing, Δz, is made much smaller than the horizontal spacing, Δx in order to adequately resolve the vertical variations while minimizing computational expense. As the model formulation is such that the upper surface is fixed by design and does not have the moving free surface usually present in other laterally averaged models, the grid spacing is uniform along each axis.

4.3.2 Time Discretization

Time differencing was performed using a semi-implicit Forward Euler scheme [60]. Previous research [6] has demonstrated that two numerical stability criteria are relevant. These are the Courant-Freidrichs-Lewy stability criterion (CFL condition)

$$\frac{\Delta t}{\Delta x}(gH)^{\frac{1}{2}} \leq 1 \tag{4.9}$$

and the viscosity criteria

$$\frac{\Delta t}{(\Delta z)^2} N_z \leq \frac{1}{4} \tag{4.10}$$

Since these criteria are deduced without considering the total amplification matrix, they can only be used as a reference, and in practice the maximum allowable timestep should be smaller than predicted by these criterion. [6] recommends halving the predicted maximum allowable timestep.

4.3.3 Boundary Conditions

The horizontal velocity was set to zero at the bay end and also at the estuary end of the ship channel model. The bay end of the channel ends in a wall, and the estuary end gradually merges with the surrounding bay. The bottom boundary was set using the bottom stress formulation described in section 3.5.3.

4.3.4 Interface Boundary Conditions

At the upper surface of the LACM, the vertical velocity was set to the vertical velocity value from the updated SELFE solution, thus ensuring continuity. Continuity of horizontal velocity was enforced weakly through the setting of the shear stresses using the updated horizontal velocity solution from SELFE (see section 4.2).

4.4 Modifications to SELFE

As mentioned earlier, care was taken to implement the multimodel approach with minimal changes to the shallow bay model (SELFE). In line with this strategy, modifications were made to SELFE routines at two locations in the code in order to set the vertical velocity and horizontal stress bottom boundary conditions. In addition, two function calls are made to LACM from SELFE. The first initializes LACM variables, locates interface elements and precalculates interpolation weights. The second is called at the end of each SELFE timestep to advance the ship channel solution by the same timestep.

4.4.1 Boundary Conditions

The boundary conditions for SELFE at non-interface locations were not changed in any way, and a description of their implementation can be found in literature [71].

4.4.2 Interface Boundary Conditions

Non-interface elements in SELFE were left undisturbed. In elements on the interface, the bottom friction terms were replaced with a new term incorporating the updated along-channel velocity from LACM, and the zero vertical velocity boundary condition were replaced with the interpolated vertical velocity from the updated LACM solution (see section 4.2).

Chapter 5

Results

5.1 Introduction

Validation of the coupled LACM – SELFE multimodel was conducted through a comparison of the coupled simulation results with a reference simulation conducted with the SELFE model on a fine resolution grid. The model comparisons were conducted on a ideal ship channel test case designed for this research. This chapter defines the ideal ship channel test case, justifies the choice of reference solution and presents comparisons of the coupled model solution to the reference solution.

5.2 Ideal Ship Channel Test Case

5.2.1 Computational Domain

To isolate fundamental circulation patterns caused by wind and tidal forcings (as opposed to those affected by heterogeneous bay morphology and river inflows), we have developed an idealized bathymetry for a circular bay bisected by a straight, uniform-width ship channel, which is connected to a large open ocean domain (see figure 5.1). A circular bay was chosen to avoid 'corner effects' in the model. A large ocean domain was used so that tidal forcings could be applied far from the ship channel entrance, allowing the reflected waves to propagate out of the circular bay. The circular bay is 16000m wide and has

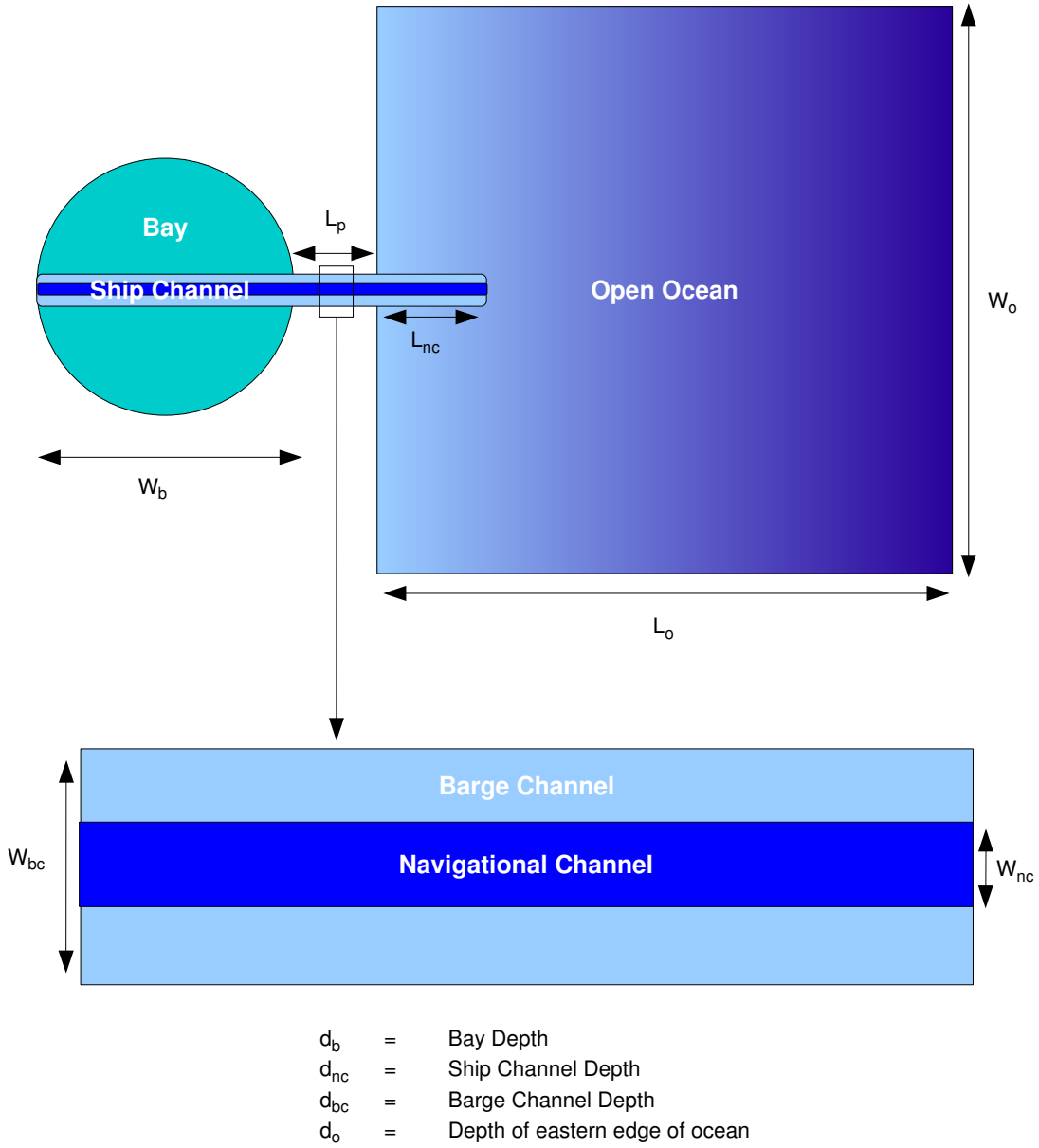

Figure 5.1: Plan view of computational domain. Values of dimensional parameters are given in Table 5.1

W_b	W_o	W_{bc}	W_{nc}	L_p	L_o
16000m	32000m	320m	160m	500m	24000m
D_b	D_o	D_{bc}	D_{nc}	**Tidal Amp.**	
3m	20m	15m	15m	0.22m	

Table 5.1: Values of dimensional parameters in Figure 5.1

a constant 3m depth except near the land boundaries where the depth slopes quadratically to zero. The ship channel consists of a central channel that is 160m wide and 15m deep surrounded by a barge channel that extends out to an overall width of 320m. Because of the difficulties in representing this rapid change in bathymetry in 3D models (see section 2.3.2) the depth of the barge channel was also set to be 15m. The western end of the ship channel is sloped quadratically to zero depth at the land boundary. The ocean domain is 24000m long and 32000m wide. Its depth varies quadratically from 4m near the bay to 20m at the open ocean boundary. These dimensions are based on values characteristic of Texas bays (see Table 1.1) and the design dimensions of the Houston Ship Channel (see Figure 1.2) adjusted to be more convenient for grid generation. The ship channel geometry and bathymetry is shown in Figure 5.1.

5.2.2 Forcing Terms

This work is focused on how wind-driven and tide-driven circulations are affected by a deep ship channel in a shallow embayment. Although an estuarine system has multiple physical forcing agents, we have chosen to explore two main agents, wind and tide, and the interaction between them. The following forcing conditions were used.

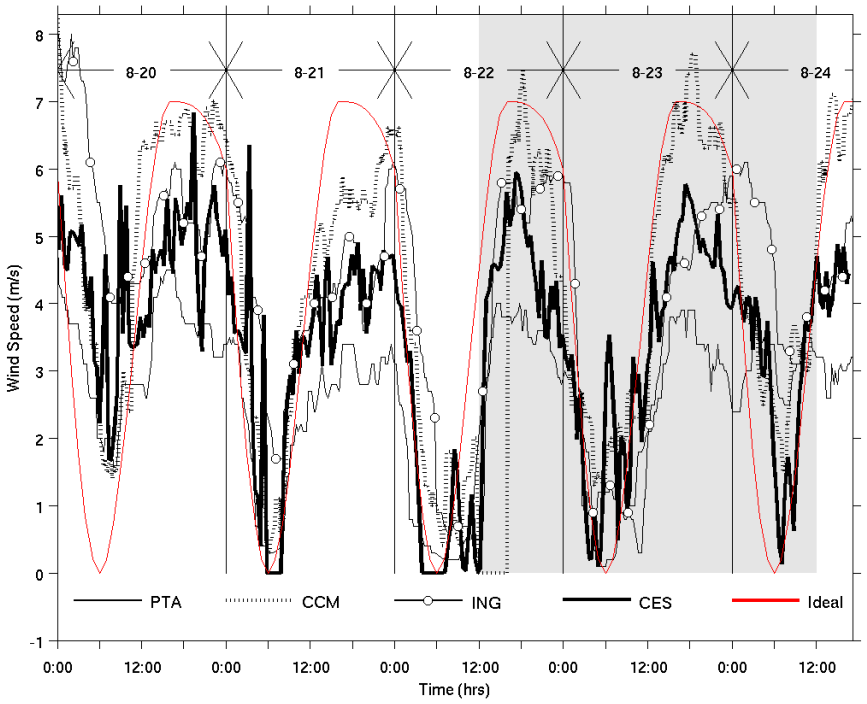

Figure 5.2: Comparison of the derived ideal diurnal wind with 4 measurement stations.(PTA, CCM, ING and CES are measured winds at 4 stations located in Corpus Christi Bay. The red line is the derived ideal diurnal wind)

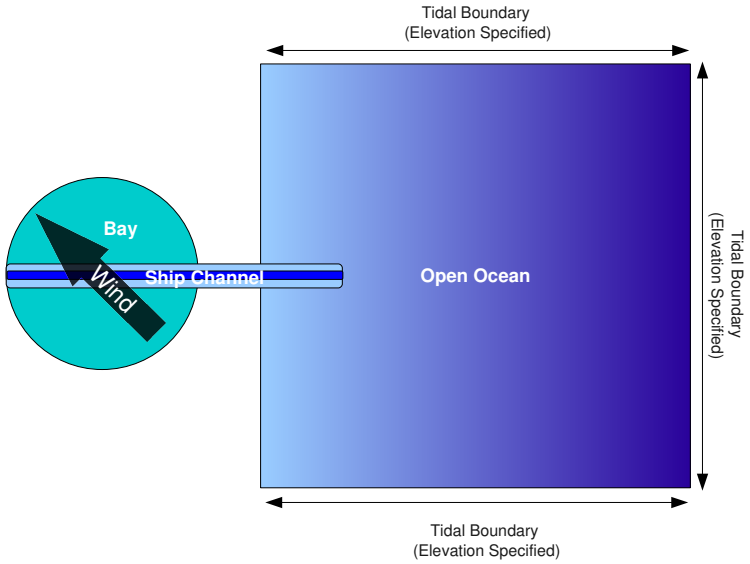

Figure 5.3: Imposed Boundary Conditions

- Ideal Diurnal Wind : A ideal diurnal wind was developed based on field measurements taken in Corpus Christi Bay during August 2005. A simple cubic interpolation was chosen to generate the ideal wind based on a few points picked visually from a plot of the wind speed at various stations in the by (see figure 5.2). A wind out of the southeast was used. This forcing was applied over the entire domain.

- Sinusoidal Tide : The tides in many Texas bays are semi diurnal and have two peaks each day. A simple sinusoidally varying tide with a time period of 12.5 hours and an amplitude of 1 foot was used as a simple representative forcing. This forcing was applied at the open ocean boundary.

The locations of the open boundary conditions and the direction of the wind in the test case are shown in Figure 5.3. All unspecified boundaries in the figure are land boundaries.

5.2.3 Computational Grid

The domain developed above has been discretized into a computational grid consisting of triangular prisms. The horizontal extent of the domain was divided into triangular elements. These elements were projected down to form 3D prisms with parallel upper and lower faces. A series of increasingly refined grids was developed. The grid was refined in the horizontal by using smaller triangular elements. In the vertical, a series of layers defined over the entire domain split the prisms at fixed depths. The resolution of a given grid is characterized by two parameters: n_h is the number of elements across the ship channel and n_v is the number of vertical layers used above the ship channel depth. The horizontal element size increases with the distance from the ship channel so that the total number of grid cells is not prohibitively large. The vertical layers were uniformly-spaced at constant z levels until the depth of the ship channel was reached, after which a few larger layers were used to capture the deeper open ocean. The test cases were developed from the sets: $n_h = [1, 2, 4, 8, 16, 32]$, $n_v = [1, 2, 4, 8, 16, 32, 64, 128]$.

Once a grid was generated, bathymetry was interpolated from a generated high resolution dataset to the nodal points of the computational grid.

Figure 5.4 shows the computational grid over the entire domain for $n_h = 1$. Figure 5.5 shows how the grid across the ship channel changes as n_h increases from 1 to 32.

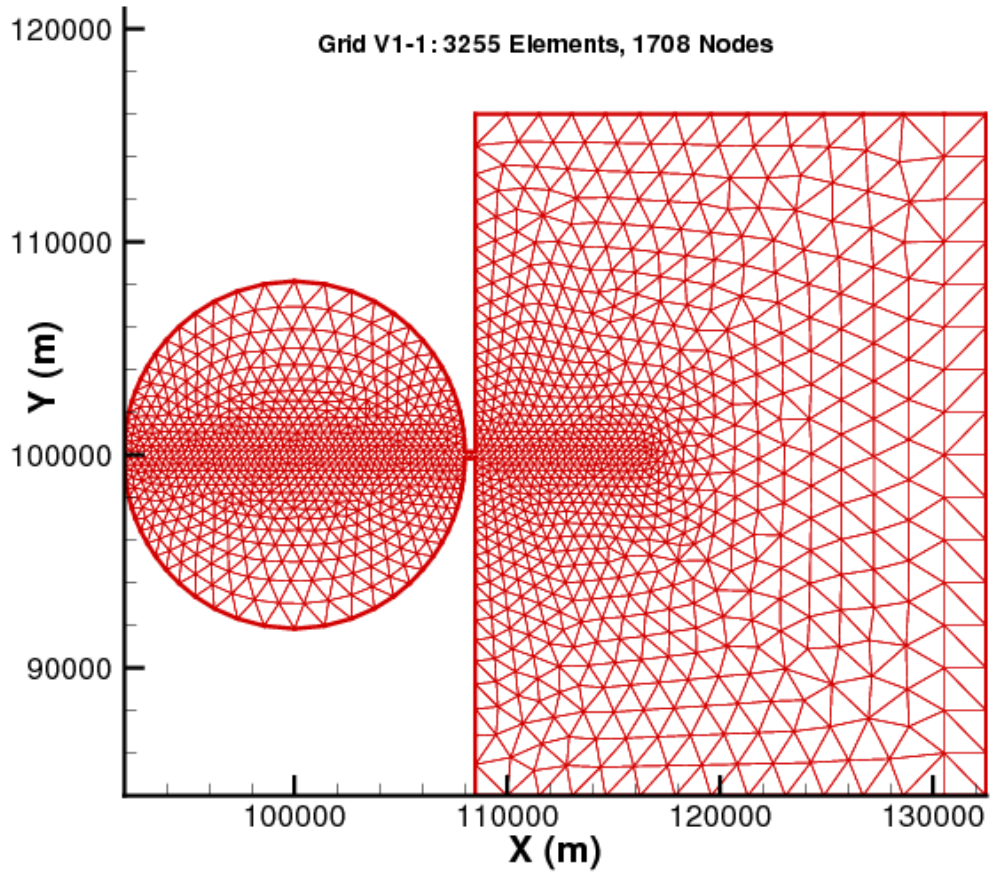

Figure 5.4: Computational Grid with $n_h = 1$

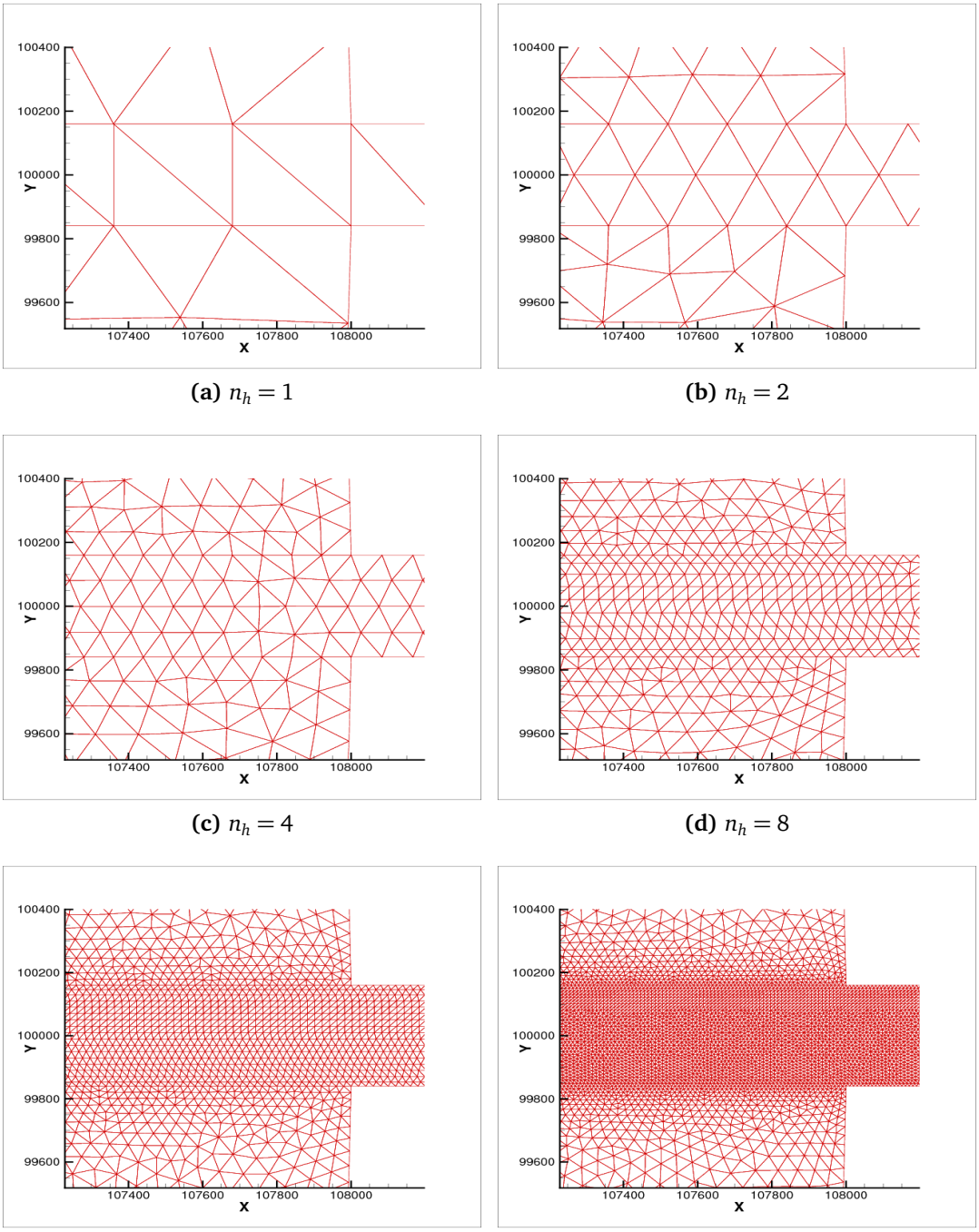

(a) $n_h = 1$ **(b)** $n_h = 2$

(c) $n_h = 4$ **(d)** $n_h = 8$

(e) $n_h = 16$ **(f)** $n_h = 32$

Figure 5.5: Zoomed in section of computational grids showing the ship channel for $n_h = [1,2,4,8,16,32]$

5.2.4 Summary of Model Parameters

Model runs were conducted with SELFE version 1.5k7 and the coupled LACM-SELFE model that was developed using the same version. Model simulations were conducted for a 15 day period with a 1 day ramp period for tides and winds. A bottom friction of 0.0025 was used. A model time step of 30 seconds was used for SELFE while a timestep of 5 seconds was used for LACM. A constant eddy viscosity of 1e-4 was used for turbulence closure except where otherwise indicated. The LACM model grid used a Δx of 100m and a Δz of 1m.

5.3 Choice of Reference Solution

To validate the multimodel strategy on the ideal ship channel test case described in this chapter, a reference simulation based on a converged solution on a fine resolution grid is required. Chapter 2 discusses the importance of horizontal and vertical grid resolution in detail. Horizontal grid resolution was set at $n_h = 8$ based on the convergence analysis presented in appendix A. Section 2.4 discusses the importance of vertical grid resolution in modeling wind driven bay circulation and the need for sufficient vertical resolution to capture surface circulation patterns is demonstrated by qualitative results shown in appendix A. A new vertical convergence study was conducted using SELFE under three different turbulence closure schemes varying n_v from 4 to 128. The SELFE model has a minimum vertical resolution of 3 vertical layers and hence no simulations were conducted for $n_v = 1$ and 2. The turbulent closure scheme tested includes a constant eddy viscosity of 1e-4, a Mellor Yamada 2.5 scheme with Galperin's stability function (MYGA) and a $k - kl$ scheme with Kantha and Clayson's stability function (KLKC). Details and further references for these schemes can be found in [69, 71].

5.3.1 Vertical Convergence

Figure 5.6 shows the effect of increasing vertical resolution on surface velocities and elevations under the three turbulence closure schemes. Under all choices of turbulence closure tested, the model does not converge even at high vertical resolutions with the surface velocities increasing as the vertical layers become thinner. This non-convergence is pronounced in the across channel component of velocity. Figure 5.7 shows, however, that the depth averaged velocities are fairly consistent across the model runs.

The non-convergence is due to a peculiar property of the turbulence closure equations as implemented in SELFE. The boundary condition for the mixing length is that it approaches distance to the surface multiplied by 0.4, which is singular for the equation. The surface velocity is critically dependent on the surface mixing (viscosity); the larger the viscosity the smaller the velocity and vice versa. Many models use one half of the surface layer thickness as the distance, and as this distance is reduced (as the grid is refined) the convergence of the results is not guaranteed (at least from the equations themselves) although there appears to be some evidence suggesting that the viscosity will remain within the same order of magnitude due to the compensation between mixing length and Turbulent Kinetic Energy. For the dominant signal (e.g., u in this case), the convergence may not be problematic, but for the weaker signal it may pose a problem (*pers. comm.* [68]). This is consistent with the observed results. It is possible that the alternative implementation of turbulence closure schemes in SELFE that use the Generalized Ocean Turbulence Model (GOTM) [71] module may have better convergence properties, but this was not explored in this research.

A comparison of the three turbulence closure schemes also shows that

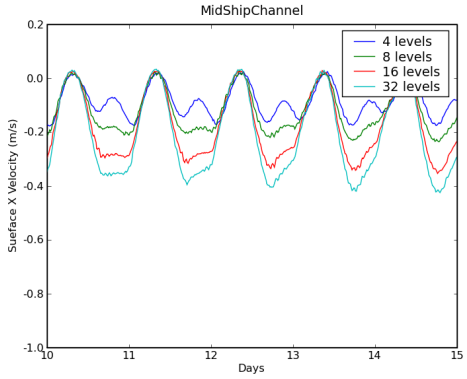

(a) Const. Eddy Visc. 1e-4 u velocity

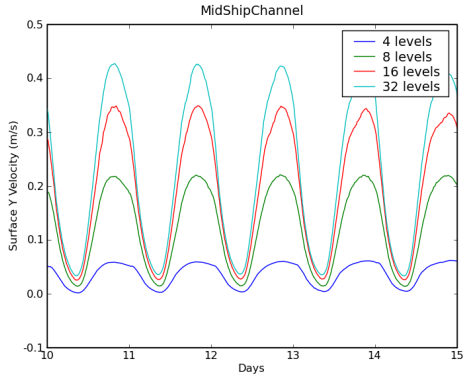

(b) Const. Eddy Visc. 1e-4 v velocity

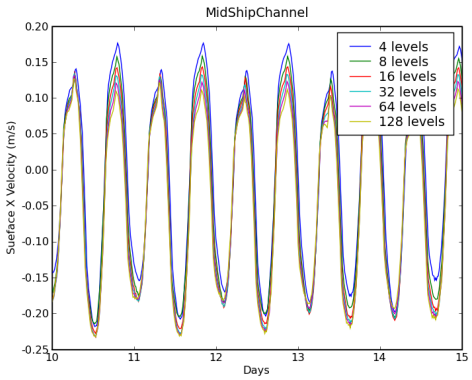

(c) KLKC Closure Scheme u velocity

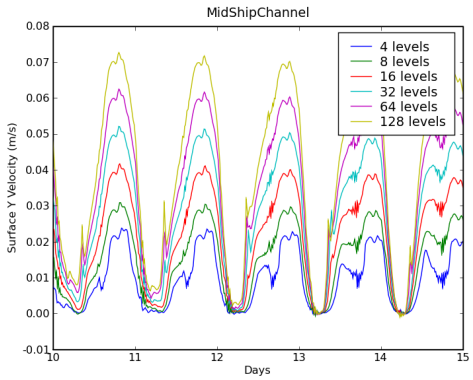

(d) KLKC Closure Scheme v velocity

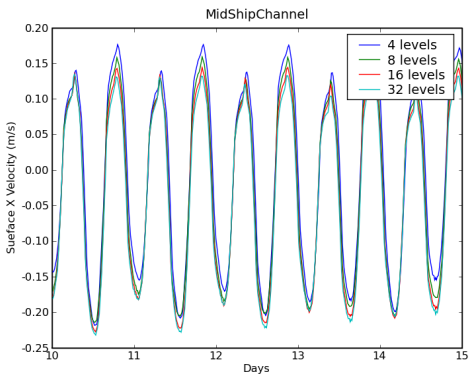

(e) MYGA Closure Scheme u velocity

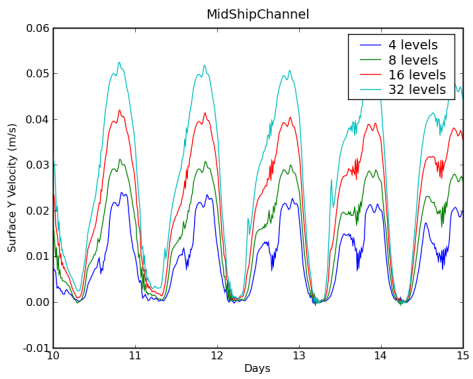

(f) MYGA Closure Scheme v velocity

Figure 5.6: Horizontal components of surface velocity under three turbulence closure schemes at increasing vertical grid resolutions

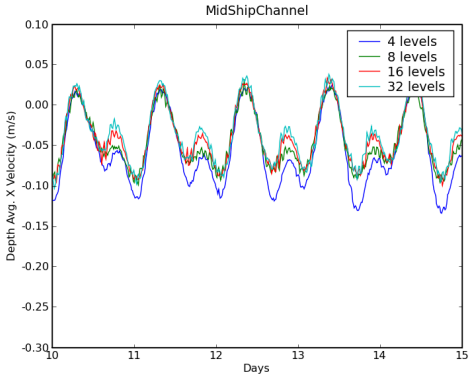

(a) Const. Eddy Visc. 1e-4 u velocity

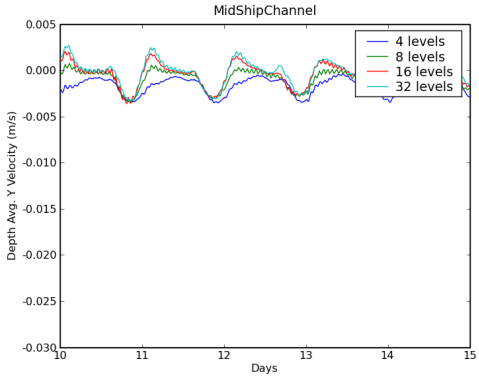

(b) Const. Eddy Visc. 1e-4 v velocity

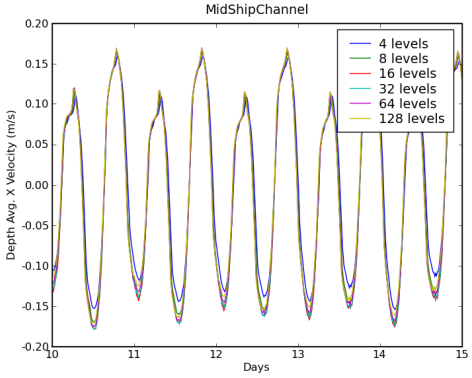

(c) KLKC Closure Scheme u velocity

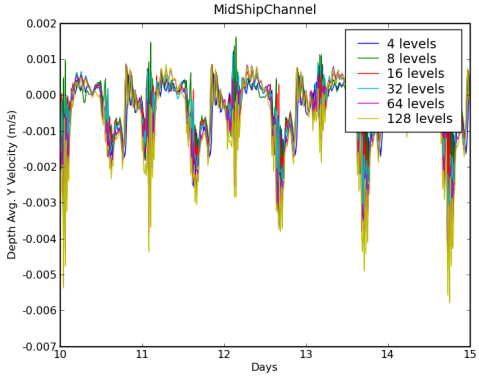

(d) KLKC Closure Scheme v velocity

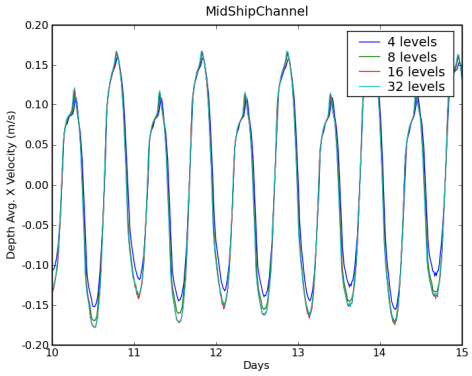

(e) MYGA Closure Scheme u velocity

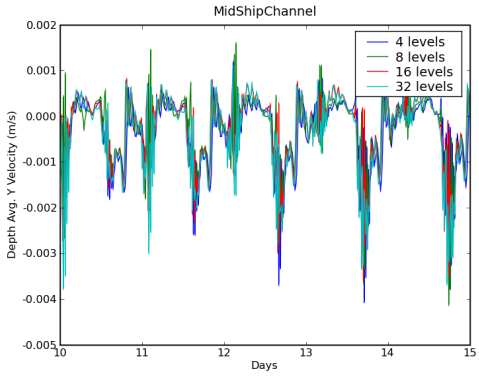

(f) MYGA Closure Scheme v velocity

Figure 5.7: Horizontal components of depth averaged velocity under three turbulence closure schemes at increasing vertical grid resolutions

the choice of turbulent closure scheme plays a major role in the determination of the surface circulation patterns.

5.3.2 Discussion

Considering the issues raised here, it is not possible to choose a converged solution for use as a reference solution in the verification of the coupled LACM-SELFE model. The original research objective of showing that the multimodel approach can achieve equal or better accuracy than a medium resolution 3D SWE model is not longer relevant since it is not clear what the converged solution should be. Instead the research objective is modified to show that the multimodel approach can match the accuracy of an equivalent resolution 3D SWE model with a much reduced computational effort. With this in mind, the $n_v = 16$ is chosen as the vertical resolution of the reference solution (along with $n_h = 8$ as the horizontal resolution). This gives the reference model a vertical resolution of approximately 1m in the ship channel. Since it is unclear which turbulence closure scheme is more accurate, the constant eddy viscosity case is used for simplicity. In the coupled LACM-SELFE simulations, a $n_h = 1$, $n_v = 4$ SELFE grid is coupled with a 12 layer ($\Delta z = 1m$) LACM grid to establish a vertical resolution comparable to the reference case.

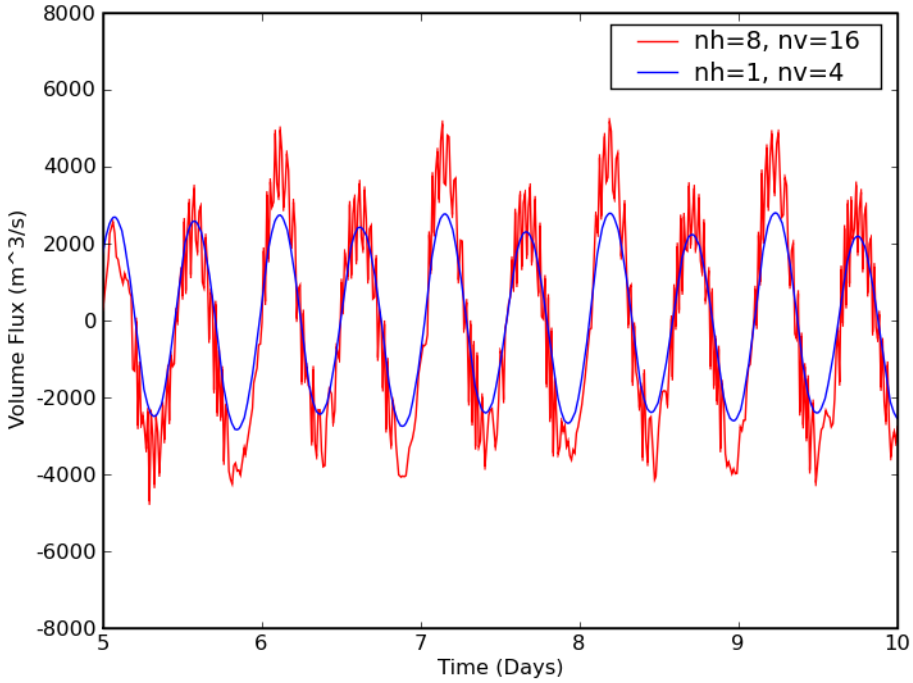

Figure 5.8: Comparison of fluxes through the channel at a fine and coarse resolution. Instabilities are present in the high resolution solution. *nh* is the number of elements across the ship channel and *nv* is the number of vertical layers

5.4 Effectiveness of Multimodel Strategy

In this section we compare results from the coupled LACM-SELFE model to the reference solution described above. We also display the results of two SELFE simulations with the ship channel removed from the domain. The first uses the same vertical and horizontal grid resolution as the reference solutions($n_h = 8$, $n_v = 16$), while the second uses the same resolution as the coupled model($n_h =$

1, $n_v = 4$). We note that there are instabilities in the reference solution (see figure 5.8. In this particular testcase, the ship channel has a uniform rectangular cross section and a lower resolution model can capture the flux reasonably well. A comparison of the low resolution solution to the reference solution shows that the high resolution SELFE model is capturing the main physics correctly but displays high frequency fluctuations that seem to be a result of the horizontal grid refinement. In the following sections we compare the multimodel solution with the reference solution with the caveat that there are instabilities in the reference solution.

5.4.1 Flow within the Ship Channel

Figure 5.9 compares the along-channel velocities within the sub surface portion of the ship channel. Velocities from the top, middle and bottom of the LACM grid in the middle of the bay are compared to an average along-channel velocity from the reference solution at the same vertical location. The averaging procedure is needed to make valid comparisons because of the higher horizontal resolution ($n_h = 8$) of the reference solution when compared to the coupled model.

The coupled model represents the velocity profile in the vertical fairly well, showing the decrease in magnitude with depth. At each level the coupled model on average matches the magnitude and phase of the along-channel velocity but misses the higher resolution fluctuations and does not capture the peaks perfectly.

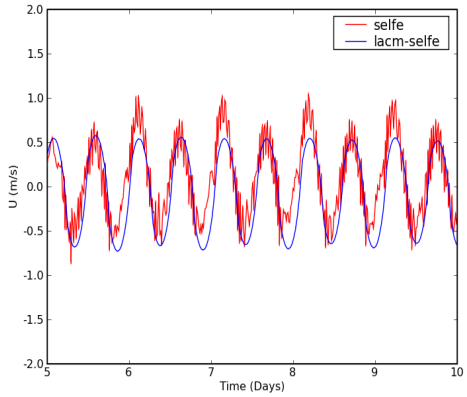

(a) Top of Ship Channel (-3m from Surface)

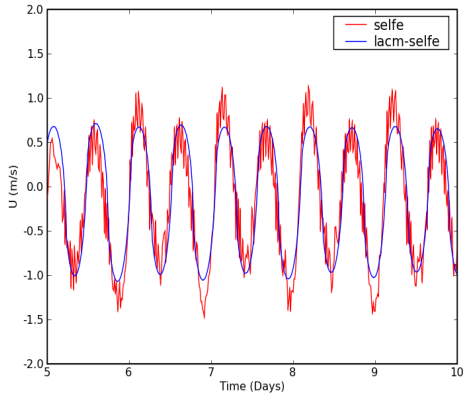

(b) Middle depth of Ship Channel (-9m from Surface)

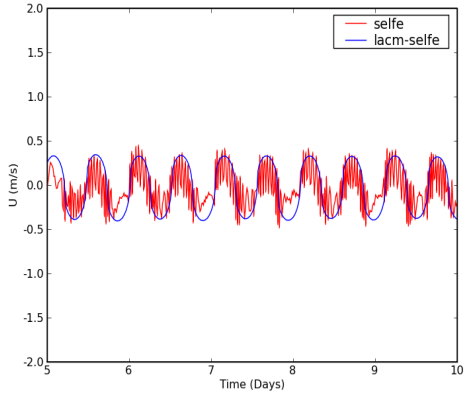

(c) Bottom of Ship Channel (-15m from Surface)

Figure 5.9: Comparison of LACM along channel velocity to reference solution at three depths at the center of the shallow bay

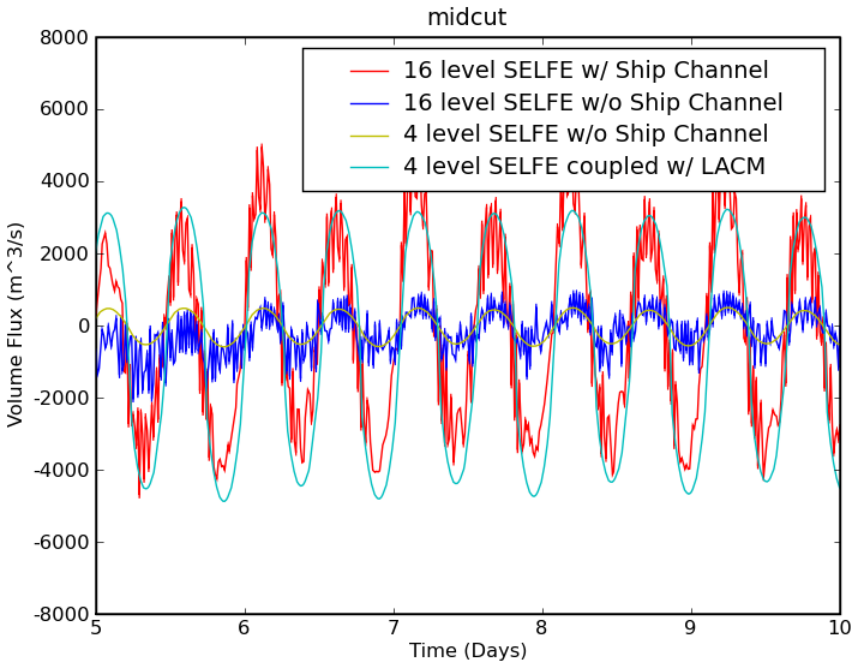

Figure 5.10: Volume Fluxes through the cut connecting the Shallow Bay to the Open Ocean

5.4.2 Volume Flux into Bay

In section 2.3, the effect of horizontal grid resolution on volume fluxes through narrow channels was discussed in detail. Figure 5.10 shows the volume flux through the cut connecting the shallow bay to the open ocean under four different model simulations. It is clear that the correct representation of the ship channel is critical in determining the volume fluxes in and out of the shallow bay. Both simulations that do not include the ship channel severely underestimate the volume fluxes. The coupled model is extremely effective at correctly simulating the volume fluxes through the cut although it does not completely capture the high frequency effects.

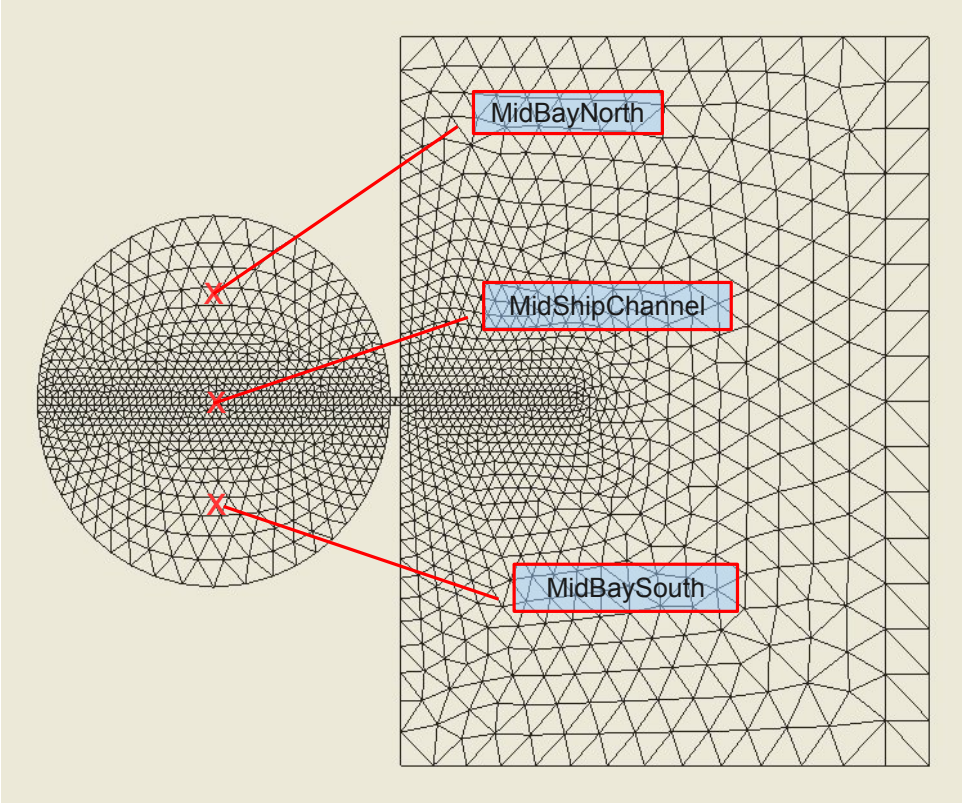

Figure 5.11: Station locations at which surface velocity comparisons were made.

5.4.3 Surface Flow

The results were compared qualitatively by plotting the surface velocity and sea surface elevation at three stations (figure 5.11). The stations include a site in the center of the ship channel, a site in the middle of the northern half of the bay and a site in the middle of the southern half of the bay called MidShipChannel, MidBayNorth and MidBaySouth respectively.

From figure 5.12 it is clear that the patterns of the surface circulation flow are determined primarily by the vertical resolution within the SELFE model.

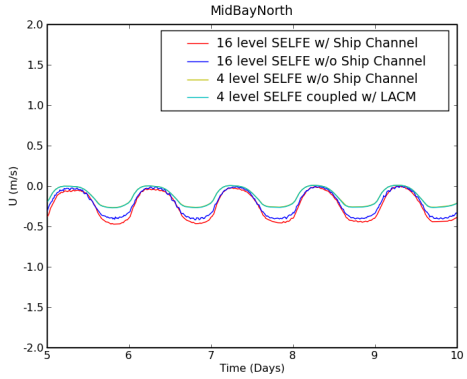

(a) MidBayNorth u velocity

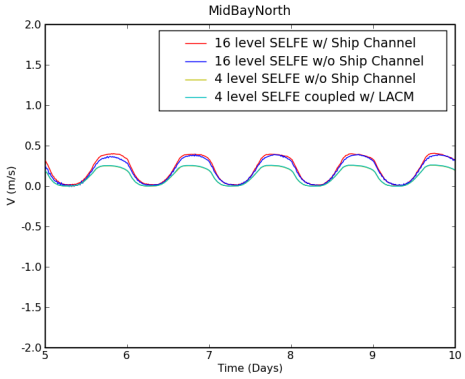

(b) MidBayNorth v velocity

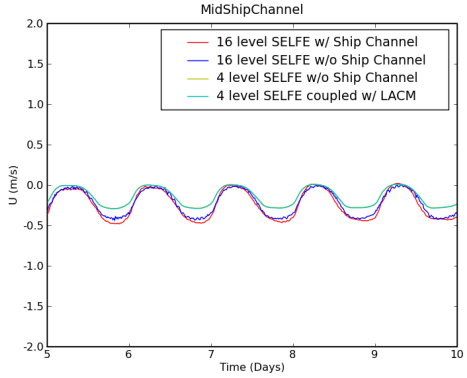

(c) MidShipChannel u velocity

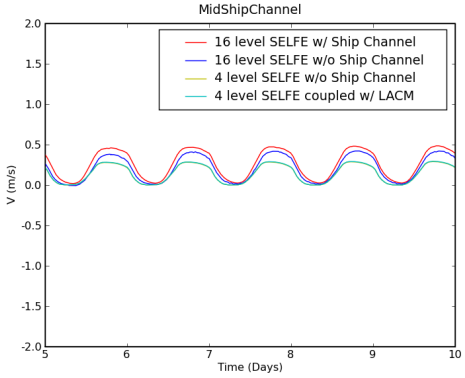

(d) MidShipChannel v velocity

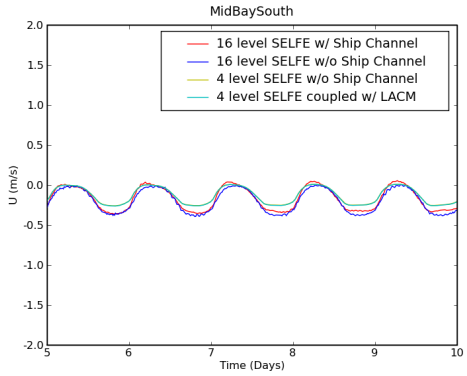

(e) MidBaySouth u velocity

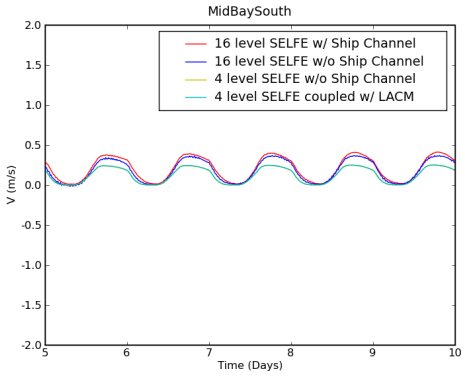

(f) MidBayNorth v velocity

Figure 5.12: Comparison of surface flow at three locations in the shallow bay

Model	Description	n_h	n_v	Time (hrs)
SELFE	Reference Solution	8	16	26.86
SELFE	No Ship Channel	1	4	0.55
LACM-SELFE	Multimodel	1	4	0.64

Table 5.2: Model Speed Comparisons

The presence or absence of the ship channel has little effect on the surface circulation. Both the 16 layer SELFE runs (with and without the ship channel) exhibit similar behavior while the 4 layer SELFE run and the 4 layer LACM-SELF run exhibit similar behavior.

5.4.4 Computational Efficiency

All simulations were conducted on an Intel Xeon X5355 CPU with a clock speed of 2.66GHz. The Intel Fortran Compiler v10.1 was used with the optimization flags *-O2 -xT*. The reference solution simulation also required use of the compilation flag *-mcmodel=large* due to the larger memory requirements of the finer resolution grid.

To determine the computational efficiency of the coupled model approach we compare its speed over the 15 day simulation to the reference fine resolution SELFE simulation and also to an unmodified SELFE simulation that uses the same shallow bay grid that is used in the coupled model. Table 5.2 lists the speeds of each of these simulations. The coupled LACM-SELFE model is approximately 16% slower than an unmodified SELFE model run on the same shallow bay grid ($n_h = 1$, $n_v = 4$) as the coupled model. This is the overhead of the ship channel model and the transmission of interface conditions between the two sub models. We note that in this case the unmodified SELFE model is

not simulating the ship channel. Even with this overhead, however, the use of the multimodel strategy enables us to accomplish a speed up of almost 42 times faster than the fine resolution reference SELFE solution.

5.4.5 Summary

In this chapter, we have shown that the newly developed multimodel (LACM-SELFE) is able to capture the important features of bay circulation for the ideal ship channel test case under wind and tidal forcings. The coupled model is able to match the accuracy of a fine resolution 3D SELFE simulation at a fraction (approximately 42 times faster) of the computational cost.

Chapter 6

Conclusions and Recommendations

6.1 Discussion

Numerical modeling of shallow microtidal semi-enclosed estuaries requires the effective simulation of physical processes with varying temporal and spatial scales. Many of these shallow estuaries contain dredged ship channels that are an order of magnitude deeper than the surrounding bay. The presence of these deep, narrow ship channels presents certain modeling challenges. Based on the research conducted, we make the following general statements on the physics of shallow bay- ship channel systems and the techniques currently used to model them:

- Two distinct flow regimes can develop in such systems. These are a wind driven surface circulation in the upper bay and a tidally driven oscillatory flow regime within the ship channel.
- 2D SWE models and low resolution 3D SWE models are inherently unable to capture this 3D flow regime.
- Insufficient vertical grid resolution causes such models to underestimate the wind driven effects, causing model simulations to be dominated by the tidal component. This causes surface circulation to be simulated incorrectly.

- Accurately representing ship channel geometry is a challenge for 2D and 3D SWE models. Misrepresentation of channel cross sections can cause large errors in volume fluxes. Using a horizontal grid resolution fine enough to capture the geometry accurately is often computationally impractical. With coarser resolution grids, care needs to be taken to align grid elements along the channel.

- At fine vertical resolutions, the choice and implementation of turbulence closure schemes can have a large effect on surface circulation. In the case studied in this research, the solution did not converge with grid refinement.

- The cross channel flow caused by the wind forcing is highly dependent on vertical resolution and choice of turbulence closure model. It is unclear what the correct magnitude of this flow is.

We make a further note that the fine resolution 3D model simulations displayed high frequency oscillations in velocity superimposed over the more normal velocity signals, indicating that the grid resolutions required to accurately represent the physical geometry of the ship channel may be too fine for the model algorithm to handle numerically.

6.2 Conclusions

In this research, we have explored using a multimodel strategy as an efficient technique to model bay circulation in shallow bay systems containing ship channels. We have demonstrated deficiencies in current approaches using 2D and 3D SWE models and have explored the need for sufficient horizontal and

vertical grid resolution to accurately capture the effect of the spatially localized ship channel on bay wide circulation patterns. In developing our multimodel strategy, we have decomposed the system into a shallow bay subdomain and a subsurface ship channel subdomain. Matching conditions have been derived across the interface between the subdomains.

This multimodel strategy has been implemented through the coupling of a 2D laterally averaged SWE ship channel model (LACM) with an off-the-shelf 3D SWE model (SELFE) through appropriate interface conditions. We have thus created a new model capable of simulating shallow bay- ship channel systems in an efficient manner. The new multimodel was applied to an ideal ship channel test case consisting of a shallow bay containing a deep ship channel separated from the open ocean by a barrier island. The model was forced with wind and tides. Comparisons of the multimodel solution to a fine resolution reference solution using the SELFE 3D SWE model showed that the multimodel was able to reproduce all major flow features effectively. Specifically, the multimodel was able to reproduce the velocity profile with depth and the volume fluxes into the bay. The multimodel approach was found to be close to 42 times faster than the equivalent fine resolution 3D model, taking 0.64 hours of CPU time versus 26.86 hours for the reference solution.

Hence, the LACM – SELFE multimodel has met our modified research goal of achieving a similar accuracy of a fine resolution 3D model run with equivalent vertical resolution at a fraction of the computational expense.

From our research, we note that for surface circulation, a vertically fine resolution model without the ship channel represented may be sufficient for many purposes. It must be remembered, however, that the absence of the ship channel in the model will cause volume fluxes and non-surface flows to be mis-

represented. The multimodel approach is able to simulate the system significantly more accurately at a relatively minor (16%) increase in computational expense, taking less than an hour to conduct a 15 day simulation of a 16km wide shallow bay containing a 15m deep ship channel.

6.3 Future Work

The multimodel approach has been shown to be an effective technique to model shallow microtidal semi-enclosed estuaries containing narrow, deep ship channels. There remain, however, several practical and theoretical issues that remain unresolved. Based on the current research results and conclusions, we propose the following work as next steps in exploring the multimodel strategy:

Realistic Turbulence Models

The ship channel model LACM was implemented using a constant eddy viscosity. Implementation of more sophisticated turbulence closures schemes are needed for the model to simulate real world systems. An open research question in this implementation is the choice of interface conditions between the 2D laterally averaged ship channel model and 3D shallow bay model. The formulation of these transmission conditions should ensure that turbulent kinetic energy is conserved across the interface.

Application to a real world system

This research has shown the effectiveness of the multimodel strategy when applied to an ideal test case. Application of the coupled model to a real world system is the logical next step. The research conducted makes it clear

that the extent and magnitude of wind driven surface flow is highly dependent on vertical resolution and the implementation of turbulence closure schemes. A further exploration of turbulent closure schemes and comparison to field data is needed to determine actual surface circulation patterns in shallow bay- ship channel systems.

Salinity and Temperature Transport

The current coupled model simulates velocities and sea surface elevations. Implementation of Salinity and Temperature transport modules into the ship channel model would greatly enhance the usefulness of the model.

Branched Channels

In real world situations, navigational channels branch and bifurcate. Inclusion of multiple connected channels in the coupled model would also be needed for practical applications.

Appendices

Appendix A

Numerical Grid Resolution Study

A.1 Introduction

Just what is sufficient grid resolution for the typical scales of Texas embayments? In this chapter we explore the effect of both horizontal and vertical grid resolution on the wind-driven and tide-driven circulation in an idealized shallow bay-ship channel system. We do this through a series of grid resolution tests on an idealized domain with a variety of forcings. We also show how the computational cost of the model increases with increase of horizontal and vertical resolution.

A.2 Ideal Ship Channel Test Case

A.2.1 Computational Domain

To isolate fundamental circulation patterns caused by wind and tidal forcings (as opposed to those affected by heterogeneous bay morphology and river inflows), we have developed an idealized bathymetry for a circular bay bisected by a straight, uniform-width ship channel, which is connected to a large open ocean domain (see figure A.1). A circular bay is chosen to avoid 'corner effects' in the model. A large ocean domain is used so that tidal forcings can be applied far from the ship channel entrance, allowing reflected waves to propagate out of the circular bay. The circular bay is 16000m wide and has

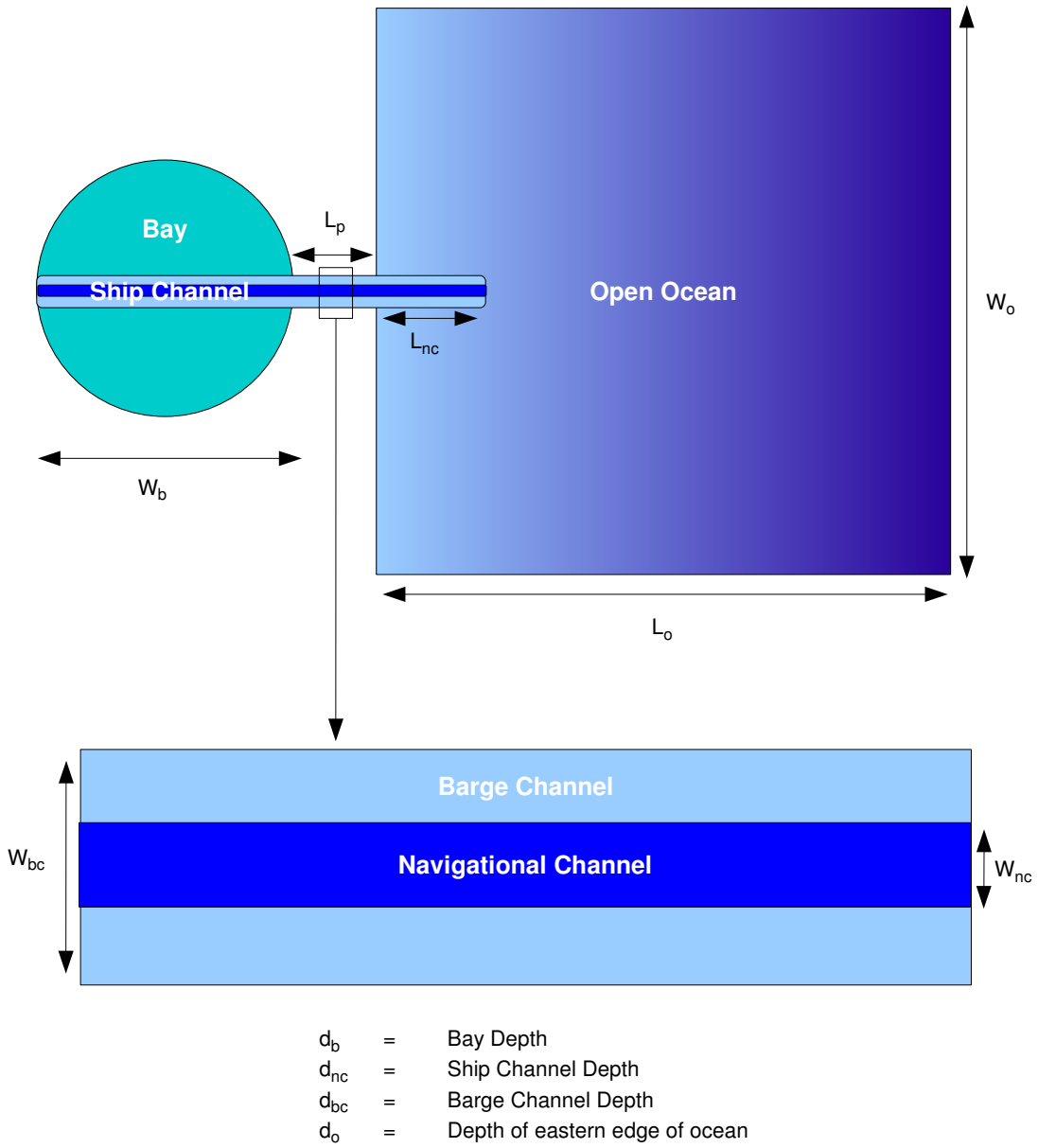

Figure A.1: Plan view of computational domain. Values of dimensional parameters are given in Table A.1

W_b	W_o	W_{bc}	W_{nc}	L_p	L_o
16000m	32000m	320m	160m	500m	24000m
D_b	D_o	D_{bc}	D_{nc}	**Tidal Amp.**	
3m	20m	4m	15m	0.22m	

Table A.1: Values of dimensional parameters in Figure A.1

a constant 3m depth except near the land boundaries where the depth slopes quadratically to zero. The ship channel consists of a central channel that is 160m wide and 15m deep surrounded by a barge channel that extends out to an overall width of 320m and a depth of 4m. The western end of the ship channel is sloped quadratically to zero depth at the land boundary. The ocean domain is 24000m long and 32000m wide. Its depth varies quadratically from 4m near the bay to 20m at the open ocean boundary. These dimensions are based on values characteristic of Texas bays (see Table 1.1) and the design dimensions of the Houston Ship Channel (see Figure 1.2) adjusted to be more convenient for grid generation. The ship channel geometry and bathymetry is shown in Figure A.1.

A.2.2 Forcing Terms

This work is focused on how wind-driven and tide-driven circulations are affected by a deep ship channel in a shallow embayment. Although an estuarine system has multiple physical forcing agents, we have chosen to explore two main agents, wind and tide, and the interaction between them. The following forcing conditions were used.

- Constant Wind : A constant wind of 7 m/s is applied over the whole domain. In the absence of any other forcing term this enables us to achieve

a steady state solution. A wind out of the southeast is used.

- Ideal Diurnal Wind : A ideal diurnal wind was developed based on field measurements taken in Corpus Christi Bay during August 2005. A simple cubic interpolation was chosen to generate the ideal wind based on a few points picked visually from a plot of the wind speed at various stations in the bay (see figure A.2). A wind out of the southeast is used. This forcing was applied over the entire domain.

- Sinusoidal Tide : The tides in many Texas bays are semi diurnal and have two peaks each day. A simple sinusoidally varying tide with a time period of 12 hours and an amplitude of 1 foot was used as a simple representative forcing. This forcing was applied at the open ocean boundary.

- Multiple Forcings : Two other cases are explored: 1) Combining constant wind with sinusoidal tide and 2) Combining diurnally-varying wind with sinusoidal tide.

The locations of the open boundary conditions and the direction of the wind on the test case are shown in Figure A.3. All unspecified boundaries in the figure are land boundaries.

A.2.3 Computational Grid

The domain developed above has been discretized into a computational grid consisting of triangular prisms. The horizontal extent of the domain was divided into triangular elements. These elements were projected down to form 3D prisms with parallel upper and lower faces. A series of increasingly refined grids was developed. The grid was refined in the horizontal by using smaller

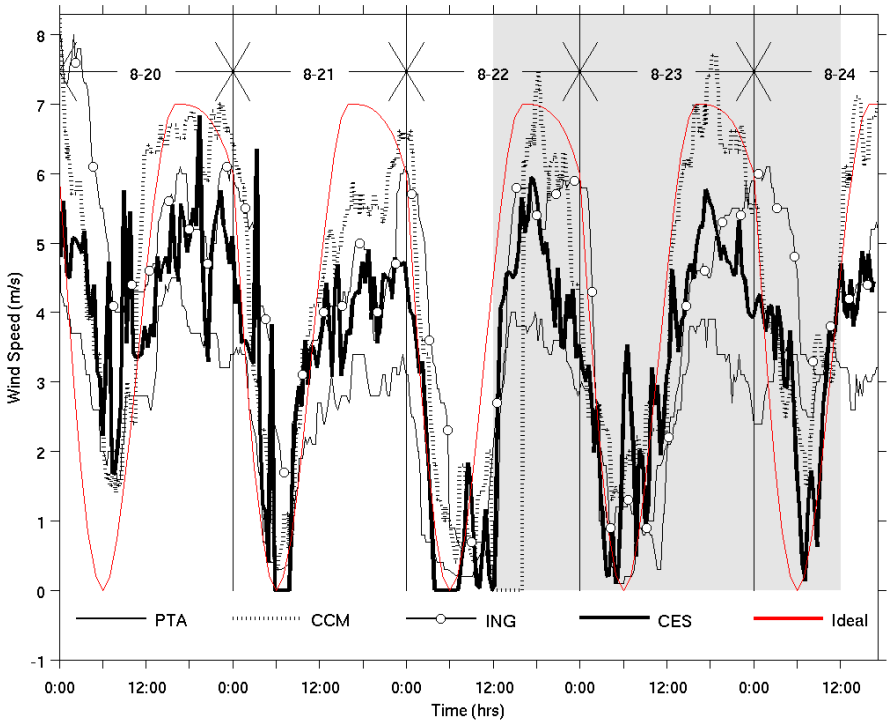

Figure A.2: Comparison of the derived ideal diurnal wind with 4 measurement stations.(PTA, CCM, ING and CES are measured winds at 4 stations located in Corpus Christi Bay. The red line is the derived ideal diurnal wind)

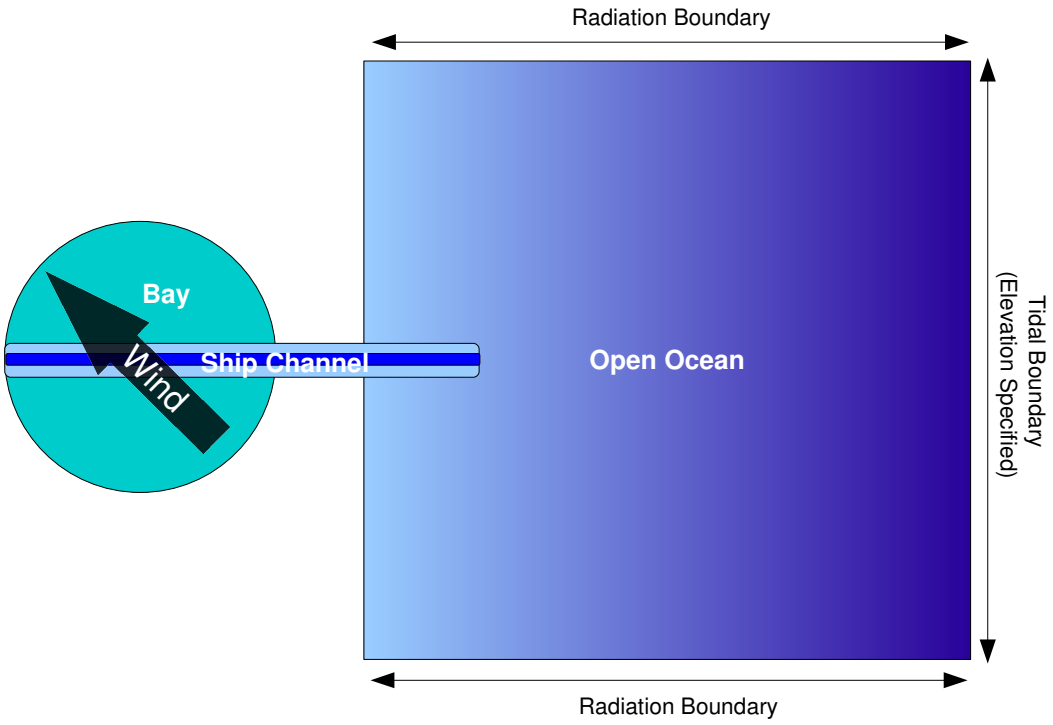

Figure A.3: Boundary Conditions

triangular elements. In the vertical, a series of layers defined over the entire domain split the prisms at fixed depths. The resolution of a given grid is characterized by two parameters: n_h is the number of elements across the ship channel and n_v is the number of vertical layers used above the ship channel depth. The horizontal element size increases with the distance from the ship channel so that the total number of grid cells is not prohibitively large. The vertical layers were uniformly-spaced at constant z levels until the depth of the ship channel was reached, after which a few larger layers were used to capture the deeper open ocean. The test cases were developed from the sets: $n_h = [1, 2, 4, 8, 16, 32]$, $n_v = [1, 2, 4, 8, 16, 32, 64, 128]$.

Once a grid was generated, bathymetry was interpolated from a generated high resolution dataset to the nodal points of the computational grid.

Figure A.4 shows the computational grid over the entire domain for $n_h = 1$. Figure A.5 shows how the grid across the ship channel changes as n_h increases from 1 to 32.

Note

As the level of grid resolution is increased, the level of physical parameter resolution can change. The scale of definition of bathymetry depends on the grid resolution [55]. At different grid resolutions the cross section of the ship channel as represented by the model can vary widely. To avoid complicating the convergence analysis, the 15m deep ship channel and 4m deep barge channel were combined into a single channel of equivalent width and an average depth of 9m.

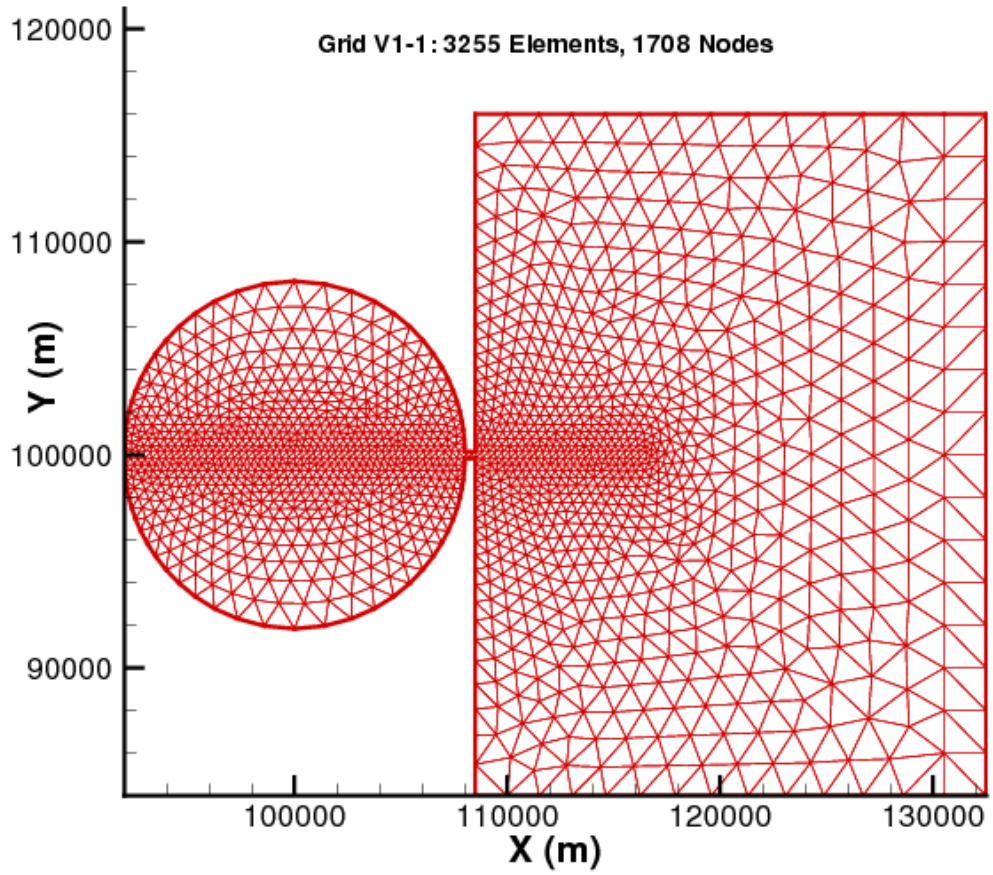

Figure A.4: Computational Grid with $n_h = 1$

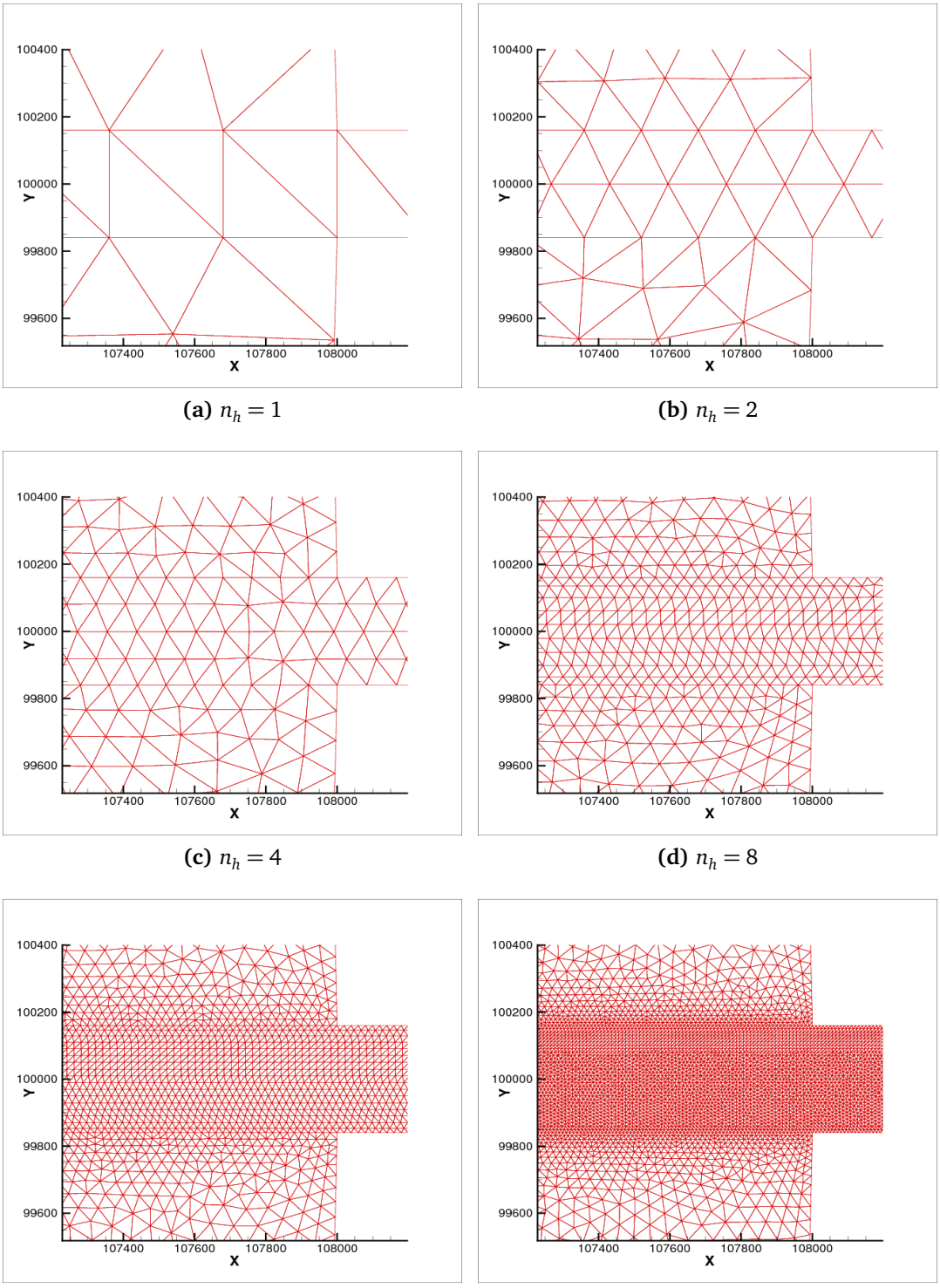

(a) $n_h = 1$ **(b)** $n_h = 2$

(c) $n_h = 4$ **(d)** $n_h = 8$

(e) $n_h = 16$ **(f)** $n_h = 32$

Figure A.5: Zoomed in section of computational grids showing the ship channel for $n_h = [1,2,4,8,16,32]$

A.2.4 Summary of Model Runs Conducted for Grid Resolution Tests

The ELCIRC hydrodynamic solver was used to conduct the numerical studies. Due to the prohibitive computational cost of using a grid with $n_h = 32$ and $n_v = 128$ (see section A.3), the initial convergence study was divided into a separate horizontal and vertical resolution study. Table A.2 shows the various model runs that were made. Simulations were conducted for 15 days with a 5 minute timestep and a 5 day ramp up period for tides. Coriolis forcing was turned off. Three turbulence closures were used:

1. Constant eddy-viscosity of 10^{-2},
2. Constant eddy-viscosity of 10^{-4},
3. and the Mellor-Yamada 2.5 closure scheme.

The results of our model runs are presented in the rest of this chapter.

A.3 Computational Cost

Using a fine resolution in the horizontal and vertical is computationally expensive. A series of simulations were conducted on an Intel Xeon 5160 3.00GHz processor with 2GB of memory to explore the increase in computational cost with increase of vertical and horizontal resolution. A 15 day time period was simulated. As we refine horizontally by increasing n_h from 1 to 32 while holding $n_v = 4$, the number of elements in the grid increases from 3255 to 246852 (see Figure A.6c) and the CPU time taken by the model increases from 3.5 minutes to 22 hours (see Figure A.6a). The increase in computational cost is a little lower than second order.

	n_h	Constant Wind	Semidiurnal Tide	Diurnal Wind + Semidiurnal Tide
full grid	1	1	1	1 2
	2	1	1	1
n_v=1	4	1	1	1
	8	1	1	1
	16	1	1	1
	32	1	1	1

	n_h	Constant Wind	Semidiurnal Tide	Diurnal Wind + Semidiurnal Tide
full grid	1	x	x	1
	2	x	x	1
n_v=4	4	x	x	1
	8	x	x	1
	16	x	x	1
	32	x	x	1

	n_v	Constant Wind	Semidiurnal Tide	Diurnal Wind + Semidiurnal Tide
full grid	1	1	1	1 2 3
	2	1	1	1 2 3
	4	1	1	1 2 3
	8	1	1	1 2 3
n_h=8	16	1	1	1 2 3
	32	1	1	1 2 3
	64	1	1	1 2 3
	128	1	1	1

	n_v	Constant Wind	Semidiurnal Tide	Diurnal Wind + Semidiurnal Tide
only bay	1	1 2 3	n.a	n.a
	2	1 2 3	n.a	n.a
	4	1 2 3	n.a	n.a
n_h=1	8	1 2 3	n.a	n.a
	16	1 2 3	n.a	n.a
	32	1 2 3	n.a	n.a
	64	1 2 3	n.a	n.a
	128	1 2 3	n.a	n.a

Table A.2: Summary of completed model runs. [1,2] indicate model runs conducted using the a constant eddy viscosity of $[10^{-2}, 10^{-4}]$ respectively. [3] indicates a model run conducted using the Mellor Yamada 2.5 turbulence closure model. [x] indicates that the run was not conducted and [n.a] indicated that it is not possible to conduct the run with the combination of boundary conditions. *full grid* refers to model runs conducted using the entire domain while *only bay* refers to runs that used grids that excluded the open ocean.

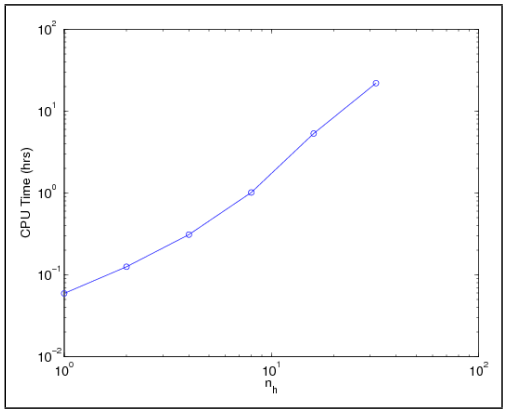

(a) Effect of increased horizontal resolution across ship channel on computational cost at $n_v = 4$. n_h is the number of elements across the channel and n_v is the number of vertical layers.

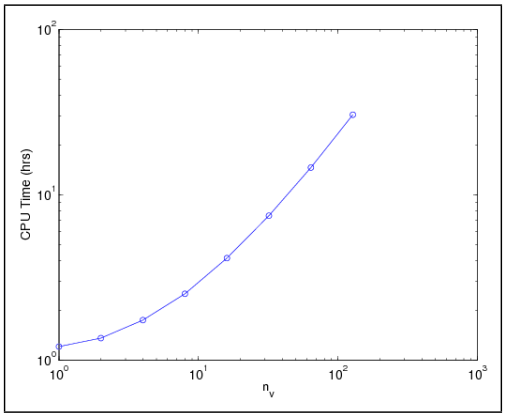

(b) Effect of increased vertical resolution on computational cost at $n_h = 8$. n_h is the number of elements across the channel and n_v is the number of vertical layers.

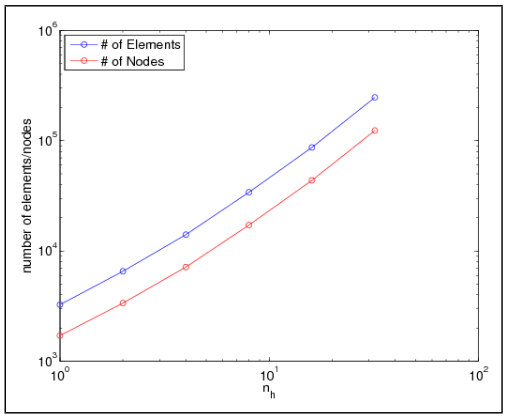

(c) Effect of increased horizontal resolution on number of elements and nodes in the computational grid, n_h is the number of elements across the ship channel.

Figure A.6: Effect of grid resolution on problem size and computational cost.

Increasing the vertical resolution from n_v from 1 to 128 while holding $n_h = 8$ increases the CPU time taken from 72 minutes to 30.5 hours (see figure A.6b). The computational cost increases linearly as n_v.

Extrapolating from figures A.6a and A.6b, we estimate that a $n_h = 32, n_v = 128$ grid would take approximately 30 days to run a 15 day simulation. An initial attempt to conduct a model run at this grid resolution met with failure due to machine limitations.

A.4 Effect of horizontal grid resolution

In this section we present results from the horizontal grid resolution tests. The horizontal grid was refined by increasing n_h from 1 to 32. The model runs were conducted at two different vertical resolutions, $n_v = 1$ and $n_v = 4$. Initial studies were done with a single vertical layer ($n_v = 1$) and it was found that while the effect of increasing the horizontal grid resolution was discernible, the 2D flow approximation greatly reduced both the magnitude of the flow through the ship channel and its dependence on horizontal grid resolution. The choice of turbulence closure had a large effect on the wind-driven surface flow, especially the y(cross-channel) velocity. These issues are explored in more detail in section A.5, The results presented in this section are from the model runs with $n_v = 4$ using a constant eddy viscosity of 10^{-2} for turbulence closure.

For brevity, we present only the results from the model runs forced with both the ideal diurnal wind and the sinusoidal tide. The results from the model runs using other forcing combinations follow the same general trend. Results are compared qualitatively by plotting velocity and sea surface elevation at three stations (figure A.7). The stations include a site in the center of the ship chan-

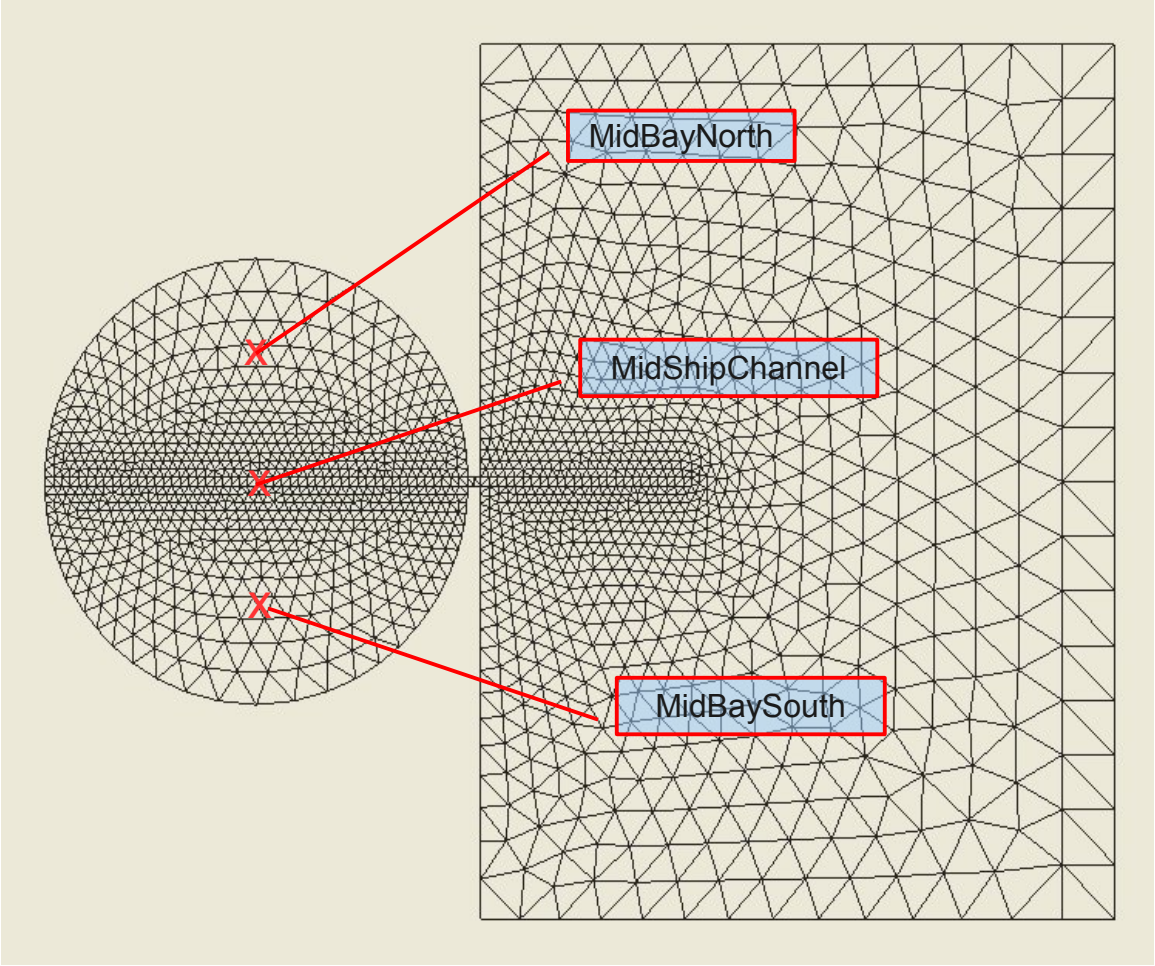

Figure A.7: Station locations at which comparisons were made.

nel, a site in the middle of the northern half of the bay and a site in the middle of the southern half of the bay called MidShipChannel, MidBayNorth and MidBaySouth respectively. An error analysis is presented in section A.4.2. The model runs using the finest horizontal grid ($n_h = 32$,$n_v = 4$) were used as representative of the true solution.

A.4.1 Station Comparisons

Figure A.8 compares the sea surface elevation at the three stations at different horizontal grid resolutions. The effect of horizontal grid resolution on sea surface elevation is minor with a maximum error of less than 5cm.

Figure A.9 compares the x(along-channel) velocity at the three stations at different horizontal grid resolutions. Comparing the graphs, we can see that away from the ship channel (figures A.9a and A.9c) the change in horizontal grid resolution has little effect. However, at the station in the middle of the ship channel (figure A.9b) the error between the $n_h = 1$ grid and the $n_h = 32$ grid can be as high as 0.45m/s. Inspecting figure A.9b we can visually determine that for $n_h = 8$ and above the solution is close to the fine grid solution.

Figure A.10 compares the y velocity at the three stations at different horizontal grid resolutions. Comparing the graphs, we can see that away from the ship channel (figures A.10a and A.10c) the change in horizontal grid resolution has little effect. The differences in velocity are of the order of 1cm/s at the peaks. The station in the middle of the ship channel also shows small differences(Figure A.10b) but also shows some some spurious oscillations on the higher resolution grids. It is surmised that the timestep used (5 minutes) is too large for these high resolution cases. In section A.5 where we explore the effect of vertical grid resolution and turbulence closure models, we see more

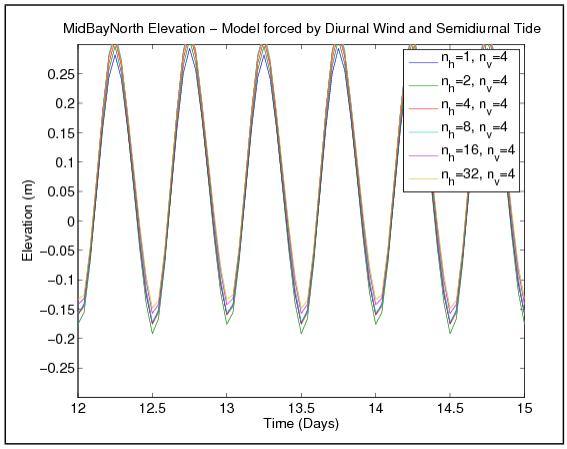

(a) Sea Surface Elevation at MidBayNorth Station

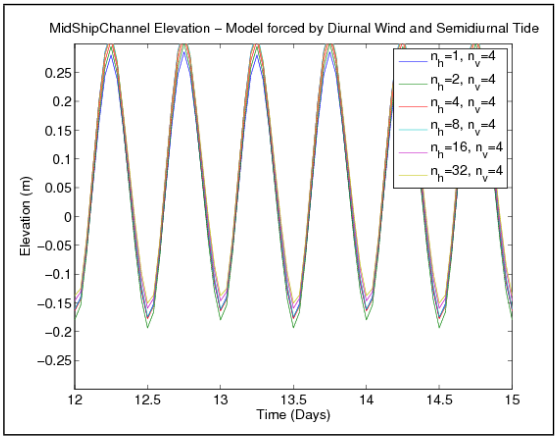

(b) Sea Surface Elevation at MidShipChannel Station

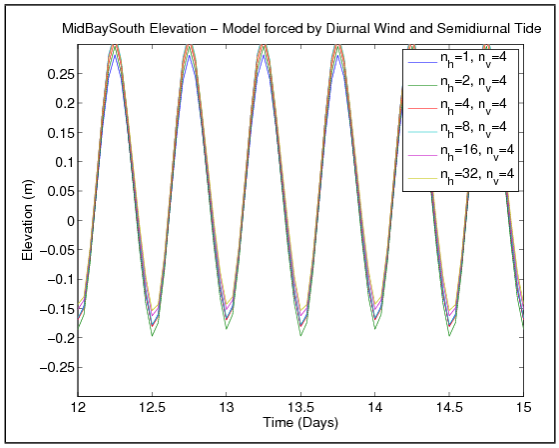

(c) Sea Surface Elevation at MidBaySouth Station

Figure A.8: Comparison of sea surface elevation at three stations at horizontal grid resolutions $n_h \in (1, 2, 4, 8, 16, 32)$ and four vertical layers n_v=4. Model run forced with ideal diurnal wind and sinusoidal tide. Constant eddy viscosity of 10^{-4} used for Turbulence Closure

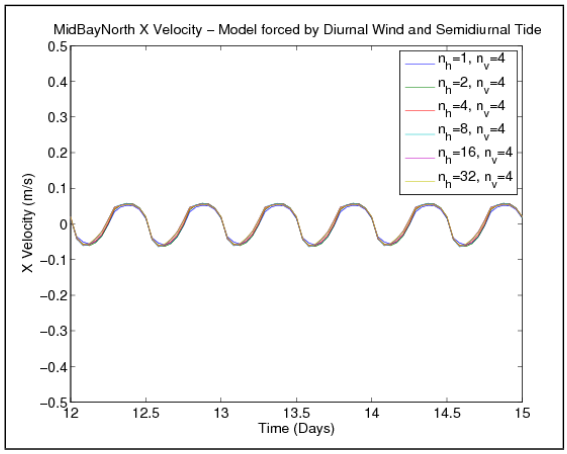

(a) x Velocity at MidBayNorth Station

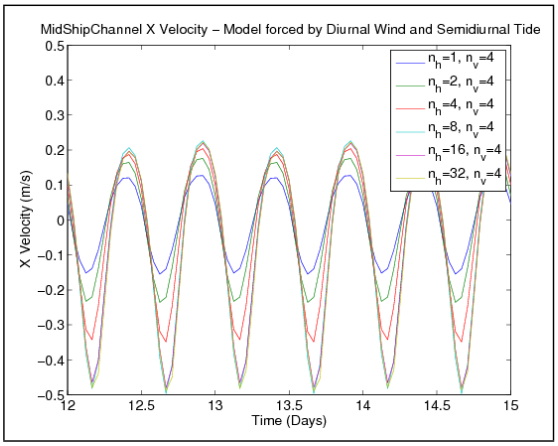

(b) x Velocity at MidShipChannel Station

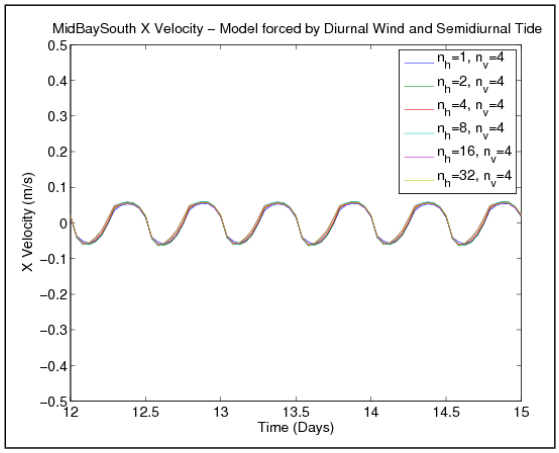

(c) x Velocity at MidBaySouth Station

Figure A.9: Comparison of x component of velocity at three stations at horizontal grid resolutions $n_h \in (1, 2, 4, 8, 16, 32)$ and four vertical layers n_v=4. Model run forced with ideal diurnal wind and sinusoidal tide. Constant eddy viscosity of 10^{-4} used for Turbulence Closure

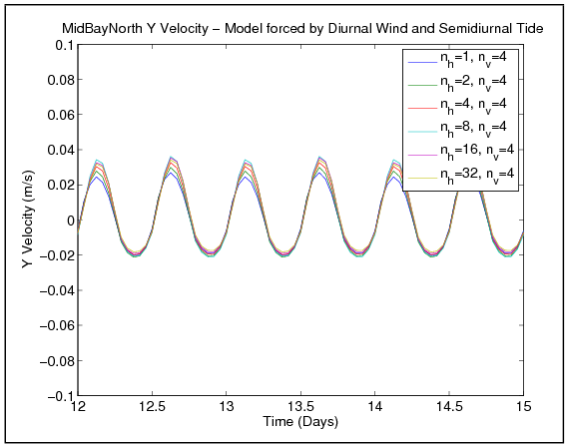

(a) y Velocity at MidBayNorth Station

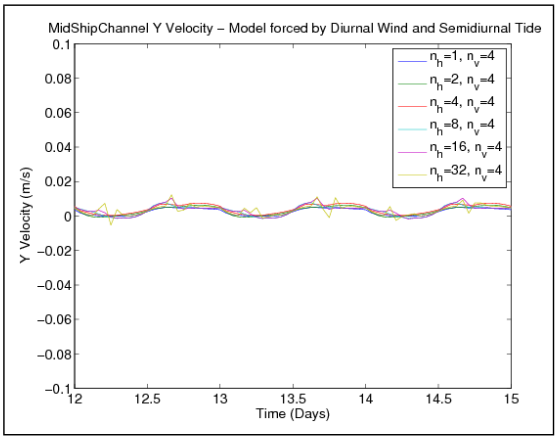

(b) y Velocity at MidShipChannel Station

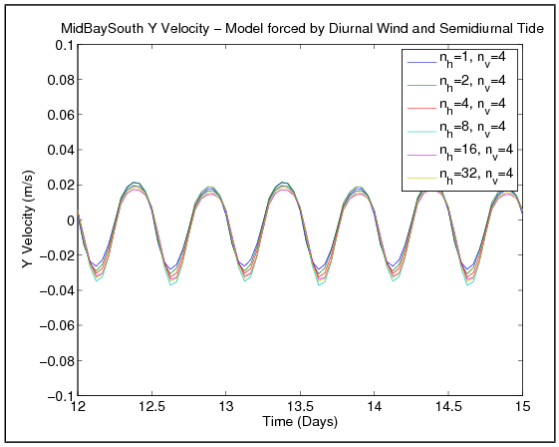

(c) y Velocity at MidBaySouth Station

Figure A.10: Comparison of y component of velocity at three stations at horizontal grid resolutions $n_h \in (1, 2, 4, 8, 16, 32)$ and four vertical layers n_v=4. Model run forced with ideal diurnal wind and sinusoidal tide. Constant eddy viscosity of 10^{-4} used for Turbulence Closure

model runs in which these oscillations occur. From the experience gained from the vertical grid resolution tests we expect that with the use of a more appropriate turbulence model and sufficient vertical grid resolution, we will see a much greater dependence of y velocity on the horizontal grid resolution.

A.4.2 Error Analysis

Looking at figures A.8 through A.10 we see that the changes in horizontal grid resolution do not affect the phase of the quantities we are comparing. Also, the differences are most pronounced at the peaks and troughs of the signal, and after the initial 5 day ramp up period the signals are regular. Based on these observations, we choose to define an error norm based on the maximum error over a 5 day period from day 10 to day 15 of the simulation. The solution on the n_h=32, n_v=4 grid is taken as the *true* solution.

Figure A.11 shows the reduction in error with increasing horizontal resolution. The largest error occurs in the x velocity at the MidShipChannel station. Looking at how this error reduces in Figure A.11b, n_h=8 seems to be a resolution at which the model is captures the flow reasonable well.

A.5 Effect of vertical grid resolution

In this section we present preliminary results from the vertical grid resolution tests. The vertical grid was refined by increasing n_v from 1 to 64. The model runs were conducted at a horizontal resolution of $n_h = 8$ and with a variety of turbulence closures.

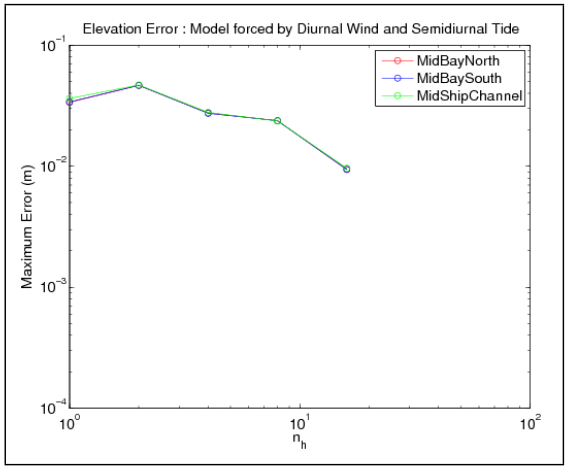

(a) Change in error in sea surface elevation with increasing horizontal grid resolution

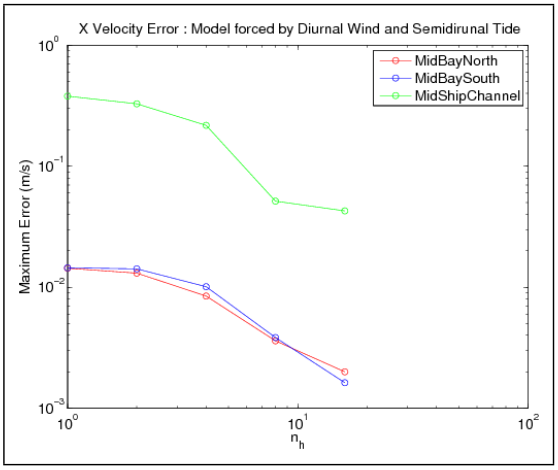

(b) Change in error in x velocity with increasing horizontal grid resolution

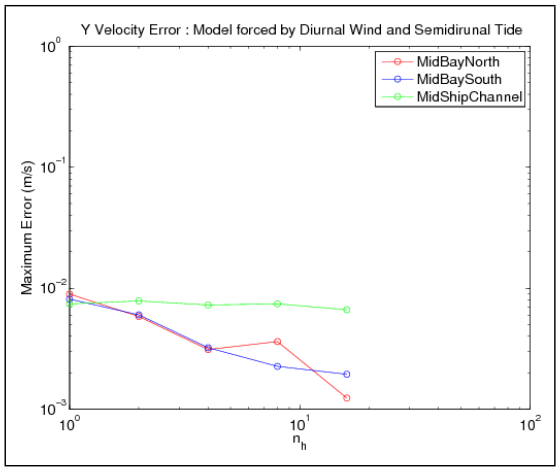

(c) Change in error in y velocity with increasing horizontal grid resolution

Figure A.11: Maximum error over days 10 to 15 at horizontal grid resolution $n_h \in (1, 2, 4, 8, 16)$ and four vertical layers n_v=4. The solution on the grid n_h=32,n_v=4 is used as the fine grid *true* solution. Model run forced with ideal diurnal wind and sinusoidal tide. Constant eddy viscosity of 10^{-4} used for Turbulence Closure

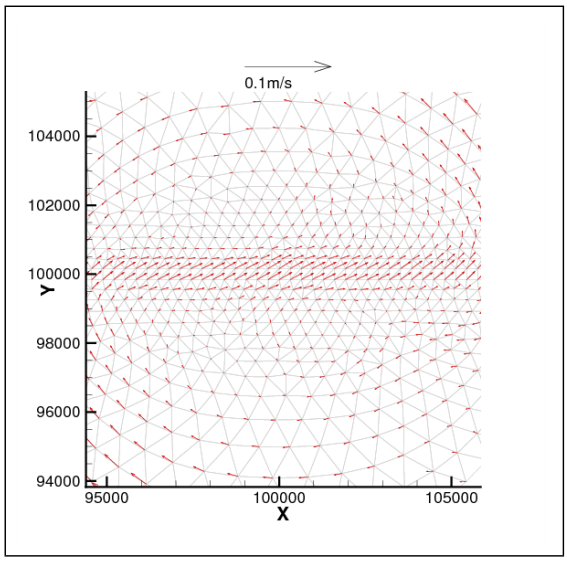

(a) Turbulence Closure Model : Constant eddy viscosity 10^{-2}

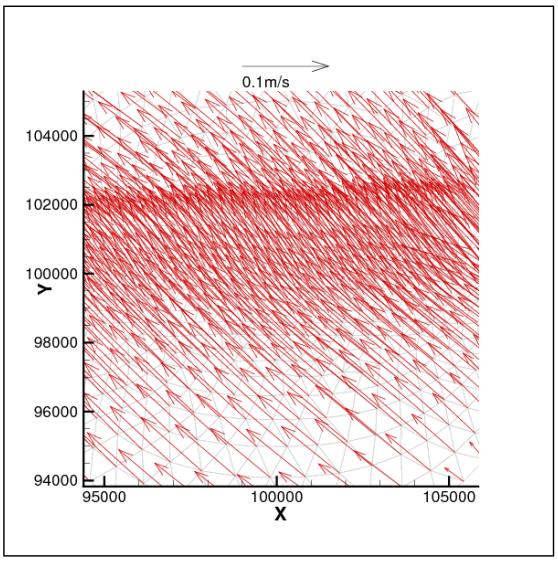

(b) Turbulence Closure Model : Constant eddy viscosity 10^{-4}

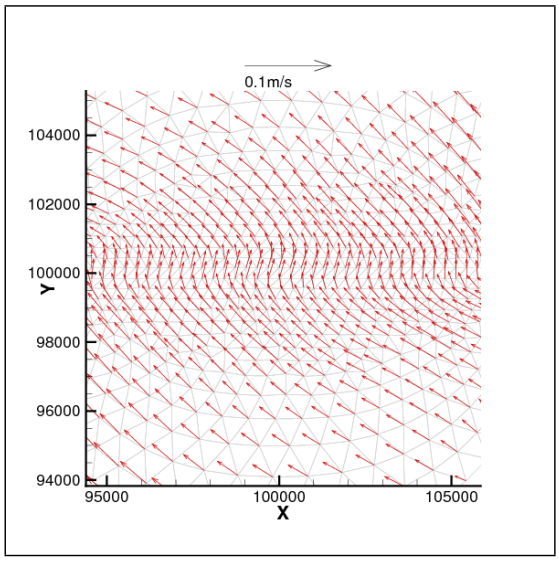

(c) Turbulence Closure Model : Mellor-Yamada 2.5

Figure A.12: Reduced domain bay grid with n_h=1, n_v=16. Model run forced by a constant South East wind of 7m/s. The Surface layers are shown for three different turbulence closures.

A.5.1 Turbulence Closure

It was found that the solution was highly dependent on the choice of turbulence closure model. In hindsight this is expected since the turbulence closure determines how deep the effects of the surface wind stress penetrate. Runs were made using a constant eddy viscosity of 10^{-2}, 10^{-2} and the Mellor Yamada 2.5 (MY2.5) closure scheme[38]. Because of the importance of the choice of turbulence closure we discuss its effect before we discuss the results of the vertical grid resolution tests.

A series of model runs were conducted on a reduced grid that only included the bay portion of the domain, the open ocean was excluded. These runs were forced by a constant wind of 7m/s from the southeast. The use of this forcing allows the model to reach a steady state. Figure A.12 shows the surface circulation of a set model runs with $n_h = 1$, $n_v = 16$ using each of the three turbulence closures.

When using a constant eddy viscosity equal to 10^{-2}, the surface circulation is strongly influenced by the presence of the ship channel (figure A.12a). When a constant eddy viscosity equal to 10^{-4} or the MY2.5 closure scheme are used the surface circulation is less influenced by the ship channel and is predominantly wind driven (figure A.12a and A.12c).

Repeating this analysis with the computational grids that encompass the entire domain met with difficulty. At higher vertical resolutions the solutions for the second two turbulence closures experienced spurious oscillations and in some cases catastrophic failures (see figure A.13 for an example of oscillations in y velocity when using MY2.5). These oscillations are not present when a lower horizontal grid resolution ($n_h = 1$) is used. It is thought that at the higher

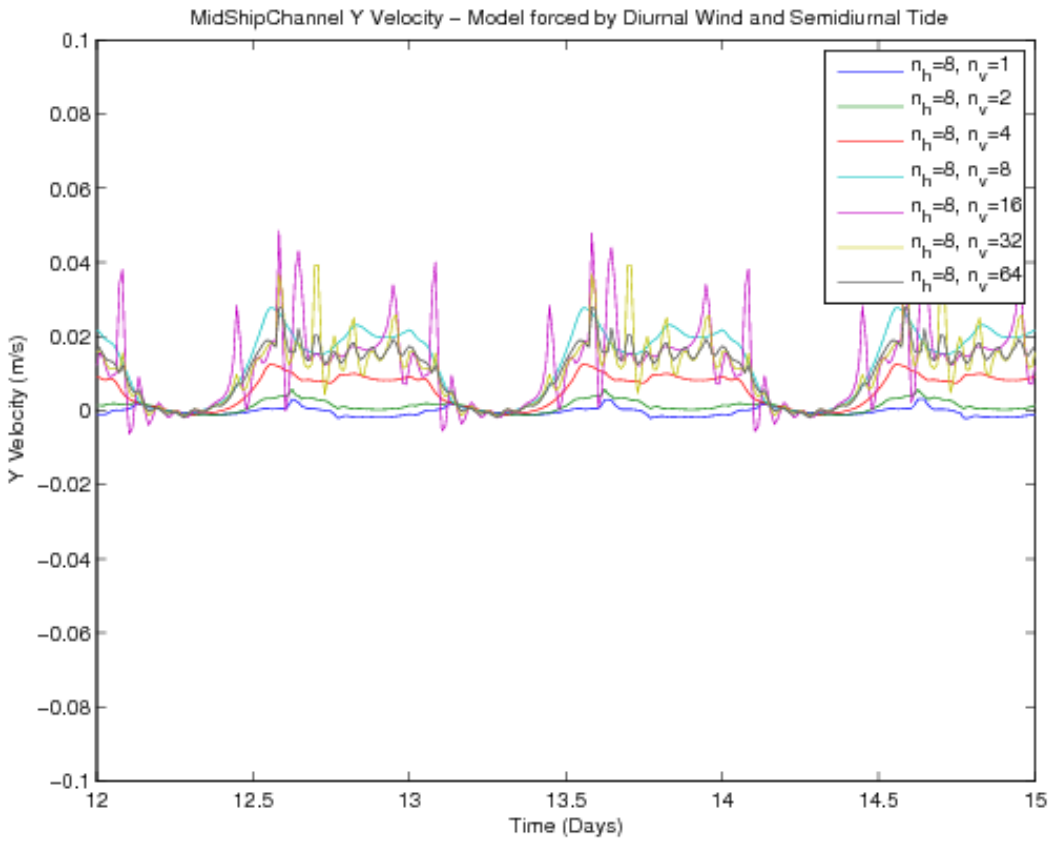

Figure A.13: Demonstration of spurious oscillations in Y velocity when using MY2.5 turbulence closure with n_h=8, $n_v \in (1, 2, 4, 8, 16, 32, 64)$

resolution the timestep used for the model runs is too large. This hypothesis is being explored at present.

A.5.2 Station Comparisons

Due to the instabilities when using other turbulence closure schemes the results presented in this section are for runs made with a constant eddy viscosity equal to 10^{-2}. With this choice of turbulence closure the effect of the wind on the bay circulation is minimal. Even so, the increasing vertical resolution has a significant effect on the sea surface elevations and the x velocity.

Examining figures A.14 through A.16 we see that the effect of increasing vertical grid resolution can be seen in the sea surface elevation and both the x and y velocities. At all three stations, the maximum errors in sea surface elevation is approximately 15cm (figure A.14). For x velocities at the stations away from the channel (figure A.15a,A.15c) the maximum error is approximately 0.05m/s while at the ship channel(Figure A.15b) it is an order of magnitude higher at over 0.5m/s. For y velocities at the stations away from the channel (figure A.16a,A.16c) the maximum error is approximately 0.02m/s while at the ship channel(Figure A.16b) we see instabilities in the solution at the higher resolutions.

A.5.3 Surface Circulation Patterns

In this section we present some qualitative comparisons of surface circulation patterns at different vertical resolutions. The set of model runs used for this comparison used a constant eddy viscosity of 10^{-2} and a horizontal resolution of $n_h = 1$. The runs were forced by an ideal diurnal wind and a semi diurnal sinusoidal tide. The vertical resolution had significant impact on surface circu-

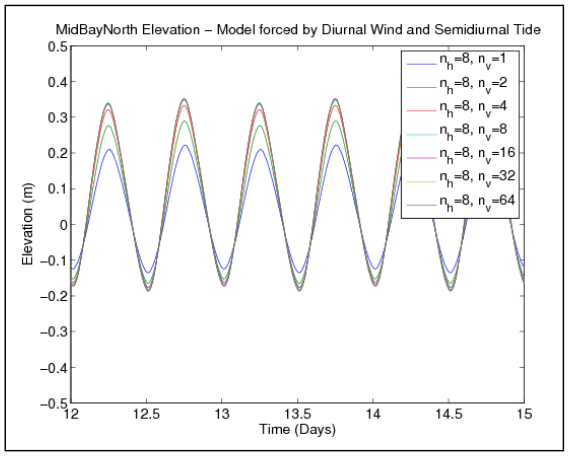

(a) Sea Surface Elevation at MidBayNorth Station

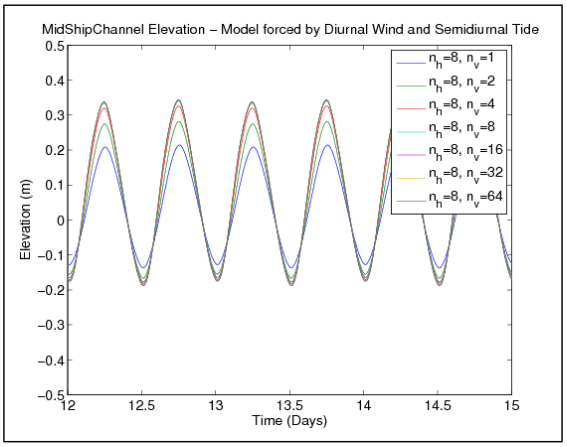

(b) Sea Surface Elevation at MidShipChannel Station

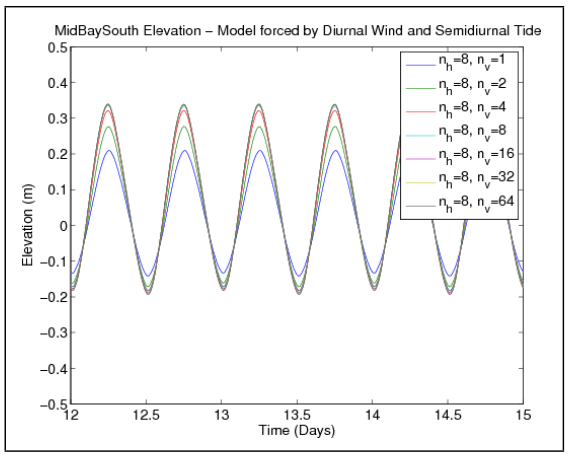

(c) Sea Surface Elevation at MidBaySouth Station

Figure A.14: Comparison of Sea Surface Elevation at three stations at vertical grid resolutions $n_v \in (1, 2, 4, 8, 16, 32, 64)$ and n_h=8. Model run forced with ideal diurnal wind and semi diurnal tide. Constant eddy viscosity of 10^{-2} used for Turbulence Closure

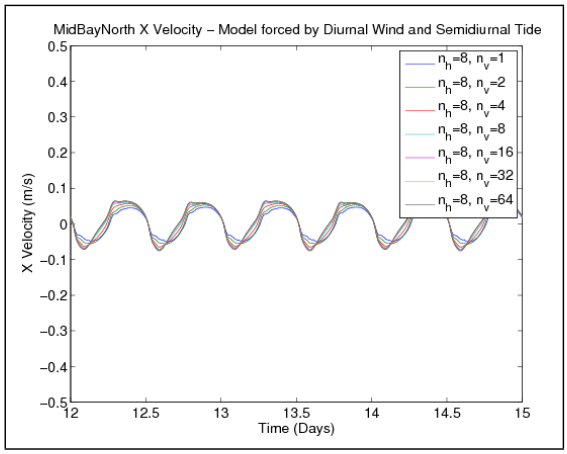

(a) x Velocity at MidBayNorth Station

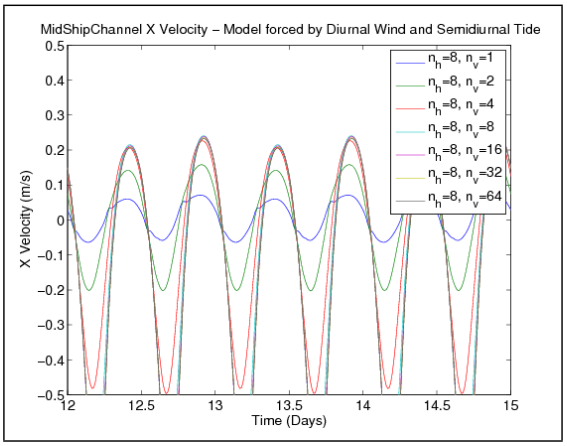

(b) x Velocity at MidShipChannel Station

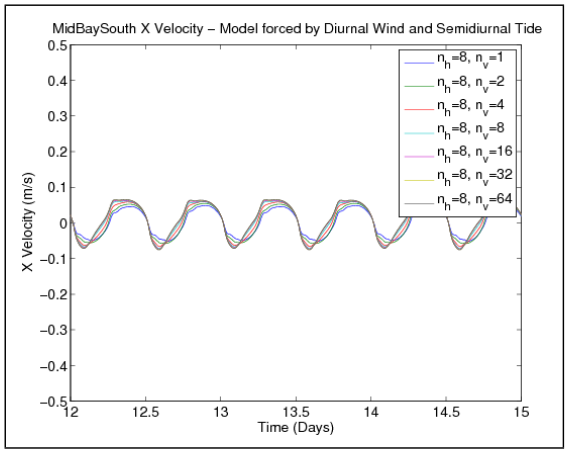

(c) x Velocity at MidBaySouth Station

Figure A.15: Comparison of x velocity at three stations at vertical grid resolutions $n_v \in (1, 2, 4, 8, 16, 32, 64)$ and n_h=8. Model run forced with ideal diurnal wind and semi diurnal tide. Constant eddy viscosity of 10^{-2} used for Turbulence Closure

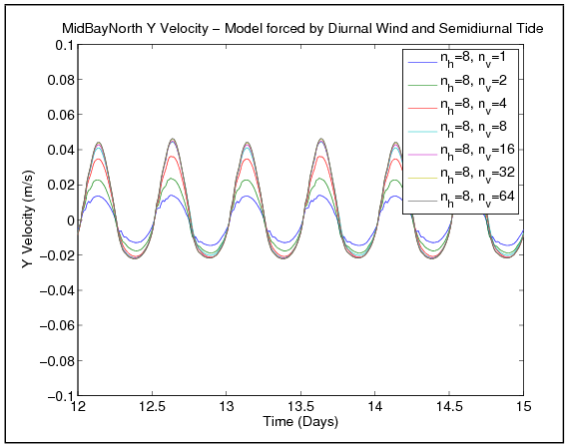

(a) y Velocity at MidBayNorth Station

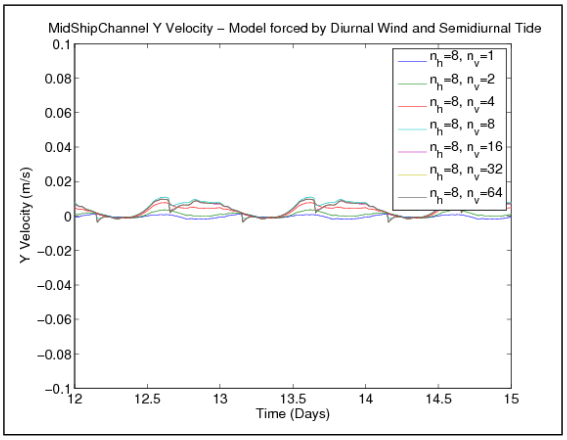

(b) y Velocity at MidShipChannel Station

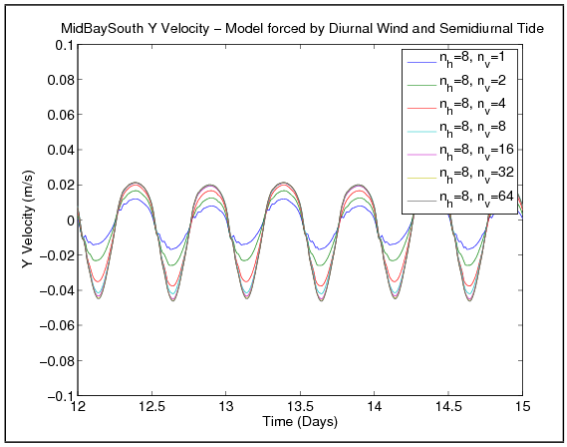

(c) y Velocity at MidBaySouth Station

Figure A.16: Comparison of y velocity at three stations at vertical grid resolutions $n_v \in (1, 2, 4, 8, 16, 32, 64)$ and n_h=8. Model run forced with ideal diurnal wind and semi diurnal tide. Constant eddy viscosity of 10^{-2} used for Turbulence Closure

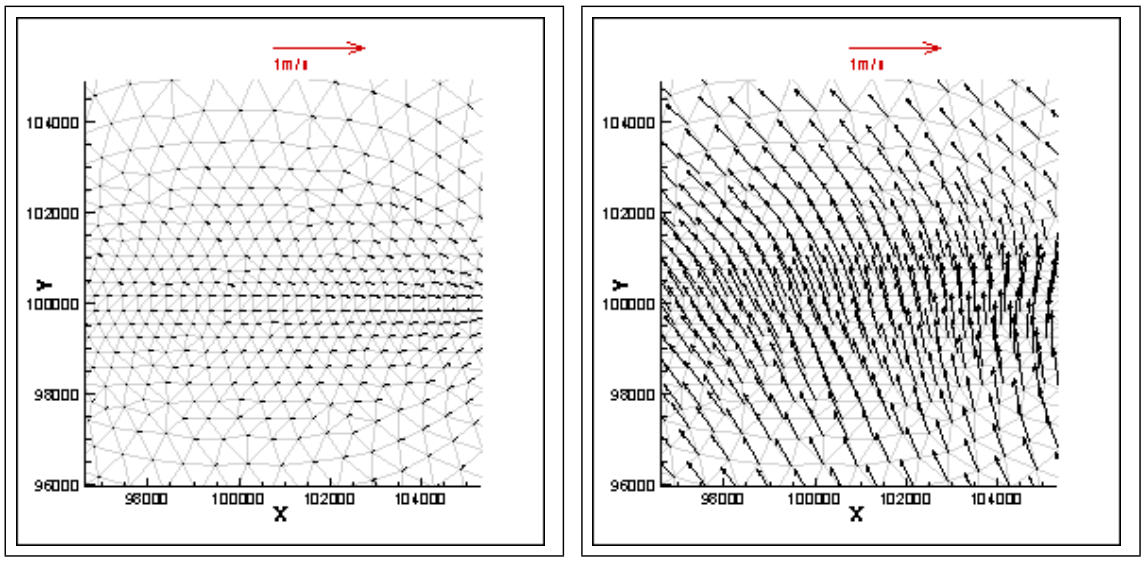

(a) Surface Circulation with n_v=1 **(b)** Surface Circulation with n_v=32

Figure A.17: Comparison of surface circulation patterns at different vertical grid resolutions n_v=1 and n_v=32 with n_h=1. Model run forced with ideal diurnal wind and semi diurnal tide. Constant eddy viscosity of 10^{-4} used for Turbulence Closure

lation patterns. In Figure A.17 we see that at a low vertical resolution($n_v = 1$) the surface flow was weak and near the channel it flowed along the channel direction. At a higher resolution($n_v = 32$), the surface layer was less influenced by tidal flow in the channel and was driven in the direction of the wind. The magnitude of the velocities are also much greater.

A.5.4 Comparison between Surface and Bottom layer flow

In this section, we show qualitatively the 3D nature of the flow in the shallow bay. We use the same set of model runs that were described in the previous section.

The bidirectional nature of the flow field in the shallow bay can be seen in figure A.18. The surface circulation and the bay bottom circulation are shown in the area close to the center of the shallow bay. The surface velocity field is driven along the direction of the wind and is fairly strong. The bottom velocity field is in the reverse direction and is weaker. The flow inside the portion of the ship channel below the bay depth is oscillatory and parallel to its walls (A.18c).

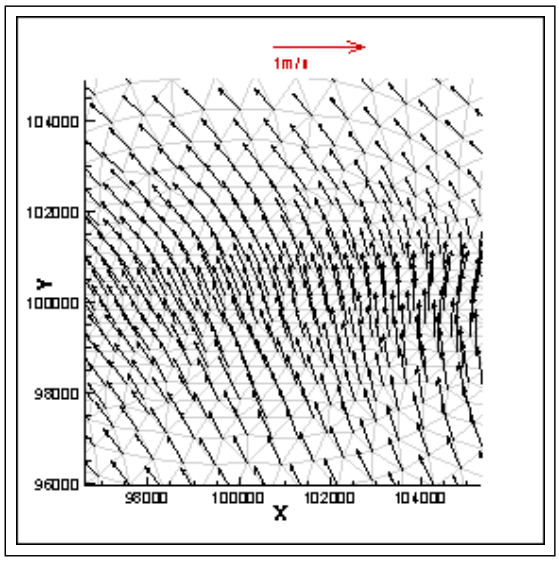

(a) Surface Circulation with n_v=32

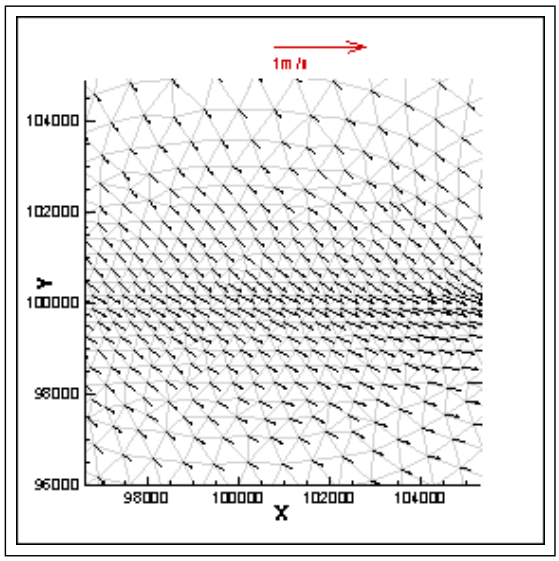

(b) Shallow Bay Bottom Circulation with n_v=32

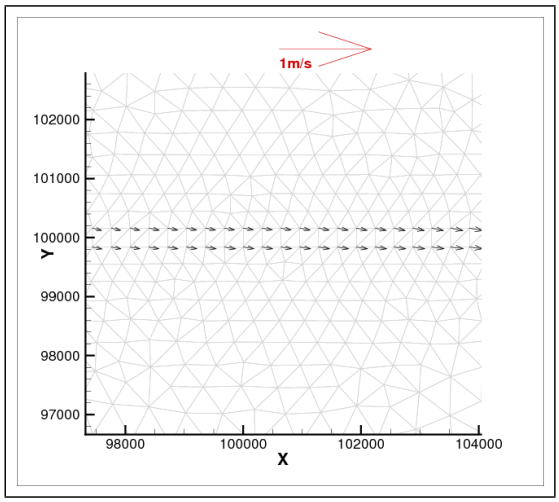

(c) Ship Channel Bottom Circulation with n_v=32

Figure A.18: Comparison of surface and bottom layer circulation patterns at vertical grid resolution n_v=32 with n_h=1. The shallow bay bottom layer shown is just above the top of the ship channel. Model run forced with ideal diurnal wind and semi diurnal tide. Constant eddy viscosity of 10^{-4} used for Turbulence Closure

A.6 Discussion

The convergence analysis presented in this chapter is by no means complete. More research is required to explore the full extent of the effect of grid resolution on wind and tide forced circulation. In particular it will be necessary to choose a suitable timestep and turbulence closure model for the vertical grid resolution tests. Also, a more complete error analysis is required to quantify some of the qualitative observations we have made.

However, based on the work completed to date and presented in this chapter, we make the following statements:

- Using a high resolution in the horizontal and vertical is computationally expensive.
- Insufficient horizontal resolution causes significant errors in the velocity field near the ship channel.
- Insufficient vertical resolution causes significant errors in both the elevation and velocity field.
- The flow regime is 3D in nature.
- A single layer (or 2D) model is inadequate to model a shallow bay-ship channel system.
- Choice of turbulence model has a strong effect on surface circulation patterns

Appendix B

Source Code Description

Filename	Description
elfe1_5k7_dp.f90	SELFE Version 1.5k7 with modified boundary conditions
dsrc2c.f90	SELFE Version 1.5k7 solver routines
lacm_globals.f90	LACM global variable declarations
lacm_interface.f90	LACM time stepping and interface routines
lacm_io.f90	LACM input/output routines
lacm_transform.f90	LACM coordinate transformation and interpolation routines

Table B.1: List of FORTRAN files that make up the LACM-SELFE Multi-model

Bibliography

[1] *Water for texas*, Texas Water Development Board, 2007.

[2] V. Aizinger, *A discontinuous galerkin method for two- and three-dimensional shallow-water equations*, Ph.D. thesis, University of Texas at Austin, 2004.

[3] V. Aizinger, C. Dawson, B. Cockburn, and P. Castillo, *The local discontinuous galerkin method for contaminant transport*, Advances in Water Resources **24** (2001), 73–87.

[4] M. Amara, D. Capatina, and D. Trujillo, *Hydrodynamical modelling and mutidimensional approximation of estuarian river flows*, Monografias del Seminario Matematico Garcia de Galdeano **27** (2003), 41–48.

[5] R.C. Berger, R.T. McAdory, J.H. Schmidt, and W.D. Martin, *Houston-galveston navigational channels, texas project; three-dimensional numerical modeling of hydrodynamics and salinity, rpt. hl-92-7*, Tech. report, U.S. Army Corps of Engineers, Waterways Experiment Station, Vicksburg, MS, 1995.

[6] A. F. Blumberg, *Numerical model of estuarine circulation*, Journal of the Hydraulics Division, American Society of Civil Engineers **103** (March 1977), 295–310.

[7] D. Bourgault and Dan E. Kelley, *A laterally averaged nonhydrostatic ocean model*, Journal of Atmospheric and Oceanic Technology **Volume 21, Issue 12** (2004), 1910–1924.

[8] J. Burroughes and K. George, *Automation of interpolation by zoned inverse distance weighting for linearly distribution of soundings*, GeoCoast **2** (2001), no. 1, 16–35.

[9] E. Burroughes J. and George K., *Interpolation of hydrographic survey data*, The Hydrographic Journal **99** (2001), 21–29.

[10] C. S. Chen, H. D. Liu, and R. C. Beardsley, *An unstructured grid, finite-volume, three-dimensional, primitive equations ocean model: Application to coastal ocean and estuaries*, Journal Of Atmospheric And Oceanic Technology **20** (2003), no. 1, 159–186.

[11] Q. Chen, H. Zhao, K. Hu, and S. L. Douglass, *Prediction of wind waves in a shallow estuary.*, Journal of Waterway, Port, Coastal & Ocean Engineering **131** (2005), no. 4, 137–148.

[12] C. A. Coclici and W. L. Wendland, *Analysis of a heterogeneous domain decomposition for compressible viscous flow*, Mathematical Models and Methods in Applied Science **11** (2001), no. 4, 565–599.

[13] C. J. Dallimore, B. R. Hodges, and J. Imberger, *Coupling an underflow model to a three-dimensional hydrodynamic model*, Journal of Hydraulic Engineering **129** (2003), no. 10, 748–757.

[14] M. deCastro, M. Gomez-Gesteira, R. Prego, J. J. Taboada, P. Montero, P. Herbello, and V. Perez-Villar, *Wind and tidal influence on water circulation in a galician ria (nw spain)*, Estuarine Coastal And Shelf Science **51** (2000), no. 2, 161–176.

[15] M. Kreienmeyer E. Stein, *Coupling of bem and fem by a multiplicative schwarz method and its parallel implementation*, Engineering Computations **15** (1998), no. 2, 173 – 189.

[16] L. Fatone, P. Gervasio, and A. Quarteroni, *Multimodels for incompressible flows*, J. math. fluid mech. **2** (2000), 126–150.

[17] Harte Research Institute for Gulf of Mexico Studies, *Gulfbase: Facts about gulf bays and estuaries*, World Wide Web electronic publication, 2006.

[18] M. Ford, J. Wang, and R. T. Cheng, *Predicting the vertical structure of tidal current and salinity in san francisco bay, california*, Water Resour. Res. **26(5)** (1990), 1027–1045.

[19] J Furnans, *Exploring hydrodynamic modeling of texas bays with a focus on corpus christi and lavaca bay*, C.r.w.r. online report 04-03, Center for Research in Water Resources, The University of Texas at Austin, 2004.

[20] J. A. Goff and S. Nordfjord, *Interpolation of fluvial morphology using channel-oriented coordinate transformation: A case study from the new jersey shelf*, Mathematical Geology **36** (2004), no. 6, 643–658.

[21] David A. Greenberg, Frederic Dupont, Florent H. Lyard, Daniel R. Lynch, and Francisco E. Werner, *Resolution issues in numerical models of oceanic and coastal circulation*, Continental Shelf Research **27** (2007), no. 9, 1317–1343.

[22] Ming-Hsi Hsu, Albert Y. Kuo, Jan-Tai Kuo, and Wen-Cheng Liu, *Procedure to calibrate and verify numerical models of estuarine hydrodynamics*, Journal of Hydraulic Engineering **125** (1999), no. 2, 166–182.

[23] TWDB Coastal Hydrology, *http://hyper20.twdb.state.tx.us/data/bays_estuaries/hydrologypage.html*, World Wide Web electronic publication, 2006.

[24] J Kachtick, *The galveston bay plan*, Tech. report, Galveston Bay National Estuary Program, 1995.

[25] K. Kawanisi, *Structure of turbulent flow in a shallow tidal estuary*, Journal Of Hydraulic Engineering-Asce **130** (2004), no. 4, 360–370.

[26] I. Kinnmark, *The shallow water wave equations: formulations, analysis and application*, Lecture Notes in Engineering (C.A. Brebbia and S.A. Orszag, eds.), Springer-Verlag, 1985.

[27] Nicolai Kliem and David Greenberg, *Diagnostic simulations of the summer circulation in the canadian arctic archipelago*, ATMOSPHERE-OCEAN **41** (2003), no. 4, 273–289.

[28] John M. Klinck, Eileen E. Hofmann, Eric N. Powell, and Margaret M. Dekshenieks, *Impact of channelization on oyster production: a hydrodynamic-oyster population model for galveston bay, texas*, Environmental Modeling and Assessment **7** (2002), 273–289.

[29] Nicholas C. Kraus and Adele Militello, *Hydraulic study of multiple inlet system: East matagorda bay, texas.*, Journal of Hydraulic Engineering **125** (1999), no. 3, 224–.

[30] Rajendra G. Kurup, David P. Hamilton, and Robert L. Phillips, *Comparison of two 2-dimensional, laterally averaged hydrodynamic model applications to the swan river estuary*, Mathematics and Computers in Simulation **51** (2000), no. 6, 627–638.

[31] B. Laval, J. Imberger, and A. N. Findikakis, *Mass transport between a semienclosed basin and the ocean: Maracaibo system*, J. Geophys. Res. **108** (2003), 27.1–27.18.

[32] M. Li, L. J. Zhong, and W. C. Boicourt, *Simulations of chesapeake bay estuary: Sensitivity to turbulence mixing parameterizations and comparison with observations*, Journal Of Geophysical Research-Oceans **110** (2005), no. C12, C12004.

[33] W. C. Liu, M. H. Hsu, and A. Y. Kuo, *Application of different turbulence closure model for stratified tidal flows and salinity in an estuarine system*, Mathematics And Computers In Simulation **59** (2002), no. 5, 437–451.

[34] Jr. Luettich, R. A.. and J. J. Westerink, *Quantitative skill assessment for coastal ocean models, coastal estuarine studies, vol. 47*, vol. 47, ch. Continental Shelf Scale Convergence Studies with a Barotropic Tidal Model, pp. 349–371, AGU, Washington, D. C., 1995.

[35] Daniel R. Lynch and Francisco E. Werner, *Three-dimensional hydrodynamics on finite elements. part i: Linearized harmonic model*, International Journal for Numerical Methods in Fluids **7** (1987), no. 9, 871–909.

[36] ———, *Three-dimensional hydrodynamics on finite elements. part ii: Nonlinear time-stepping model*, International Journal for Numerical Methods in Fluids **12** (1991), no. 6, 507–533.

[37] Daniel R. Lynch, Francisco E. Werner, Jean Marc Molines, and Marianela Fornerino, *Tidal dynamics in a coupled ocean/lake system*, Estuarine, Coastal and Shelf Science **31** (1990), no. 3, 319–343.

[38] G. L. Mellor and T. Yamada, *Development of a turbulence closure model for geophysical fluid problems.*, Reviews in Geophysics **20** (1982), 851–875.

[39] V. Merwade, D. Maidment, and J. Goff, *Anisotropic considerations while interpolating river channel bathymetry*, Journal of Hydrology **331** (2006), no. 3-4, 731–741.

[40] E. Miglio, S. Perotto, and F. Saleri, *A multiphysics strategy for free surface flows*, Proceedings of the 15th International Conference on Domains Decomposition Methods, 2003.

[41] ———, *Model coupling techniques for free-surface flow problems: Part i.*, Nonlinear Analysis **63** (2005), no. 5-7, e1885–e1896.

[42] ———, *Model coupling techniques for free-surface flow problems: Part ii.*, Nonlinear Analysis **63** (2005), no. 5-7, e1897–e1908.

[43] J.M. Molines, M. Fornerino, and C. Le Provost, *Tidal spectroscopy of a coastal area: observed and simulated tides of the lake maracaibo system*, Continental Shelf Research **9** (1989), no. 4, 301–323.

[44] Northern Area Office, *Hydrographic report: Channels with project depths 25 feet or over*, Tech. report, U.S Army Corps of Engineers, Galveston District, 2001.

[45] W. W. Pandoe and B. L. Edge, *Three-dimensional hydrodynamic model, study cases for quarter annular and idealized ship channel problems,* Ocean Engineering **30** (2003), no. 9, 1117–1135.

[46] Joseph Pedlosky, *Geophysical fluid dynamics*, Springer-Verlag, New York, 1987.

[47] B. Petrie, *Sea level variability in the bras d'or lakes*, Atmosphere-Ocean **37** (1999), no. 2, 221–239.

[48] B. Petrie and G. Bugden, *The physical oceanography of the bras d'or lakes*, Proceedings of the Nova Scotia Institute of Science, vol. 42, 2002, pp. 9–36.

[49] L.J. Pietrafesa, G.S. Janowitz, T.Y. Chao, R.H. Weisberg, F. Askari, and E. Noble, *The physical oceanography of the pamlico sound*, UNC Sea Grant Publication **UNC-WP-86-5** (1986), 125.

[50] A. Pinones, A. Valle-Levinson, D. A. Narvaez, C. A. Vargas, S. A. Navarrete, G. Yuras, and J. C. Castilla, *Wind-induced diurnal variability in river plume motion*, Estuarine Coastal And Shelf Science **65** (2005), no. 3, 513–525.

[51] D. Pothina and C. G. Guthrie, *Evaluating inverted siphons as a means of mitigating salinity intrusion in the keith lake/salt bayou system, jefferson county, texas*, Final report for grant mx96401704, epa gulf of mexico program, Texas Water Development Board, 2009.

[52] A. Quarteroni and L. Stolcis, *Heterogeneous domain decomposition for compressible flows*, Proceedings of the ICFD Conference on Numerical Methods for Fluid Dynamics (M. Baines and W.K. Morton, eds.), Oxford University Press, Oxford, 1995, pp. 113–128.

[53] A. Quarteroni and A. Valli, *Domain decomposition methods for partial differential equations*, Oxford University Press Inc., New York, 1999.

[54] Jr. Richard A. Schmalz, *Testing an all weather nowcast/forecast system for galveston bay*, 9th International Conference on Estuarine and Coastal

Modeling Charleston (Malcolm L. Spaulding, ed.), vol. 209, ASCE, 2005, pp. 36–36.

[55] Patrick J. Roache, *Verification and validation in computational science and engineering*, Hermosa, 1998.

[56] M. T. Stacey, S. G. Monismith, and J. R. Burau, *Observations of turbulence in a partially stratified estuary*, Journal Of Physical Oceanography **29** (1999), no. 8, 1950–1970.

[57] Corpus Christi Wind Surfing, *http://www.corpuschristiwindsurfing.com/weather.html*, World Wide Web electronic publication, 2007.

[58] C. Ulses, C. Grenz, P. Marsaleix, E. Schaaff, C. Estournel, S. Meule, and C. Pinazo, *Circulation in a semi-enclosed bay under influence of strong freshwater input*, Journal Of Marine Systems **56** (2005), no. 1-2, 113–132.

[59] R. A. N. Vaz and J. H. Simpson, *Turbulence closure modeling of estuarine stratification*, Journal Of Geophysical Research-Oceans **99** (1994), no. C8, 16143–16160.

[60] C.B. Vreugdenhil, *Numerical methods for shallow-water flow*, Water Science and Technology Library, Kluwer Academic Publishers, 1994.

[61] J. Wang, *A two-channel laterally averaged estuarine circulation model (laecim)*, J. Geophys. Res. **103(C9)** (1998), 18,381–18,391.

[62] J. C. Warner, C. R. Sherwood, H. G. Arango, and R. P. Signell, *Performance of four turbulence closure models implemented using a generic length scale method*, Ocean Modelling **8** (2005), no. 1-2, 81–113.

[63] T. Weiyan, *Shallow water hydrodynamics*, Elsevier Oceanography Series, Elsevier, 1992.

[64] J.J. Westerink and P. Roache, *Next generation environmental models computational methods*, ch. Issues in convergence studies in geophysical flow computations, SIAM, Philadelphia, PA, 1996.

[65] Joannes J. Westerink, Jesse C. Feyen, John H. Atkinson, Richard A. Luettich, Clint N. Dawson, Mark D. Powell, Jason P. Dunion, Hugh J. Roberts, Ethan J. Kubatko, and Hasan Pourtaheri, *A new generation hurricane storm surge model for southern louisiana*, Bulletin of the American Meteorological Society **in review** (2004).

[66] Mary F. Wheeler and Malgorzata Peszynska, *Computational engineering and science methodologies for modeling and simulation of subsurface applications*, Advances in Water Resources **25** (2002), no. 8-12, 1147–1173.

[67] L. Xie and D. B. Eggleston, *Computer simulations of wind-induced estuarine circulation patterns and estuary-shelf exchange processes: The potential role of wind forcing on larval transport*, Estuarine, Coastal and Shelf Science **49** (1999), no. 2, 221–234.

[68] Y. Zhang, *email comunication 03/10/2009*.

[69] Y. Zhang and A.M. Baptista, *Second elcirc/selfe user group meeting, charleston, sc, nov. 2-3, 2005*.

[70] Y. Zhang, A.M. Baptista, and E.P. Myers, *A cross-scale model for 3d baroclinic circulation in estuary-plume-shelf systems: I. formulation and skill assessment*, Continental Shelf Res. (2004), accepted.

[71] Yinglong Zhang and Antonio M. Baptista, *Selfe: A semi-implicit eulerian-lagrangian finite-element model for cross-scale ocean circulation*, Ocean Modelling **21** (2008), no. 3-4, 71–96.

[72] L. Y. Zheng, C. S. Chen, and H. D. Liu, *A modeling study of the satilla river estuary, georgia. i: Flooding-drying process and water exchange over the salt marsh-estuary-shelf complex*, Estuaries **26** (2003), no. 3, 651–669.

[73] L. Y. Zheng and R. H. Weisberg, *Tide, buoyancy, and wind-driven circulation of the charlotte harbor estuary: A model study*, Journal Of Geophysical Research-Oceans **109** (2004), no. C6, C06011.

Vita

Dharhas Pothina was born in Vijayawada, India on December 12, 1975 to Parasuram and Yethirajamma Pothina. When he was two years old, his family moved to England, where he lived for ten years before returning to India. He completed high school in India and was accepted to the Indian Institute of Technology Madras, where he completed his undergraduate degree in aerospace engineering in 1999. While working on his Masterś degree in aerospace engineering at the University of Texas, he met his wife Jada. He graduated in May 2002, and they were married in August of that year. After discontinuing doctoral studies in aerospace, Dharhas began working for the Texas Water Development Board, where he continued pursuing his interest in fluid dynamics and modeling through his work as part of a team studying the bays and estuaries of Texas. It was not long before he decided to continue his studies in Environmental and Water Resource Engineering at the University of Texas department of Civil Engineering. He now has one beautiful daughter, Seraya Grace who is almost two years old and another daughter is expected soon. Dharhas plans to continue working in the field of estuarine modeling and is looking forward to spending his free time with his family and their cat Sparky instead of working on this dissertation.

Permanent address: 11700 Ruffed Grouse Dr.
Austin, Texas 78758

This dissertation was typeset with LaTeX[†] by the author.

[†]LaTeX is a document preparation system developed by Leslie Lamport as a special version of Donald Knuth's TeX Program.